RIDE COMFORT EFFECTS OF INERTER IMPLEMENTATION AT HEAVY VEHICLE SUSPENSION SEAT

AĞIR TİCARİ ARAÇ SÜSPANSİYONLU KOLTUĞUNDA İNERTER UYGULAMASI VE KONFORA OLAN ETKİLERİ

BUĞRA AYDIN

ASST. PROF. DR. EMIR KUTLUAY

Supervisor

Submitted to

Graduate School of Science and Engineering of Hacettepe University

as a Partial Fulfillment to the Requirements

for the Award of the Degree of Master of Science

in Mechanical Engineering

April 2024

ABSTRACT

RIDE COMFORT EFFECTS OF INERTER IMPLEMENTATION AT HEAVY VEHICLE SUSPENSION SEAT

Buğra Aydın

Master of Science , Mechanical Engineering

Supervisor: Asst. Prof. Dr. Emir KUTLUAY

April 2024, 201 pages

The benefits of the relative new passive vibration isolation device, known as an Inerter or J-Damper, have been examined in terms of ride comfort for heavy commercial vehicle seat and cabin suspensions. The investigations were conducted using the equations of motion for a 5-axle tractor-trailer combination with 14 degrees of freedom associated with such a vehicle. Inerter devices were applied in various combinations in the cabin and seat suspensions, and each combination was realized by adding increasing inertance to spring and damper pairs corresponding to different natural frequencies and damping ratios. Weighted RMS acceleration values and RMS displacements were calculated in the frequency domain for each parameter set, and the changes obtained with increasing inertance were illustrated graphically.

Weighted RMS accelerations were calculated using methods defined by the ISO-2631:1997 standard. Road surface irregularities were defined according to the ISO-8608:2016 standard.

The results indicated that within the selected range, an increase in inertance led to a decrease in weighted accelerations and displacements. This suggests that the implementation of

inerter devices in the seat and cabin suspensions of heavy commercial vehicles can improve ride comfort.

Keywords: inerter, inerter based seat suspension, heavy vehicle inerter seat and cab suspension, ride comfort, ride comfort with inerter

ÖZET

AĞIR TİCARİ ARAÇ SÜSPANSİYONLU KOLTUĞUNDA İNERTER UYGULAMASI VE KONFORA OLAN ETKİLERİ

Buğra Aydın

Yüksek Lisans, Makine Mühendisliği

Danışman: Asst. Prof. Dr. Emir KUTLUAY

Nisan 2024, 201 sayfa

Inerter olarak adlandıralan ve J-Damper olarak da bilinen göreceli yeni pasif titreşim izole edici cihazın ağır ticari araç koltuk ve kabin süspansiyonunda getirdiği faydalar sürüş konforu bakımından incelenmiştir. İncelemeler, 5 akslı çekici-dorse kombinasyonu ile bu tipte bir araca ait 14 hareket sebestliğine sahip hareket denklemleri ile yapılmıştır. İnerter cihazları, kabinde ve koltukta farklı kombinasyonlarda uygulanmış ve her kombinasyon, farklı doğal freakanslara ve sönüm oranlarına denk gelen yay-amotisör çiftlerine, 0'dan başlayıp artan inertans eklenerek gerçekleştirilmiştir. Her bir parametre seti için ağırlıklı etkin ivme değeri ve etkin deplasman, frekans bölgesinde hesaplanmış ve inertans artışı ile birlikte elde edilen değişimler grafikler ile gösterilmiştir.

Ağırlıklı etkin ivmeler, ISO-2631:1997 standardının belirlerdiği metotlar ile hesaplanmıştır. Yol yüzey düzgünsüzlükleri ise ISO-8608:2016 standardına göre oluşturulmuştur.

Sonuçlar, seçilmiş olan aralıkta, inertans artışı ile birlikte etkin ağırlıklı ivmelerde ve aynı zamanda etkin deplasmanlarda düşüş oluştuğunu, yani inerter cihazlarının ağır ticari araç koltuk süspansiyonunda ve kabin süspansiyonunda uygulanması halinde sürüş konforunun iyileşeceğini göstermiştir.

Keywords: inerter, inerter based seat suspension, heavy vehicle inerter seat and cab suspension, ride comfort, ride comfort with inerter

CONTENTS

Page

TABLES

FIGURES

ABBREVIATIONS

PSD	:	**P**ower **S**pectral **D**ensity
DOF	:	**D**egrees **O**f **F**reedom
FEM	:	**F**inite **E**lements **M**ethod
FFT	:	**F**ast **F**ourier **T**ransformation
RMS	:	**R**oot **M**ean **S**quare
VDV	:	**V**ibration **D**ose **V**alue

1. INTRODUCTION

Heavy vehicles play a significant role in today's transportation system. They are relied upon for tasks ranging from delivering individual purchases to transporting parts that keep factories running. Consequently, road transportation is expected to operate continuously. To achieve this, manpower is as crucial as the drivers themselves. Ride discomfort negatively affects drivers' fatigue levels and needs to be minimized.

Ride comfort can generally be evaluated in three parts: noise, vibration, and harshness. These measures are essentially subjective and can vary from individual to individual. This thesis focuses on vibrations caused by road irregularities. While ride comfort is a subjective measure, there are widely accepted objective measures that enable its evaluation using standardized methods. The ISO-2631 standard defines limits for vibrations related to health, comfort, and motion sickness. For comfort evaluation, there are also defined limits assessing human reactions to vibratory environments, ranging from extremely uncomfortable to not uncomfortable. [1]

Heavy vehicles differ from passenger vehicle counterparts in several aspects due to their primary purpose: carrying heavier and bulkier goods. This difference results in larger and higher designs with suspensions that must perform well under varying loading conditions, from an empty vehicle to a fully laden one. This variability significantly limits axle suspension designs. One solution to this challenge is air bellow suspensions. Such systems can maintain the natural frequency of the design relatively constant and perform well under any loading condition, enhancing both comfort and road holding capabilities. The use of such systems has now been extended to cab and seat suspensions, thereby greatly improving ride comfort. [2] demonstrates that there are instances where drivers are exposed to vibrations that fall within the health caution zone according to the definitions of ISO-2631.

However, ride comfort can be further enhanced to reduce fatigue levels, which not only improves driver efficiency but also meets the high demand for better ride quality from drivers. This thesis investigates the effects of a relatively new vibration control element,

the inerter, when implemented in heavy vehicles. An inerter, also known as a j-damper, is a two-terminal device that produces force based on the acceleration difference across its terminals. Essentially, it resists changes in acceleration at its terminals, a property known as inertance, measured in kilograms. [3]

1.1. Scope Of The Thesis

This thesis primarily focuses on the ride comfort benefits of inerters in Cab Over Engine (COE) type Tractor-Semitrailers. Various factors influence the comfort of such vehicles, including loading conditions, type of semi-trailer, axle suspension type, cab suspension type and its location, seat suspension, engine-gearbox bushings, frame compliance, and lastly, the driver's physical characteristics. Within the scope of this thesis, all specifications pertain to a single fully laden case. A mathematical model of such a vehicle is developed, and the vibration isolation performance is evaluated using this model. Inerters are positioned at both the cab and seat suspensions. Road irregularities are defined in accordance with the ISO-8608 standard.

1.2. Contributions

In this thesis, the vibration isolation performance benefits of parallel inerters are investigated using a 14-degree-of-freedom (DOF) model of a heavy vehicle ride comfort. Changes in weighted RMS accelerations and suspension deflections are plotted across a range of natural frequencies and damping ratios to generalize the results. This approach enables the prediction of the benefits of inerters when integrated into suspensions within these ranges.

- Parallel inerter applied to heavy vehicle seat fore-aft isolator and the changes in the isolation performance is shown
- Parallel inerter applied to heavy vehicle seat vertical suspension and the changes in the isolation performance is shown

- Parallel inerter applied to heavy vehicle cab suspension and the changes in the isolation performance is shown

1.3. Organization

The organization of the thesis is as follows:

- Chapter 1 presents our motivation, contributions, and the scope of the thesis.
- Chapter 2 provides a literature review of related works in the field.
- Chapter 3 introduces the mathematical approaches.
- Chapter 4 demonstrates the results and findings from the simulations.
- Chapter 5 summarizes the results obtained throughout the thesis.

2. LITERATURE REVIEW

2.1. Ride Comfort Studies of Heavy Vehicles

The primary methodology for studying ride comfort is presented by Wong [4], as illustrated in Figure 2.1. This approach typically involves three main components: a model for road irregularities, a model for vehicle vibrations, and a procedure for vibration evaluation. Jiang's literature survey on ride comfort indicates that many authors follow this general approach, with variations in the methods used to describe road profiles, the fidelity of the vehicle model, and the methods used for vibration evaluation [5].

Figure 2.1 A general ride comfort study method [4]

Road profiles are typically described using their respective fitted Power Spectral Density (PSD) functions. Kropac [6] provides examples of one, two, and three-band road PSD descriptions, as shown in Figure 2.2. This thesis adopts the ISO-8608:2016 standard for road PSD descriptions.

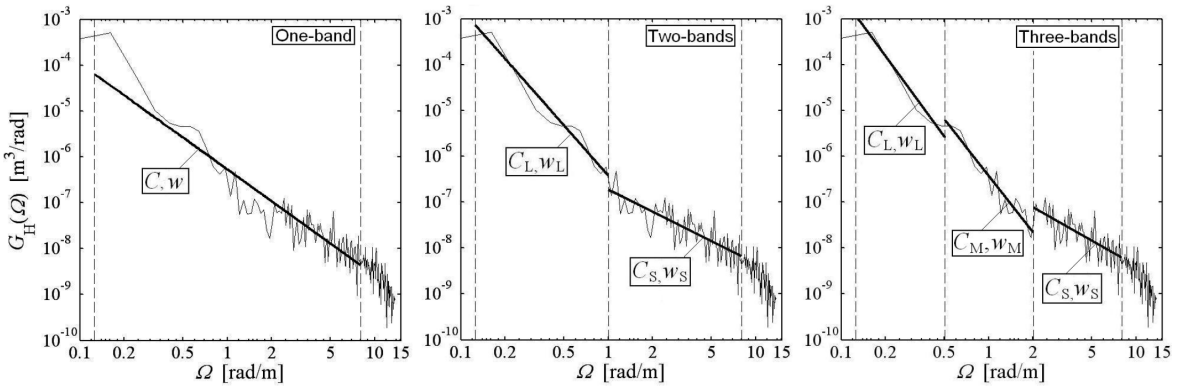

Figure 2.2 PSD approximation lines with one, two, and three wavelength bands [6]

The mathematical description of the vehicle plays a crucial role in obtaining the necessary vibrations. Some key properties of the models include:

- Number of DOF: 6-21
- Number of axles: 2-5
- Cab mountings: stiff or suspended
- Inclusion of seat-human model: exists or lumped into cab mass
- Engine and gearbox mountings: stiff or suspended
- Flexibility of chassis frames accounted for: rigid, modal superposition, or finite element model
- 5th wheel coupling model for tractor-semitrailers: rigid coupling or spring simplification

While more complex models generally provide a better description of vibrations, they also require more parameters to be estimated and demand more computational power. Simplifications should be made carefully. For modeling decisions, studies like Trangsrud's [7] can be referenced. For instance, Figure 2.3 demonstrates how the engine DOF affects the vibration PSD at the driver's seat in both vertical and longitudinal directions.

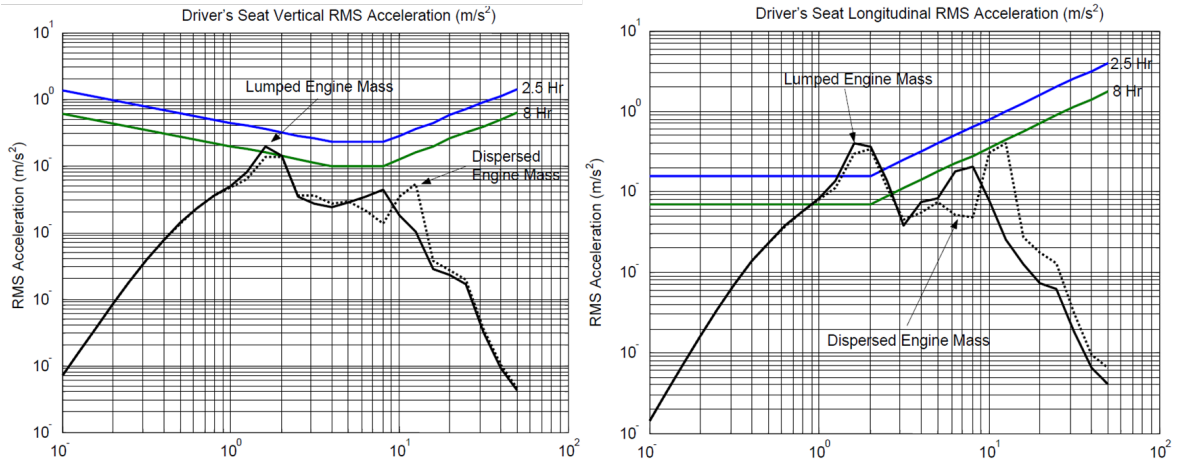

Figure 2.3 Engine DOF effects on seat vibration PSD [7]

Perseguim et al. utilized a multibody model incorporating FEM in their work [8]. Figure 2.4 displays the first torsion mode of the frame obtained through testing, occurring at 7.7 Hz with a 0.302 damping ratio. Figure 2.5 presents the time domain displacement and its FFT obtained through simulation, revealing three main modes causing the most discomfort in the fore-aft direction, one occurring at a very low frequency.

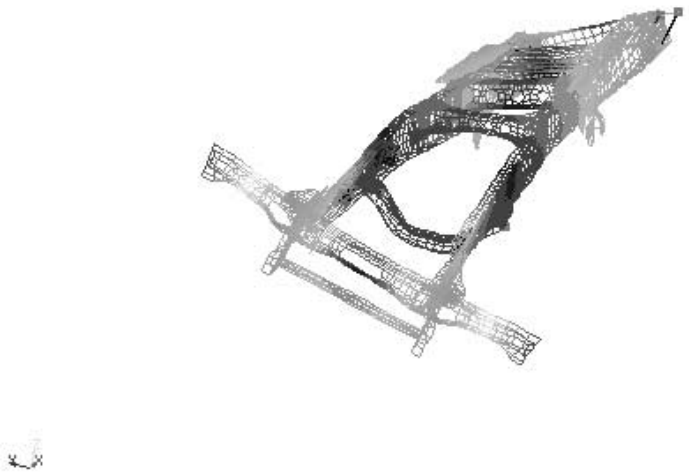

Figure 2.4 Frame first torsion mode [8]

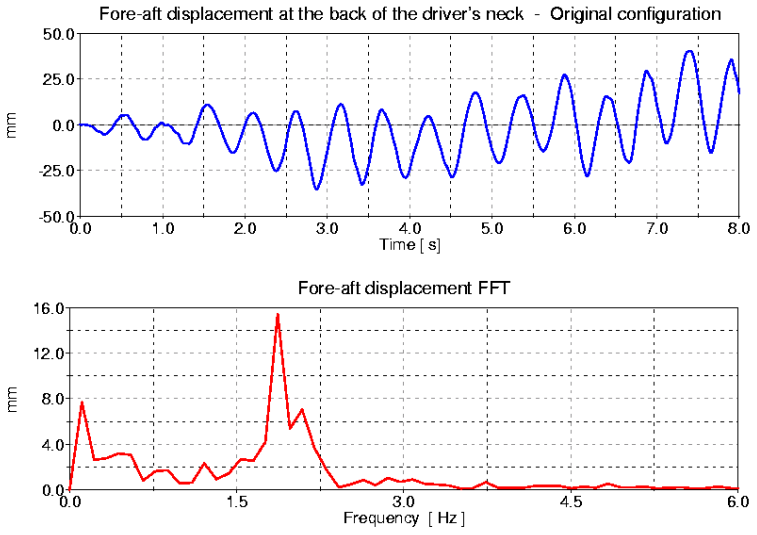

Figure 2.5 Driver's neck fore-aft displacement and FFT [8]

In conclusion, a ride comfort study necessitates a description of the road elevation profile, an appropriate vehicle model, and a procedure for vibration evaluation.

2.2. ISO 2631

ISO-2631 is widely accepted and used for ride comfort studies. Proposed methods often involve different positions, with seated individuals being common for ride studies since drivers typically sit while driving. The main principle involves measuring the vibrations transmitted to humans at the seat pan. These vibrations are processed in the respective principal axes. Figure 2.6 shows the axes considered for the sitting human body on the seat pan. On this figure the axes for the feet contact point also drawn. In general, for comfort evaluation of whole body vibration obtained at the seat pan for the given axes and the overall vibration magnitude calculated from individual component and then compared to given indication values. While obtaining individual vibration magnitudes at the axes, frequency based filtering is applied to emphasize the vibrations in the more irritating frequency range. Frequency weightings for the x and z axes provided by ISO-2631:1997 standard is given in Figure 2.7. These weightings suggest that the 4-10 Hz range is more important for vertical vibrations, while the 0.5-2 Hz range is more irritating in the fore-aft directional vibrations to the human body. This is seen by the frequency bands where the weightings are greater than the rest of the plot.

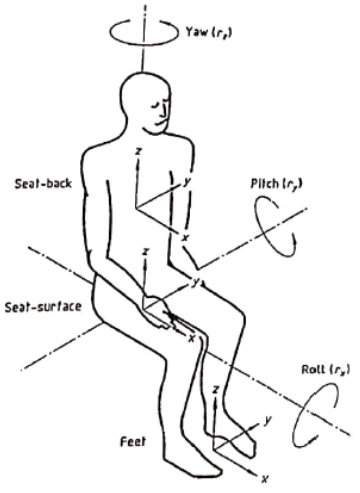

Figure 2.6 Basicentric axes of the human body for seated position [1]

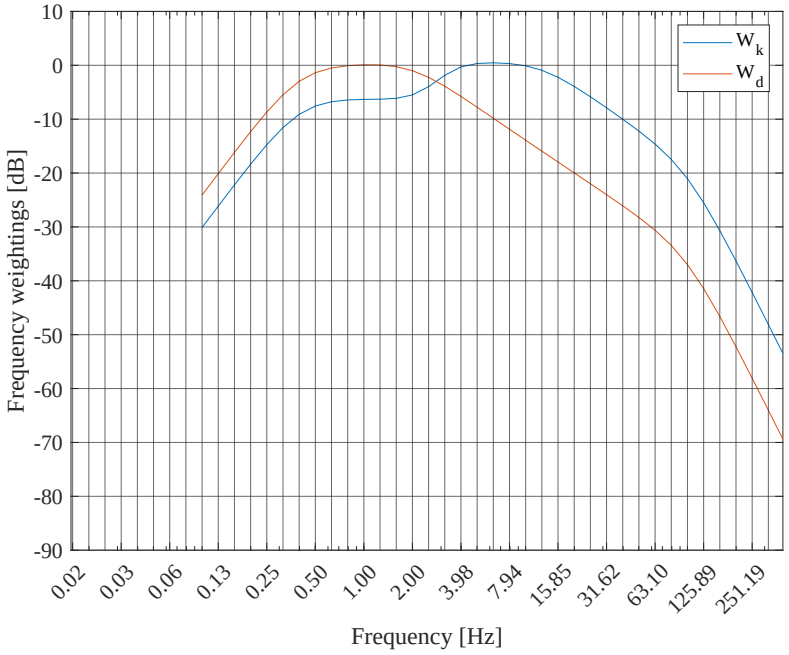

Figure 2.7 ISO2631:1997 Frequency-dependent weightings for x and z principle axes.

2.3. ISO 8608

Road irregularities are typically the primary source of vibrations used in ride comfort studies, making a concrete definition essential. Among various definitions, ISO's definition for road irregularity in the 8608 standard is widely accepted and utilized by many researchers. ISO-8608:2016 categorizes roads into eight classes, from A (best) to H (worst). For each class, upper and lower limits for degree of roughness are defined, and mean values for each road class are provided for simulation studies. These roughness degrees are used to calculate the Power Spectral Density (PSD) using the formula below. The ISO PSD graphs can be seen in the figure **??**

$$G_d(n) = G_d(n_0)\left(\frac{n}{n_0}\right)^{-w} \tag{1}$$

where n is the spatial frequency in cycles/meter, n_0 is the reference spatial frequency (0.1 cycles/meter), and w is the exponent for the fitted PSD. ISO8608:2016 suggests a frequency range between 0.01 and 10 for spatial frequency content. Care should be taken when using

frequencies outside this range, as the magnitudes can become very high for lower frequencies and very low for higher frequencies [9].

For simulations or calculations, a definition in the time domain is often required. This can be achieved by converting the spatial frequency into frequency in the time domain (Hz) based on velocity. While the road's irregularity remains constant regardless of the vehicle's velocity, the excitation frequency for the vehicle changes in the time domain with the vehicle's speed. The necessary conversion can be performed using Equation 2. An example conversion is shown in Figure 2.8 [10].

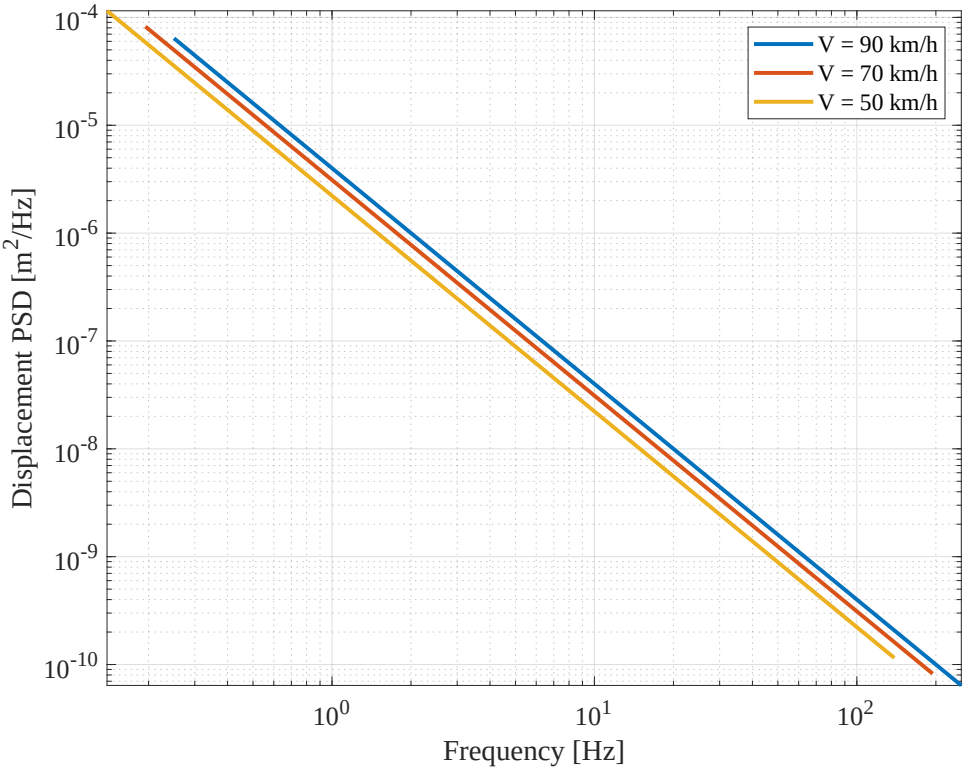

Figure 2.8 PSD definition in Hz for road class A at different velocities

$$G_d(f) = \frac{G_d(n_0) f^{-w}}{V} \tag{2}$$

where, $f = n * V$ f is frequency in Hertz V is velocity in meters/second.

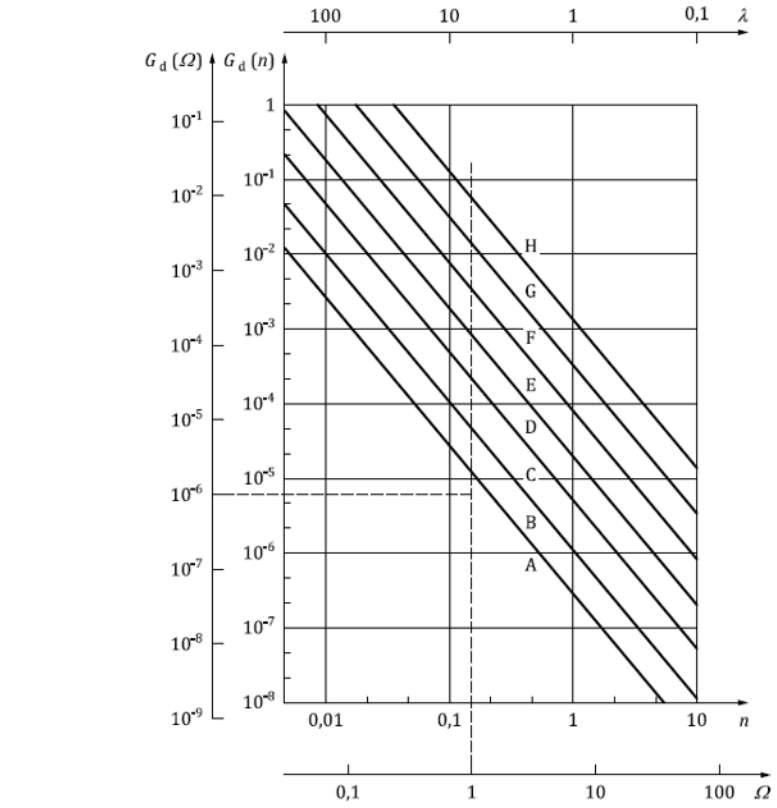

Key

λ	wavelength, m	n	spatial frequency, cycles/m
$G_d(n)$, $G_d(\Omega)$	displacement power spectral density, m^3	Ω	angular spatial frequency, rad/m

Figure 2.9 ISO-8608:2016 PSD description of road classifications

2.4. Inerter

An inerter is a device with two terminals that produces force in response to the acceleration differences between its terminals, resisting changes in velocity. It is used in high-performance applications as a complementary passive vibration control element. Figure 2.10 shows a schematic of a ball screw-type inerter. In such a mechanism, rotational inertia is converted to linear inertia, or inertance, measured in kg units.

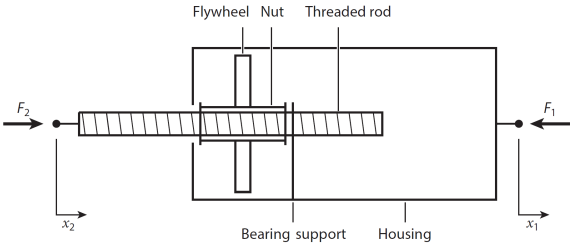

Figure 2.10 Ball screw-type inerter schematic [11]

The force produced by such an inerter can be calculated using Equations 3 and 4.

$$F_1 = b(\ddot{x}_2 - \ddot{x}_1) - m_1\ddot{x}_1 \tag{3}$$

$$F_2 = b(\ddot{x}_2 - \ddot{x}_1) + m_2\ddot{x}_2 \tag{4}$$

where, $b = (2\pi\gamma/\rho)^2 m$

b is the inertance value, γ is the radius of gyration of the flywheel, ρ is the pitch of the screw, m is the mass of the flywheel, m_2 is the mass of the threaded rod, and m_1 is the total mass of the rest of the device, including the nut, bearings, housing, and flywheel. When $m_2 < m_1$, Equations 3 and 4 can be simplified to an ideal inerter equation, as shown in Equation 5 [11].

$$F_1 = F_2 = b(\ddot{x}_2 - \ddot{x}_1) \tag{5}$$

An example realization of a ball screw inerter is depicted in Figure 2.11 and the 2 terminals, case and the screw is visible.

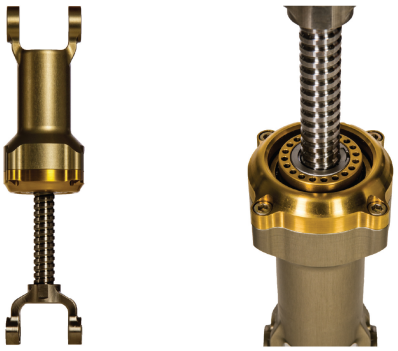

Figure 2.11 Realization of ball screw-type inerter [11]

Inerters can be incorporated into suspensions in various configurations. Smith provides eight different suspension layouts in his work [3], six of which include an inerter, as shown in Figure 2.12. Layouts S3 and S4 are known as parallel and series configurations, respectively.

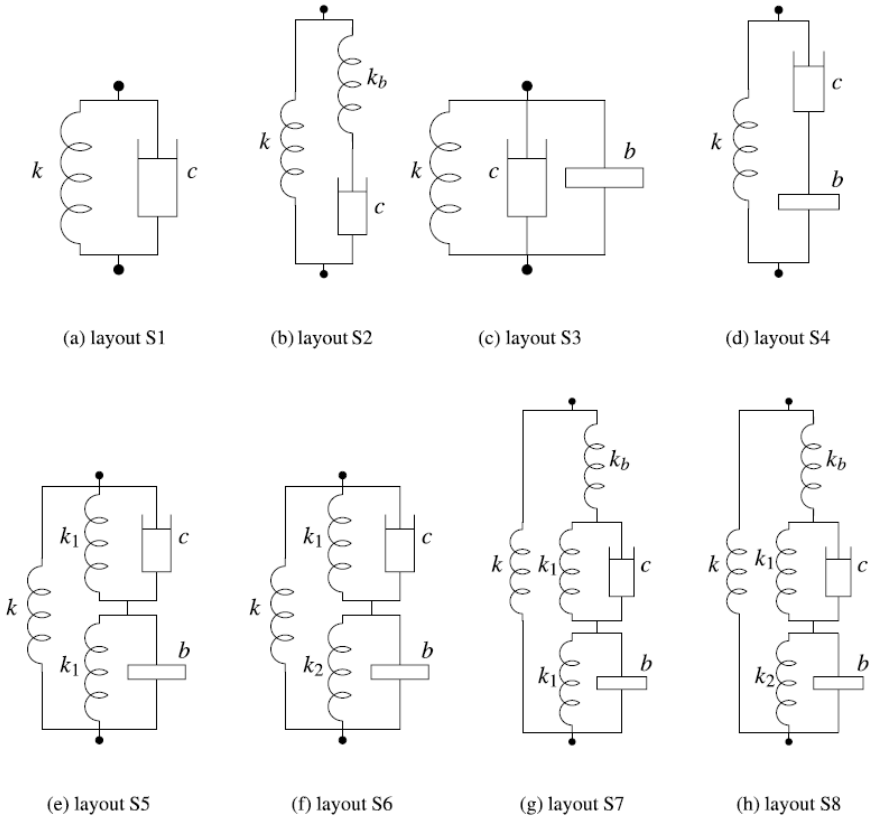

Figure 2.12 Suspension layouts provided by Smith [3]

From these layouts, S4 which is also known as the serial inerter is physically not practical as the positions of the damper and inerter is not controlled. This is because there is no force acting between terminals of the damper and inerter when they are deflected from the original positions and hence they could be anywhere between the connected elements. To overcome this issue, layouts S5 to S8 contain springs to centre the damper and inerter and these springs are called centring springs. Layouts S5 and S6 are the variation of the same configuration with the same spring and different spring stiffness for centring springs. And so the layouts S7 and S8. The main difference between the layouts S5-6 and S7-8 is the inclusion of the serial connected springs.

The transmissibility of a single DOF vibration system with and without a parallel inerter is presented in Figure 2.13, from a study by Kuhnert et al. [12]. This graph indicates an earlier occurrence of the natural frequency, followed by an anti-resonant frequency, both of which are advantageous for vibration isolation performance. However, the isolation performance deteriorates after the anti-resonant frequency, as the transmissibility does not decay and instead becomes flat. Despite this behavior, an inerter can be beneficial for the ride comfort of road vehicles because, in general, the vibration amplitude of road profiles decreases with increasing frequencies, and lower frequencies are more important for ride comfort studies.

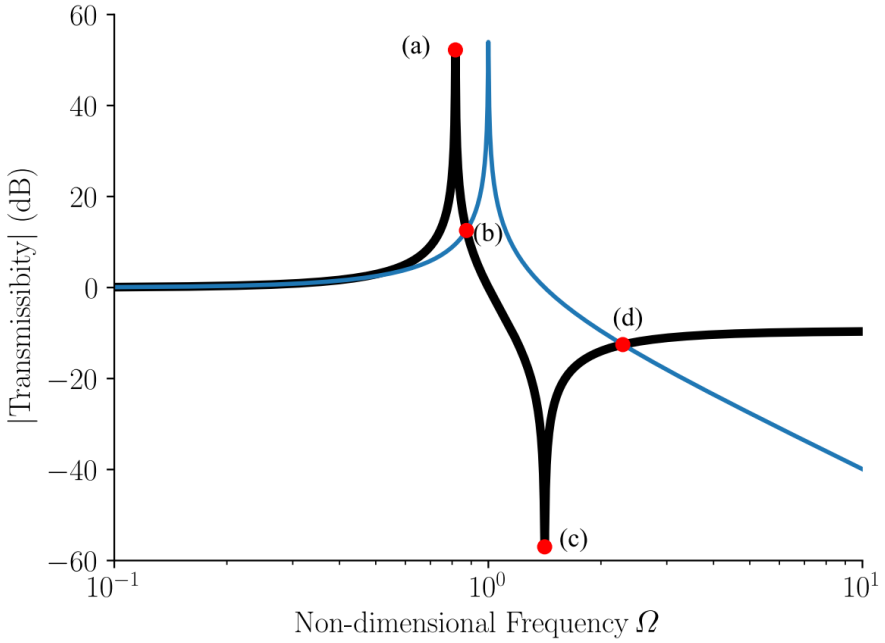

Figure 2.13 Transmissibility of suspension systems with and without parallel inerter [3]

In their work, Kuhnert et. al. shows that with a parallel inerter, the decay on the transmissibility is lost. This phenomena can be revealed by examining the transfer function of this 1-DOF system. They have used the model given in the figure 2.14 for the parallel inerter.

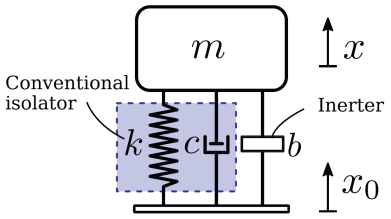

Figure 2.14 1-DOF inerter based isolator model exmined by Kuhnert et. al. [12]

The mass m is supported through a spring k, a damper c and an inerter b. The system excited by the input x_0 and the position of the mass is x. The equation of motion for this 1-DOF isolation system can be written as given in the equation 6.

$$m\,\ddot{x} = -b\,(\ddot{x} - \ddot{x}_0) - c\,(\dot{x} - \dot{x}_0) - k\,(x - x_0) \tag{6}$$

They write the transmissibility function of this 1-DOF system with non-dimensional terms by defining, $\Omega = \omega/\omega_n$, $\omega_n = \sqrt{k/m}$, $\zeta = c/(2\sqrt{mk})$ and $\mu = b/m$ where w_n is undamped natural frequency, ζ is the damping ratio and μ is the ratio of inertance value to the mass. With these non-dimensional parameters, they provide the transmissibility function as given in equation 8 by assuming a harmonic excitation of the form $x_0 = X_0 e^{jwt}$, hence harmonic response of the form $x = Xe^{jwt}$. Then they use the impedance of each component to construct the transmissibility function with non-dimensional terms as;

$$Q = \frac{X}{X_0} = \frac{Z_I}{Z_m + Z_I} \tag{7}$$

where,

$Z_I = Z_k + Z_c + Z_b$ is the total impedance of the system,

$Z_k = \frac{k}{jw}$ is the impedance of the spring,

$Z_c = c$ impedance of the damper,

$Z_b = jwb$ is the impedance of the inerter and

$Z_m = jwm$ is the impedance of the mass.

The resulting non-dimensional transmissibility function is provided in their work is given in equation 8.

$$Q = \frac{1 - \mu\Omega^2 + j2\zeta\Omega}{1 - (1+\mu)\Omega^2 + j2\zeta\Omega} \tag{8}$$

In figure 2.13, the loss of decay is apparent when an inerter is added to the system. For this graph the damping ratio, ζ, is set to 0.001 and inertance to mass ratio, μ, is set to 0 and 0.5 in the equation 8 for the systems without with inerter respectively. By inspection, it is seen that when no inerter exists, i.e. $\mu = 0$, then the numerator of the transmissibility function given by 8 becomes first order, and when inerter added, numerator becomes 2nd order which reveals

that the inerter adds a zero to system. This causes change in the inclination of the numerator term from 20dB/decade for non-inerter to 40dB/decade for the inerter based isolator system after the corner frequency of the numerator terms.

To show this phenomena, the plots given in the figure 2.13 is recreated in which the magnitude terms are drawn separately by the mean of numerator and denominator terms together with their summation which is the magnitude of response of the complete system. The damping ratio and the inertance ratio are kept the same as in their work.

For the conventional system with no inerter, the graph is given in figure 2.15. On this plot, the denominator and numerator terms are plotted with blue dashed line and red dashed line respectively. The corner frequency of the numerator term is 500 i.e. 500 times of the natural frequency. To make it visible graph is plotted up to $\Omega = 10^4$. Lower limit kept as the original value, $\Omega = 0.1$. The magnitude of the numerator term stays close to zero up to corner frequency. Hence, the total response magnitude of the system is dictated by the numerator term up to 500 time of the natural frequency. After this corner frequency, numerator term has an inclination of 20 dB/decade. This affects the total response and the seperation between total response (black solid line) and the denominator term (blue dashed line) becomes visible and the decay becomes -20 dB/decade from -40 dB/decade. So the decay is preserved with different declination before and after the numerator terms corner frequency.

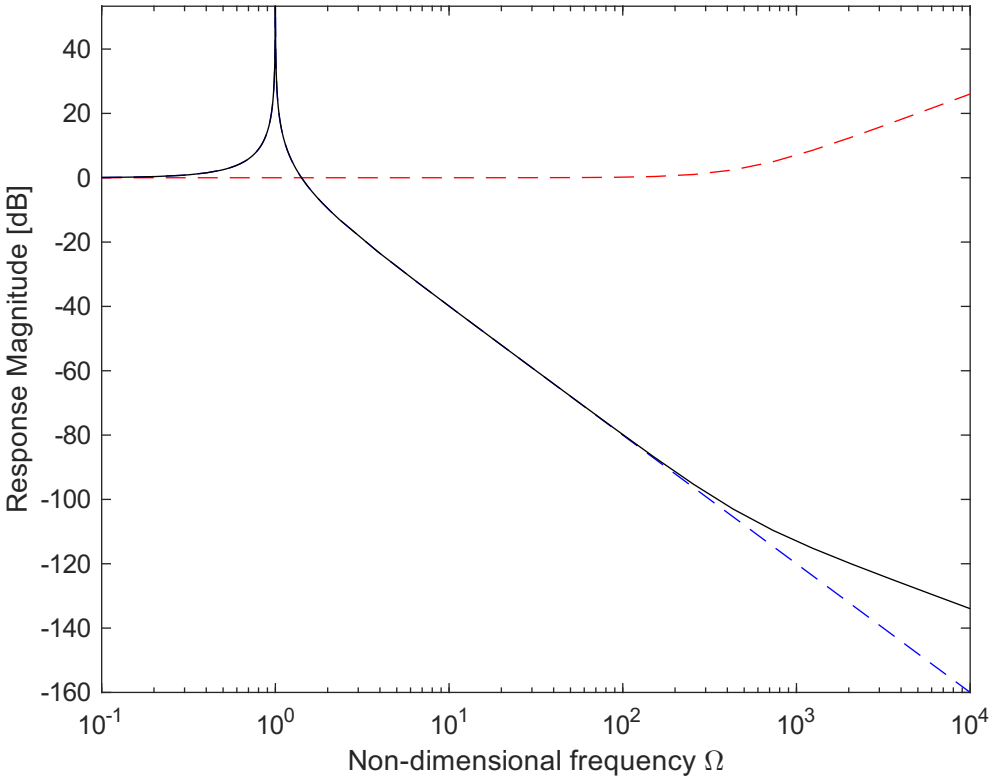

Figure 2.15 Bode magnitude plot construction for conventional isolation system. red dashed line is numerator term, blue dashed line is denominator term and black solid line is the total response of the system.

The same graph is also constructed for the inerter based isolation system and given in the figure 2.16. In this case μ is set to 0.5 which meas that the inerter has the inertance value of half of the mass. The numerator term in equation 8 becomes 2nd order and its magnitude is plotted with red dashed line. As seen, 2nd order numerator causes an anti-resonant and after then it has inclination of 40dB/decade. Denominator term has a -40dB/decade declination after its corner frequency. Hence, total response becomes flat after corner frequency of the numerator term. Plotting limits are kept the same for convenient.

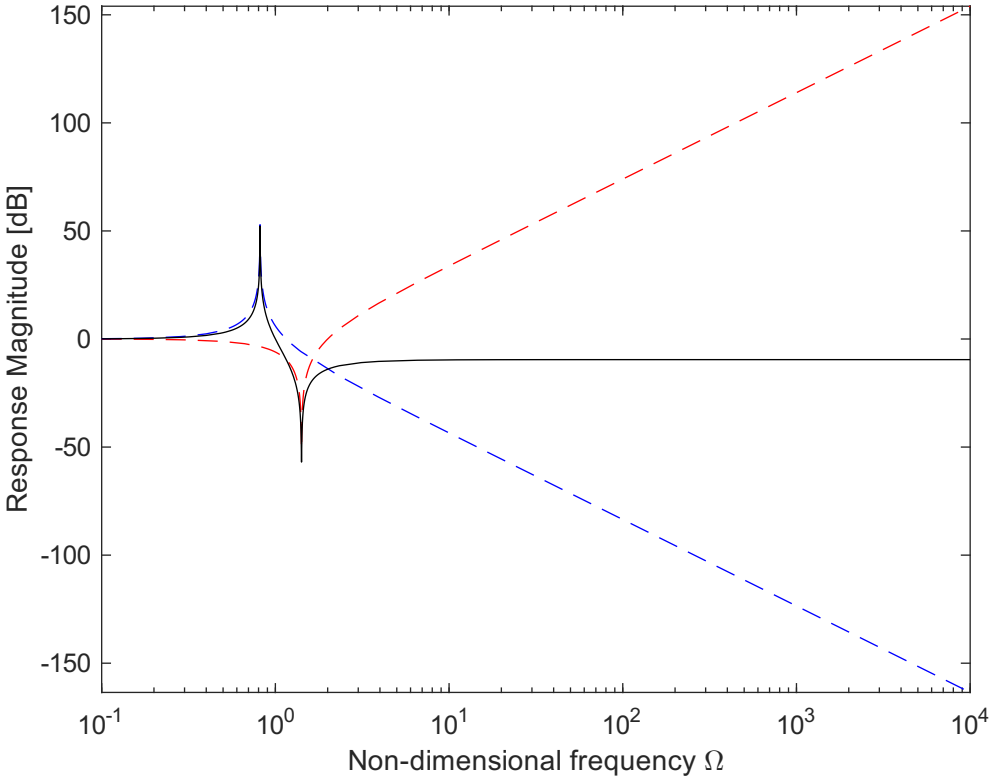

Figure 2.16 Bode magnitude plot construction for parallel inerter based isolation system. Red dashed line is numerator term, blue dashed line is denominator term and black solid line is the total response of the system.

Even though the decay is lost with inerter, parallel inerter based isolation system can provide benefits by the mean of ride comfort when the frequency dependent ISO-2631:1997 weightings given in the figure 2.7 considered. Weightings suggest that the important frequency bands are narrow and futhermore, after the important bands weightings has steep declination. This might indicate that the occurrence of loss of decay when an inerter added in parallel configuration might not affect the overall ride comfort if the anti-resonant frequency can be kept in the important band of the ISO weightings. Moreover, considering the road profile PSD functions provided by the ISO-8608:2016 standard given in the figure 3.2 it is seen that the signal magnitudes becomes very small with increasing frequency. This also suggests that the loss of decay occurring with the parallel inerter might be insignificant when the ride comfort is evaluated with the road irregularity excitation.

Inerters are relatively new devices, and the literature is limited in studies investigating their benefits when utilized in heavy vehicle seat suspension. Ning et al. [13] conducted a study on a variable inertance device applied to heavy vehicle seat suspension. Their work demonstrates the positive effects of an inerter on vibrations transmitted to the driver through both simulations and experimental methods. Figure 2.17 illustrates how the variable inerter is achieved using a controllable damper in their work. The equivalent inertance value can be controlled by setting the damper to its lowest possible value, which is nearly 0 Ns/m, and to its maximum possible value, which is infinite i.e., the damper is locked. Thus, the inertance value can be varied between b_1 and $b_1 + b_2$. With this configuration, the variable device's inertance value depends on the input frequency, as given by Equation 9.

$$b_{eqv} = b_1 + \frac{b_2 c^2}{c^2 + b^2 w^2} \tag{9}$$

where w is frequency.

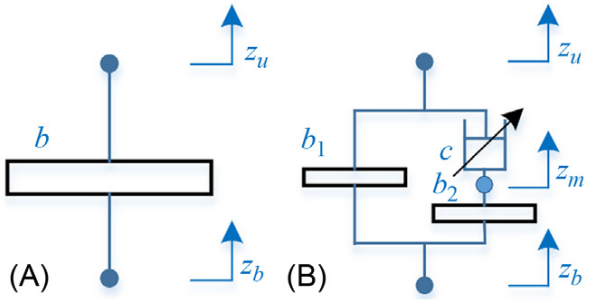

Figure 2.17 Constant and variable inerter devices proposed by Ning et. al. [13]

Equation 9 is used to calculate the equivalent inertance values yielding depend on both damper value and frequency. And in the figure 2.18, the change in the inertance value with increasing frequency is provided by Ning. et. al. for different set values of damper. This graph shows that the variable inertance device has a decreasing inertance with increasing frequency. And, it is also observable that with higher damper values, the equivalent inertance value decreases slower than the smaller damper counterpart.

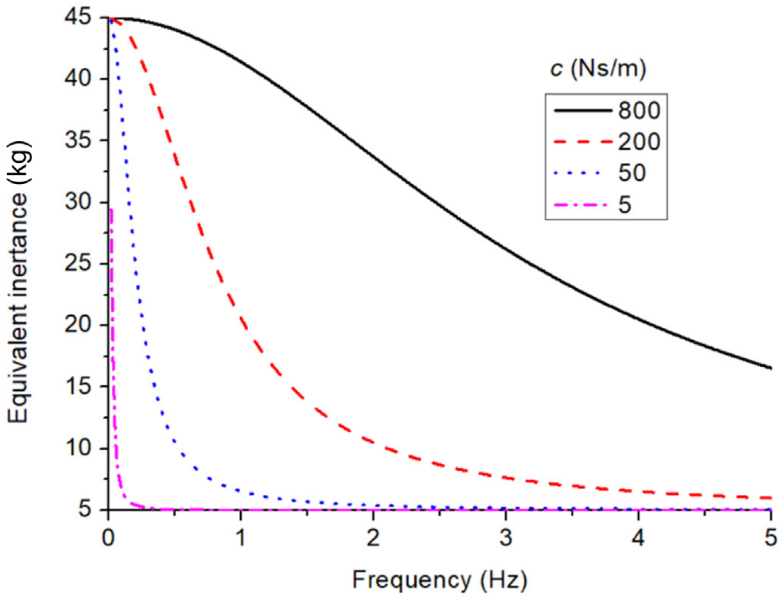

Figure 2.18 Frequency dependent equivalent inertance for different dampers [13]

The developed device was implemented as a vibration isolation element in a seat suspension system, which is a 1 DOF system where the input is base excitation. Experimental results were obtained for conventional suspension and inerter-based suspensions with different configurations. When no current is applied, the Variable Inertance Device exhibits low inertance, and when 1 ampere is applied, the inertance is high. There is also a controlled form that aims to leverage both high and low inertance to achieve optimal performance. The transmissibility results are shown in Figure 2.19.

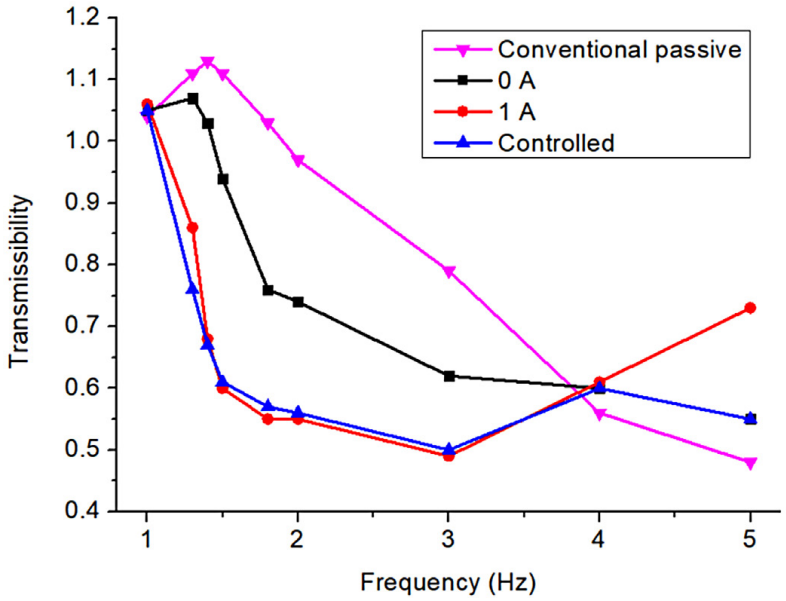

Figure 2.19 Transmissibility for different inertance values [13]

The transmissibility plot in this figure indicates that the Variable Inertance Device with high inertance offers better isolation performance at lower frequencies than conventional suspension, but its performance deteriorates after about 4 Hz. The low inertance Variable Inertance Device shows worse isolation performance than the high inertance counterpart up to almost 4 Hz however the deterioration is not high as high inertance considering the provided plot. The applied control law, as previously mentioned, leverages both behaviors by adjusting the applied current appropriately. Therefore, this controlled Variable Inertance Device exhibits the best isolation performance within the specified frequency range. It has the behaviour of high inertance device up to about 4 Hz and after then it has the behaviour of the low inertance device.

Ning et. al. conduct also a random excitation experiment and provide the comfort indicators as RMS, FW-RMS(Frequency Weighted-RMS) and VDV, fouth power vibration dose value. VDV is a measure which is more sensitive to the acceleration peaks and uses 4th power of the time history signal instead of 2nd, hence the peaks are more pronounced. The formula for VDV is defined in equation 10 [1].

$$VDV = \left\{ \int_0^T \left[a_w(t) \right]^4 dt \right\}^{\frac{1}{4}} \tag{10}$$

Table 2.1 Performance comparison of the Variable Inertance Devices to passive system for random excitattion input. Regenerated from [13]

	Conventional passive	VA			
		0 A	1 A	Controlled	Reduction
RMS (m/s^2)	1.044	0.895	0.653	0.654	37.3%
FW-RMS (m/s^2)	0.779	0.535	0.448	0.439	43.6%
VDV $(m/s^{1.75})$	2.445	1.474	1.230	1.177	51.8%

In table 2.1 it is seen that the Variable Inertance Device provides better vibration isolation than the conventional counterpart. The differences vary depend on the configuration of the device. The RMS results shows that the high inertance device (1 A) has slightly lower acceleration than the controlled form. For other results, controlled form has the least values. However, High inertance device has also very close values to controlled form. FW-RMS (Frequency Weighted-RMS) results represent the overall comfort assessment value according to ISO-2631 and it is seen that conventional passive isolation system falls into the "fairly uncomfortable" reaction category while isolation systems incorporating variable inertance device fall all into "a little uncomfortable" category.

These results are important as it shows that despite the deteoirated isolation performance for higher frequencies, an inerter based isolation system can perform overall better. However, it should be mentioned that the devices proposed and experimented by Ning. et. al. has variable inertance. This does not only mean that the inertance value can be controlled but the device also has a changing inertance with the varying frequency as shown previously in the figure 2.18.

Another aspect is the direction of the vibrations. Heavy vehicles, as mentioned before, has bulkier and taller bodies than most of the other road vehicles especially than the passenger vehicles and fore-aft motions becomes greater. Sweatman and McFarlane have shown with their report that the seat fore-aft vibration is important as much as the vertical vibrations. Among many other measurements, they have measured the seat pan vibrations on different fully laden semi-trucks. Experiments conducted on different pathways in Australia and the measurement are frequency weighted [14] and depicted in figures 2.20 and 2.21. The frequency based RMS values are calculated based on Australian standard which is based on ISO-2631:1985. So, each center frequency of one third octave band has its own RMS value and calculated for vertical and longitudinal directions separately. Figures are given for 8 different vehicles and it is obvious that each vehicle has its own characteristics by the mean of acceleration amplitude and frequency distribution. In general, vertical vibrations seem to be greater in the 2-4 Hz band. Sweatman and McFarlane emphasize the fore-aft seat pad vibrations occurring in 10-15 Hz band. When BM3 and BM1 are not concerned, high magnitudes also exist in the 2-4 HZ band. However, in the longitudinal direction there is no band where the magnitude considerable higher than the rest of the graph as in the graph provided for the vertical direction. With the exception of BM3, which has lower vibrations in both directions, longitudinal vibrations seem to be effective from 1 Hz up to 20 Hz band with major deviations in the frequency distributions from one vehicle to another. Another, interesting behaviour occurs with the vehicle F4. This vehicle seems to have greater fore-aft vibrations throughout the entire given frequency range.

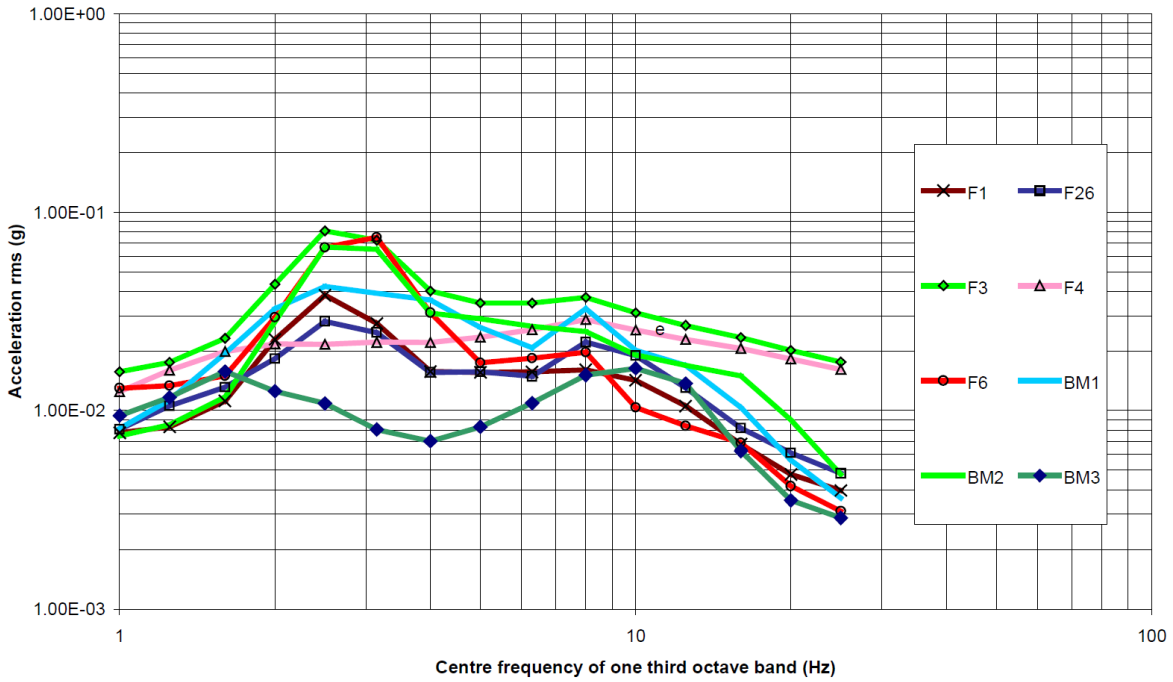

Figure 2.20 Seatpad vertical accelerations by vehicles from the report by Sweatman and McFarlane [14]

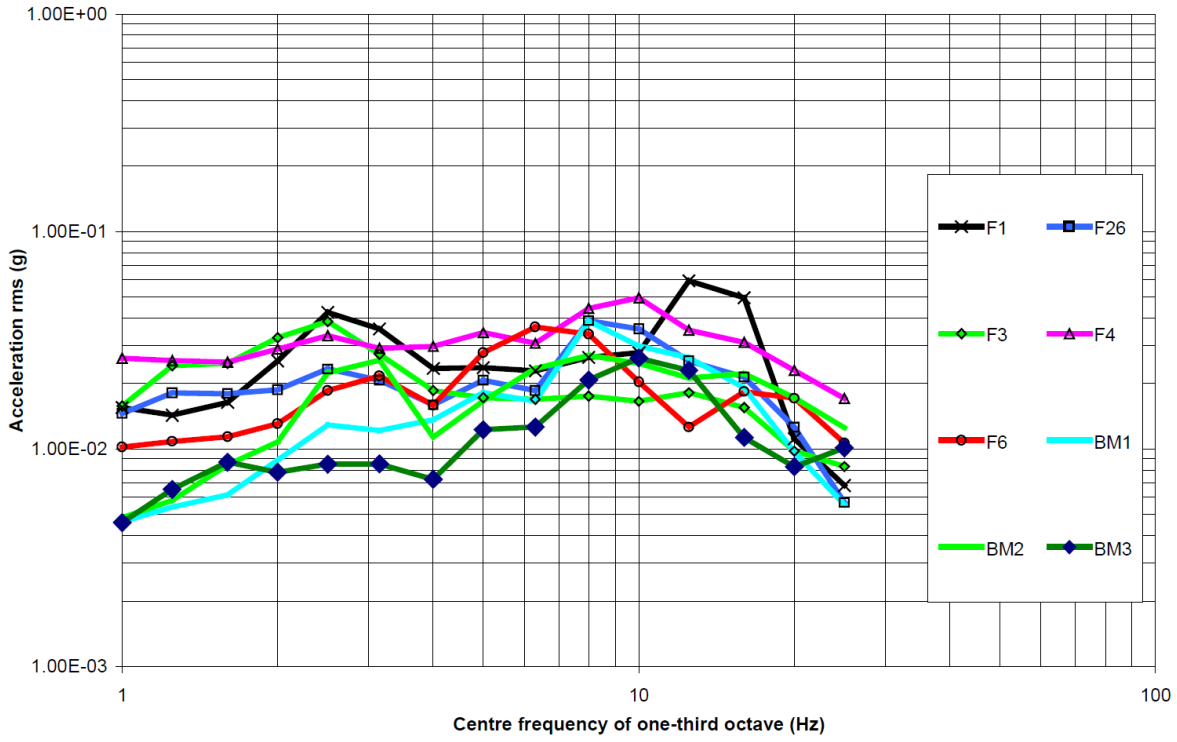

Figure 2.21 Seatpad fore-aft accelerations by vehicles from the report by Sweatman and McFarlane [14]

Literature review shows the necessity of further minimization of vibrations transmitted to the human body in both vertical and longitudinal directions and the benefits of inerters on isolation performance. Inerters are relatively new devices and attracts attention [12]. Through the literature review, no publications investigating the isolation performance of passive inerters on seat or cab suspensions of vehicles could be reached. Moreover, in general, fore-aft isolators of heavy vehicle are generally omitted in the literature. The lack of research with these considerations is aimed to be answered with this thesis.

3. PROPOSED METHOD

The general method proposed by Wong [4], illustrated in Figure 2.1, will primarily serve as the framework for this study. This method comprises three stages. To align with the thesis's objectives, an additional step has been introduced to demonstrate the benefits of an inerter across various suspension configurations and settings. As a result, the proposed method encompasses four steps, which will be elaborated upon in the subsequent sections.

Calculations will be conducted in the frequency domain rather than the time domain, as this approach offers simplicity and facilitates quicker, more accurate results. A limitation of this method is that the vibration results are confined to RMS values. This limitation becomes particularly significant when nonlinear models are employed, where higher vibration levels can be accurately represented, and the running RMS method, as described by ISO-2631:1997, can be applied. To determine the necessity of this approach, one must first ascertain the crest factor, which is the ratio of the peak vibration value to the RMS value of the same vibration data. It is recommended that when the crest factor exceeds 9, the running RMS method should be reported alongside the basic RMS method, as detailed in the relevant section. Despite these considerations, the basic RMS method remains the primary evaluation method, and the frequency domain calculation is widely adopted by many researchers [15], [16], [17], [18].

3.1. Road Irregularity Description

To characterize road imperfections and their impact on vehicle vibrations, power spectral density (PSD) analysis is commonly employed. PSD offers insights into the frequency content and amplitude of road surface roughness, essentially decomposing the road profile into different frequency components and their respective amplitudes. This information is vital for designing suspension systems that effectively dampen vibrations, ensuring a comfortable ride for passengers.

The ISO 8608 standard is frequently utilized to standardize the reporting and obtain a PSD description of road irregularities. This standard offers guidelines for characterizing road surface irregularities using parameters such as road roughness index, roughness wavelength, and amplitude. These parameters can also be employed to synthesize a road profile for time-domain simulation studies. To achieve this, a series of sine waves within the required frequency range can be generated, with amplitudes following the fitted PSD provided by ISO-8608. By introducing random phase angles to each wave and summing them, a random road profile can be synthesized [19]. Figure 3.1 depicts an example of such a synthesized road profile based on the mean values of ISO-8608:2016 Class A road, while Figure 3.2 presents its PSD estimation alongside the target PSD.

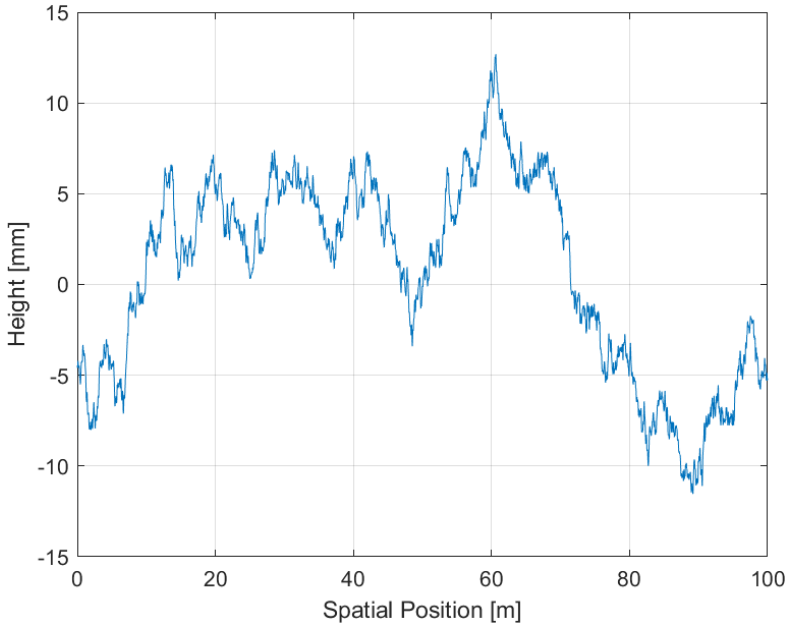

Figure 3.1 Example road profile synthesized according to ISO8608:2016 Class A road mean values

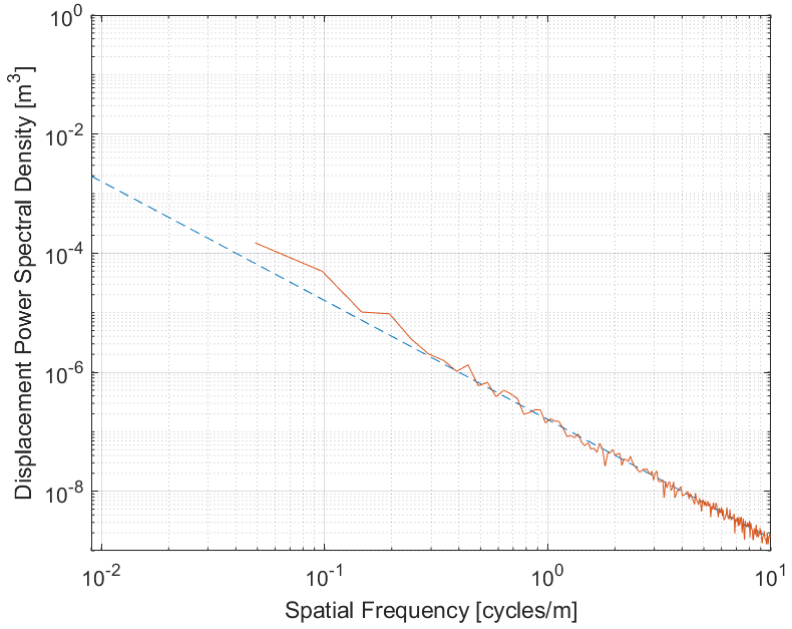

Figure 3.2 Target PSD (dashed line) and PSD of the synthesized road profile in Figure 3.1

In this thesis, however, the analysis will primarily be conducted in the frequency domain, utilizing the ISO-8608:2016 fitted PSD definition provided in Equation 1, and employing Equation 2 for frequency unit conversion when necessary.

3.2. Vehicle Model

In this section, the vehicle model is presented. A 2-axle tractor and 3-axle semi-trailer constitute a commonly used type of heavy vehicle in Europe, as depicted in Figure 3.3. Thus, the model comprises a total of 5 axles. A survey [5] indicates that pitch plane half-car models are frequently used due to their ability to incorporate vertical, pitch, and fore-aft motions. Consequently, a pitch plane half-car model is also employed and adapted for this thesis.

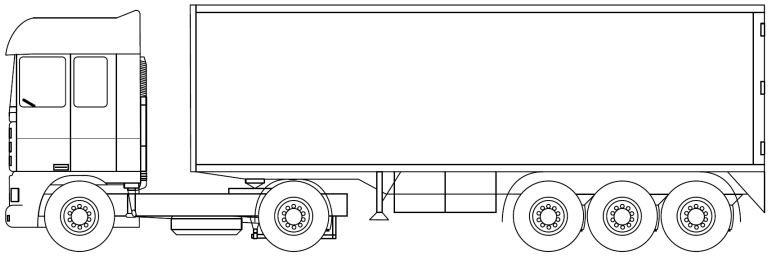

Figure 3.3 2-axle tractor and 3-axle semi-trailer [20]

Evers [20] utilized a complex 44-DOF 2-axle tractor and 3-axle semi-trailer model in his research on active cabin suspension systems for his PhD thesis. While this model incorporates frame torsional compliance, air drag force, and cab air suspension control law, it is too complex to gain insights into the effects of individual components. However, he also provides and utilizes reduced-order versions of this model, including a 9-DOF pitch plane half-car model. In this reduced-order model, the force interaction between the tractor and semi-trailer is simplified by an anonymous force.

In this thesis, the model depicted in Figure 3.4 is employed and it is mainly adapted from Evers' study by reducing the 44 DOF model into pitch plane. Seat and human models are added as described in the following sections. This model consists of 5 axles, a tractor chassis, cab, seat-human, and a semi-trailer. The tractor and semi-trailer are connected via a revolute joint. The cab is connected to the chassis through three suspensions: front fore-aft, front vertical, and rear vertical suspensions, resulting in a 3-DOF cab (bounce, fore-aft, and pitch). The seat-human combination is modeled as a single point mass connected to the cab via two

suspensions: seat vertical and seat fore-aft. It rotates in unison with the cab and possesses 2 degrees of freedom. The tractor chassis offers bounce, fore-aft, and pitch motion freedoms. The trailer has only 1 DOF, which is pitch freedom, and can only rotate about the 5th wheel coupling, modeled as a rigid revolute joint.

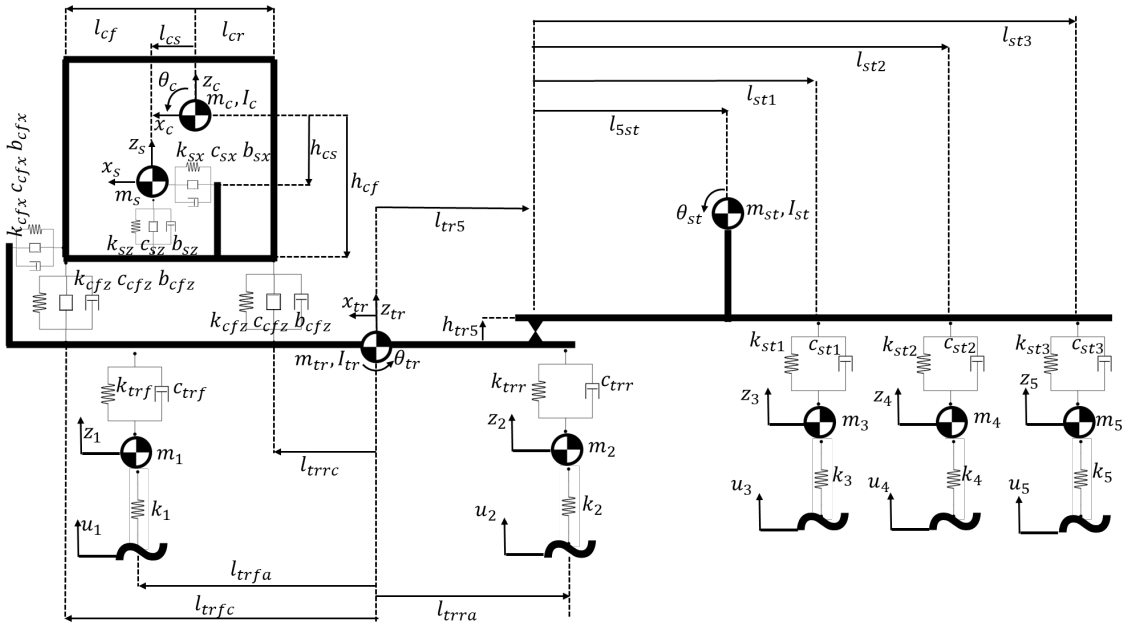

Figure 3.4 14-DOF tractor and semi-trailer model used in this thesis

3.2.1. Seat-Human Model

In the literature, it is observed that seat suspension is often disregarded, and cab accelerations are considered for comfort assessments. While this approach may provide an estimation, ISO-2631 [1] stipulates that measurements should be taken at the vibration-transmitting interface, suggested as the seat pan. To address this measurement requirement, a simulation model should separate the human body and seat. However, this complicates the model significantly. In this thesis, the seat and human masses are combined into a single mass, which is then connected to the cab through seat suspensions. This approach combines two models from studies by Stein et al. [21] and Rakheja et al. [22].

3.2.2. Seat Fore-Aft Suspension

Stein et al. investigated the fore-aft vibration isolation performance of a heavy vehicle seat fore-aft suspension. They utilized a simplified single-DOF model for modeling, and measurements taken from a tractor and semi-trailer combination were used to validate the model. Their model is depicted in Figure 3.5. For this thesis, the model without end stops is employed to maintain linearity. Parameters for two different seats were estimated—one with high friction and the other with a very low friction coefficient. The seat with the lower friction coefficient was adapted, and the friction force was neglected.

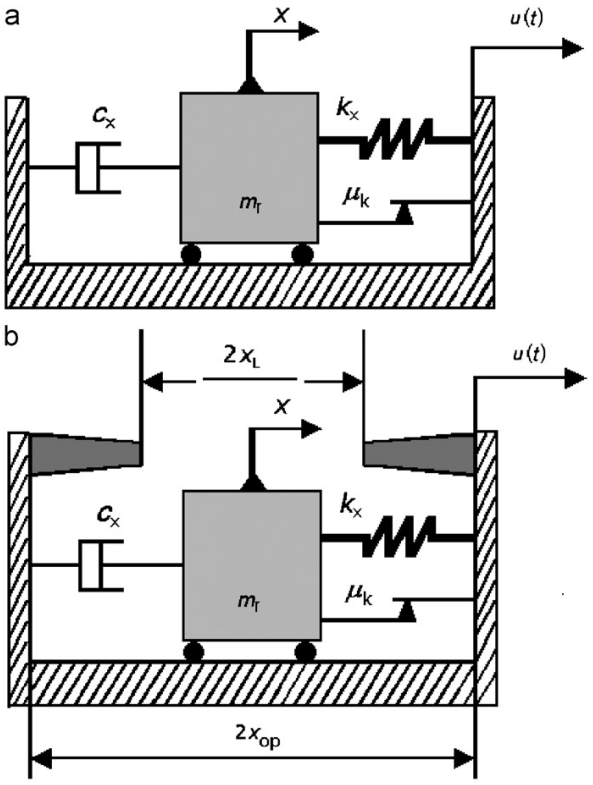

Figure 3.5 Single-DOF seat fore-aft suspension model, without end stops (a) and with end stops (b) [21]

3.2.3. Seat Vertical Suspension

Rakheja et al. investigated the vibration isolation performances of three different seats with vertical suspensions [22]. They utilized a 2-DOF model, as shown in Figure 3.6.

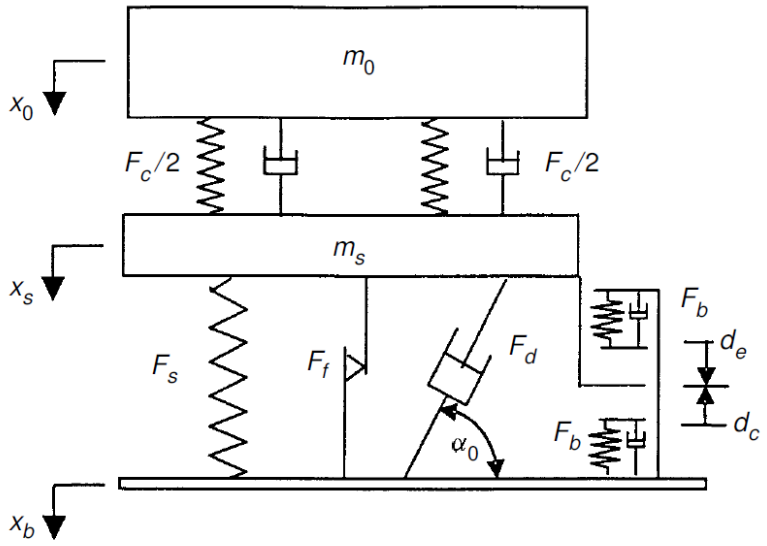

Figure 3.6 2-DOF seat suspension model [22]

As mentioned in Chapter 3.2.1., in this thesis, the seat and human mass are lumped together. To utilize the model provided by Rakheja et al., the seat cushion is simplified to be rigid, essentially merging the seat and human mass. Furthermore, frictional forces, end stops, and damper non-linearity are neglected, and the suspension parameters are linearized. Parameters pertaining to Seat-B in [22] are adapted.

3.2.4. System Parameters

Model parameters are mainly taken from the PhD thesis of Evers [20]. This research provides several models from which a 44 DOF model is the main model and others are reduced order forms. Provided models are validated with extensive field tests. The model used in this is a combination of 3 different submodels; tractor-semitrailer, seat vertical suspension, seat fore-aft model. Their origins and adaptation methods are described in previous sections. The resulting parameters and descriptions are given in the tables 3.1, 3.2 and 3.3.

Table 3.1 Mass property parameters for the model

Symbol	Value	Unit	Description
m_s	105.4	kg	Seat and human mass
m_c	650	kg	Cab mass
m_{tr}	2144	kg	Tractor chassis mass
m_{st}	15170	kg	Semi-trailer chassis mass
m_1	350	kg	Tractor front axle mass
m_2	620	kg	Tractor rear axle mass
m_3	450	kg	Semi-trailer front axle mass
m_4	450	kg	Semi-trailer middle axle mas
m_5	450	kg	Semi-trailer rear axle mass
I_c	550	kgm^2	Cab inertia
I_{tr}	23295	kgm^2	Tractor chassis inertia
I_{st}	100000	kgm^2	Semi-trailer chassis inertia

Table 3.2 Suspension property parameters for the model

Symbol	Value	Unit	Description
k_{sx}	8510	N/m	Seat fore-aft suspension stiffness
k_{sz}	7961.6	N/m	Seat vertical suspension stiffness
k_{cfx}	6000000	N/m	Cab front suspension fore-aft bushing stiffness
k_{cfz}	20000	N/m	Cab front suspension vertical suspension stiffness
k_{crz}	20000	N/m	Cab rear suspension vertical suspension stiffness
k_{trf}	300000	N/m	Tractor front axle suspension stiffness
k_{trr}	600000	N/m	Tractor rear axle suspension stiffness
k_{st1}	400000	N/m	Semi-trailer front axle suspension stiffness
k_{st2}	400000	N/m	Semi-trailer middle axle suspension stiffness
k_{st3}	400000	N/m	Semi-trailer rear axle suspension stiffness
k_1	1200000	N/m	Tractor front tyre stiffness
k_2	2200000	N/m	Tractor rear tyre stiffness
k_3	1200000	N/m	Semi-trailer front tyre stiffness
k_4	1200000	N/m	Semi-trailer middle tyre stiffness
k_5	1200000	N/m	Semi-trailer rear tyre stiffness
c_{sx}	606	Ns/m	Seat fore-aft suspension damper
c_{sz}	788	Ns/m	Seat vertical suspension damper
c_{cfx}	25000	Ns/m	Cab front suspension fore-aft bushing damper
c_{cfz}	7400	Ns/m	Cab front suspension vertical suspension damper
c_{crz}	5900	Ns/m	Cab rear suspension vertical suspension damper
c_{trf}	11000	Ns/m	Tractor front axle suspension damper
c_{trr}	22000	Ns/m	Tractor rear axle suspension damper
c_{st1}	10000	Ns/m	Semi-trailer front axle suspension damper
c_{st2}	10000	Ns/m	Semi-trailer middle axle suspension damper
c_{st3}	10000	Ns/m	Semi-trailer rear axle suspension damper
b_{sx}	0-30	kg	Seat fore-aft suspension inertance
b_{sz}	0-30	kg	Seat vertical suspension inertance
b_{cfx}	0-300	kg	Cab front suspension fore-aft inertance
b_{cfz}	0-300	kg	Cab front suspension vertical inertance
b_{crz}	0-300	kg	Cab rear suspension vertical inertance

Table 3.3 Geometry property parameters for the model

Symbol	Value	Unit	Description
l_{cf}	0.94	m	Distance from Cab CoG to front suspension mount
h_{cf}	-0.97	m	Height from cab CoG to front suspension mount
l_{cr}	-1.14	m	Distance from Cab CoG to rear suspension mount
l_{cs}	0.23	m	Distance from Cab CoG to Seat CoG
h_{cs}	-0.65	m	Height from Cab CoG to Seat CoG
l_{trfa}	1.03	m	Distance from tractor CoG to front axle suspension
l_{trra}	-2.77	m	Distance from tractor CoG to rear axle suspension
l_{trfc}	2.57	m	Distance from tractor CoG to front cab suspension
l_{trrc}	0.49	m	Distance from tractor CoG to rear cab suspension mount
l_{tr5}	-1.82	m	Distance from tractor CoG to 5th wheel coupling
h_{tr5}	0.25	m	Height from tractor CoG to 5th wheel coupling
l_{5st}	-5.61	m	Distance from 5th wheel coupling to trailer CoG
h_{5st}	0.5	m	Height from 5th wheel coupling to trailer CoG
l_{st1}	-6.31	m	Distance from 5th wheel coupling to trailer 1st axle
l_{st2}	-7.62	m	Distance from 5th wheel coupling to trailer 2nd axle
l_{st3}	-8.93	m	Distance from 5th wheel coupling to trailer 3rd

3.2.5. Equations of Motion of the Model

Equations of motion is the set of differential equations which describes a systems response. It can be obtained by newtonian apprroach. This method is easy until the number of DOF, or number of bodies under interaction is low but it gets rapidly tangled with increasing number of equations and prone to mistakes.

Lagrangian method on the other hand is an energy based method which is more suitable with high number of DOF systems. Equation 11 is the general form including energy dissipation.

$$\frac{d}{dt}\left(\frac{\delta T}{\delta \dot{q}_r}\right) - \frac{\delta T}{\delta q_r} + \frac{\delta R}{\delta \dot{q}_r} + \frac{\delta V}{\delta q_r} = F_r, r = 1, 2, 3, ...n \tag{11}$$

where,

T is the kinetic energy,

V is the potential energy,

R is the dissipation function of the system,

F_r is the force applied to the system.

In the model described in section 3.2., there is no external forces acting on the system, rather, there are kinematic inputs which are the road irregularities. Hence, F_r is 0 for all equations. To apply Lagrangian given in the equation 11, the generalized coordinates are considered as in the figure 3.4 and descriptions are given in the table 3.4.

Table 3.4 Generalized coordinates and descriptions

Generalized coordinate	**Description**
x_s	x position of seat-human
z_s	z position of seat-human
x_c	z position of cab
z_c	x position of cab
θ_c	pitch position of cab
x_{tr}	x position of tractor chassis
z_{tr}	z position of tractor chassis
θ_{tr}	pitch position of tractor chassis
θ_{st}	pitch position of trailer chassis
z_1	tractor front axle (axle 1)
z_2	tractor rear axle (axle)
z_3	trailer front axle (axle 3)
z_4	trailer middle axle (axle 4)
z_5	trailer rear axle (axle 5)

The kinetic energy functions of the system can be written as in the equations from 12 to 19.

$$T_{seat-human} = \frac{m_s\,\dot{x}_s^2}{2} + \frac{m_s\,\dot{z}_s^2}{2} \tag{12}$$

$$T_{seatinerter} = \frac{b_{\mathrm{sx}}\left(\dot{x}_c - \dot{x}_s + h_{\mathrm{cs}}\,\dot{\theta}_c\right)^2}{2} + \frac{b_{\mathrm{sz}}\left(\dot{z}_s - \dot{z}_c + l_{\mathrm{cs}}\,\dot{\theta}_c\right)^2}{2} \tag{13}$$

$$T_{cab} = \frac{I_c\,\dot{\theta}_c^2}{2} + \frac{m_c\,\dot{x}_c^2}{2} + \frac{m_c\,\dot{z}_c^2}{2} \tag{14}$$

$$T_{cabinerter} = \frac{b_{\mathrm{cfx}} \left(\dot{x}_c - \dot{x}_{\mathrm{tr}} + h_{\mathrm{cf}}\, \dot{\theta}_c\right)^2}{2} + \frac{b_{\mathrm{cfz}} \left(\dot{z}_c - \dot{z}_{\mathrm{tr}} - l_{\mathrm{cf}}\, \dot{\theta}_c + l_{\mathrm{trfc}}\, \dot{\theta}_{\mathrm{tr}}\right)^2}{2} + \frac{b_{\mathrm{crz}} \left(\dot{z}_c - \dot{z}_{\mathrm{tr}} - l_{\mathrm{cr}}\, \dot{\theta}_c + l_{\mathrm{trrc}}\, \dot{\theta}_{\mathrm{tr}}\right)^2}{2} \tag{15}$$

$$T_{tractor} = \frac{I_{\mathrm{tr}}\, \dot{\theta}_{\mathrm{tr}}^2}{2} + \frac{m_{\mathrm{tr}}\, \dot{x}_{\mathrm{tr}}^2}{2} + \frac{m_{\mathrm{tr}}\, \dot{z}_{\mathrm{tr}}^2}{2} \tag{16}$$

$$T_{semi-trailer} = \frac{m_{\mathrm{st}} \left(\dot{x}_{\mathrm{tr}} + h_{5\mathrm{st}}\, \dot{\theta}_{\mathrm{st}} + h_{\mathrm{tr5}}\, \dot{\theta}_{\mathrm{tr}}\right)^2}{2} + \frac{I_{\mathrm{st}}\, \dot{\theta}_{\mathrm{st}}^2}{2} + \frac{m_{\mathrm{st}} \left(l_{5\mathrm{st}}\, \dot{\theta}_{\mathrm{st}} - \dot{z}_{\mathrm{tr}} + l_{\mathrm{tr5}}\, \dot{\theta}_{\mathrm{tr}}\right)^2}{2} \tag{17}$$

$$T_{axles} = \frac{m_1\, \dot{z}_1^2}{2} + \frac{m_2\, \dot{z}_2^2}{2} + \frac{m_3\, \dot{z}_3^2}{2} + \frac{m_4\, \dot{z}_4^2}{2} + \frac{m_5\, \dot{z}_5^2}{2} \tag{18}$$

$$T_{total} = T_{seat-human} + T_{seatinerter} + T_{cab} + T_{cabinerter} + T_{tractor} + T_{semi-trailer} + T_{axles} \tag{19}$$

The potential energy functions of the system can be written as in the equations from 20 to 25.

$$V_{seat-springs} = \frac{k_{\mathrm{sx}} \left(x_c - x_s + h_{\mathrm{cs}}\, \theta_c\right)^2}{2} + \frac{k_{\mathrm{sz}} \left(z_s - z_c + l_{\mathrm{cs}}\, \theta_c\right)^2}{2} \tag{20}$$

$$V_{cab-springs} = \frac{k_{\mathrm{cfx}} \left(x_c - x_{\mathrm{tr}} + h_{\mathrm{cf}}\, \theta_c\right)^2}{2} + \frac{k_{\mathrm{cfz}} \left(z_c - z_{\mathrm{tr}} - l_{\mathrm{cf}}\, \theta_c + l_{\mathrm{trfc}}\, \theta_{\mathrm{tr}}\right)^2}{2} + \frac{k_{\mathrm{crz}} \left(z_c - z_{\mathrm{tr}} - l_{\mathrm{cr}}\, \theta_c + l_{\mathrm{trrc}}\, \theta_{\mathrm{tr}}\right)^2}{2} \tag{21}$$

$$V_{tractor-springs} = \frac{k_{\mathrm{trf}} \left(z_1 - z_{\mathrm{tr}} + l_{\mathrm{trfa}}\, \theta_{\mathrm{tr}}\right)^2}{2} + \frac{k_{\mathrm{trr}} \left(z_2 - z_{\mathrm{tr}} + l_{\mathrm{trra}}\, \theta_{\mathrm{tr}}\right)^2}{2} \tag{22}$$

$$V_{trailer-springs} = \frac{k_{\mathrm{st1}} \left(z_3 - z_{\mathrm{tr}} + l_{\mathrm{st1}}\, \theta_{\mathrm{st}} + l_{\mathrm{tr5}}\, \theta_{\mathrm{tr}}\right)^2}{2} + \frac{k_{\mathrm{st2}} \left(z_4 - z_{\mathrm{tr}} + l_{\mathrm{st2}}\, \theta_{\mathrm{st}} + l_{\mathrm{tr5}}\, \theta_{\mathrm{tr}}\right)^2}{2} + \frac{k_{\mathrm{st3}} \left(z_5 - z_{\mathrm{tr}} + l_{\mathrm{st3}}\, \theta_{\mathrm{st}} + l_{\mathrm{tr5}}\, \theta_{\mathrm{tr}}\right)^2}{2} \tag{23}$$

$$V_{tyres} = \frac{k_1 \left(u_1 - z_1\right)^2}{2} + \frac{k_2 \left(u_2 - z_2\right)^2}{2} + \frac{k_3 \left(u_3 - z_3\right)^2}{2} + \frac{k_4 \left(u_4 - z_4\right)^2}{2} + \frac{k_5 \left(u_5 - z_5\right)^2}{2} \tag{24}$$

$$V_{total} = V_{seat-prings} + V_{cab-springs} + V_{tractor-springs} + V_{trailer-springs} + V_{tyres} \tag{25}$$

And the dissipation functions are given from equation 26 to equation 30.

$$R_{seat-dampers} = \frac{c_{\mathrm{sx}} \left(\dot{x}_c - \dot{x}_s + h_{\mathrm{cs}}\, \dot{\theta}_c\right)^2}{2} + \frac{c_{\mathrm{sz}} \left(\dot{z}_s - \dot{z}_c + l_{\mathrm{cs}}\, \dot{\theta}_c\right)^2}{2} \tag{26}$$

$$R_{cab-dampers} = \frac{c_{\mathrm{cfx}}\left(\dot{x}_c - \dot{x}_{\mathrm{tr}} + h_{\mathrm{cf}}\,\dot{\theta}_c\right)^2}{2} + \frac{c_{\mathrm{cfz}}\left(\dot{z}_c - \dot{z}_{\mathrm{tr}} - l_{\mathrm{cf}}\,\dot{\theta}_c + l_{\mathrm{trfc}}\,\dot{\theta}_{\mathrm{tr}}\right)^2}{2} + \frac{c_{\mathrm{crz}}\left(\dot{z}_c - \dot{z}_{\mathrm{tr}} - l_{\mathrm{cr}}\,\dot{\theta}_c + l_{\mathrm{trrc}}\,\dot{\theta}_{\mathrm{tr}}\right)^2}{2} \tag{27}$$

$$R_{tractor-dampers} = \frac{c_{\mathrm{trf}}\left(\dot{z}_1 - \dot{z}_{\mathrm{tr}} + l_{\mathrm{trfa}}\,\dot{\theta}_{\mathrm{tr}}\right)^2}{2} + \frac{c_{\mathrm{trr}}\left(\dot{z}_2 - \dot{z}_{\mathrm{tr}} + l_{\mathrm{trra}}\,\dot{\theta}_{\mathrm{tr}}\right)^2}{2} \tag{28}$$

$$R_{trailer-dampers} = \frac{c_{\mathrm{st1}}\left(\dot{z}_3 - \dot{z}_{\mathrm{tr}} + l_{\mathrm{st1}}\,\dot{\theta}_{\mathrm{st}} + l_{\mathrm{tr5}}\,\dot{\theta}_{\mathrm{tr}}\right)^2}{2} + \frac{c_{\mathrm{st2}}\left(\dot{z}_4 - \dot{z}_{\mathrm{tr}} + l_{\mathrm{st2}}\,\dot{\theta}_{\mathrm{st}} + l_{\mathrm{tr5}}\,\dot{\theta}_{\mathrm{tr}}\right)^2}{2} + \frac{c_{\mathrm{st3}}\left(\dot{z}_5 - \dot{z}_{\mathrm{tr}} + l_{\mathrm{st3}}\,\dot{\theta}_{\mathrm{st}} + l_{\mathrm{tr5}}\,\dot{\theta}_{\mathrm{tr}}\right)^2}{2} \tag{29}$$

$$R_{total} = R_{seat-dampers} + R_{cab-dampers} + R_{tractor-dampers} + R_{trailer-dampers} \tag{30}$$

These energy functions are inserted into the Lagrangian formulation to obtain the equations of motion of the vehicle model. For this the generalized coordinates, q, is constructed by following the table 3.4 and given in the equation 31.

$$q' = \begin{pmatrix} x_s & z_s & x_c & z_c & \theta_c & x_{\mathrm{tr}} & z_{\mathrm{tr}} & \theta_{\mathrm{tr}} & \theta_{\mathrm{st}} & z_1 & z_2 & z_3 & z_4 & z_5 \end{pmatrix} \tag{31}$$

The resulting equations of motion is given in the equations 32 - 45.

$$\ddot{x}_s\ (b_{\mathrm{sx}} + m_s) = \\ b_{\mathrm{sx}}\,\ddot{x}_c + c_{\mathrm{sx}}\,\dot{x}_c - c_{\mathrm{sx}}\,\dot{x}_s + k_{\mathrm{sx}}\,x_c - k_{\mathrm{sx}}\,x_s + b_{\mathrm{sx}}\,h_{\mathrm{cs}}\,\ddot{\theta}_c + c_{\mathrm{sx}}\,h_{\mathrm{cs}}\,\dot{\theta}_c + h_{\mathrm{cs}}\,k_{\mathrm{sx}}\,\theta_c \tag{32}$$

$$\ddot{z}_s\ (b_{\mathrm{sz}} + m_s) = \\ b_{\mathrm{sz}}\,\ddot{z}_c + c_{\mathrm{sz}}\,\dot{z}_c - c_{\mathrm{sz}}\,\dot{z}_s + k_{\mathrm{sz}}\,z_c - k_{\mathrm{sz}}\,z_s - b_{\mathrm{sz}}\,l_{\mathrm{cs}}\,\ddot{\theta}_c - c_{\mathrm{sz}}\,l_{\mathrm{cs}}\,\dot{\theta}_c - k_{\mathrm{sz}}\,l_{\mathrm{cs}}\,\theta_c \tag{33}$$

$$\begin{aligned}\ddot{x}_c\ (b_{\mathrm{cfx}} + b_{\mathrm{sx}} + m_c) = b_{\mathrm{cfx}}\,\ddot{x}_{\mathrm{tr}} + b_{\mathrm{sx}}\,\ddot{x}_s - c_{\mathrm{cfx}}\,\dot{x}_c + c_{\mathrm{cfx}}\,\dot{x}_{\mathrm{tr}} - c_{\mathrm{sx}}\,\dot{x}_c + \\ c_{\mathrm{sx}}\,\dot{x}_s - k_{\mathrm{cfx}}\,x_c - k_{\mathrm{sx}}\,x_c + k_{\mathrm{cfx}}\,x_{\mathrm{tr}} + k_{\mathrm{sx}}\,x_s - b_{\mathrm{cfx}}\,h_{\mathrm{cf}}\,\ddot{\theta}_c - b_{\mathrm{sx}}\,h_{\mathrm{cs}}\,\ddot{\theta}_c - \\ c_{\mathrm{cfx}}\,h_{\mathrm{cf}}\,\dot{\theta}_c - c_{\mathrm{sx}}\,h_{\mathrm{cs}}\,\dot{\theta}_c - h_{\mathrm{cf}}\,k_{\mathrm{cfx}}\,\theta_c - h_{\mathrm{cs}}\,k_{\mathrm{sx}}\,\theta_c\end{aligned} \tag{34}$$

$$\begin{aligned}\ddot{z}_c\ (b_{\mathrm{cfz}} + b_{\mathrm{crz}} + b_{\mathrm{sz}} + m_c) = b_{\mathrm{cfz}}\,\ddot{z}_{\mathrm{tr}} + b_{\mathrm{crz}}\,\ddot{z}_{\mathrm{tr}} + b_{\mathrm{sz}}\,\ddot{z}_s - c_{\mathrm{cfz}}\,\dot{z}_c - \\ c_{\mathrm{crz}}\,\dot{z}_c + c_{\mathrm{cfz}}\,\dot{z}_{\mathrm{tr}} + c_{\mathrm{crz}}\,\dot{z}_{\mathrm{tr}} - c_{\mathrm{sz}}\,\dot{z}_c + \\ c_{\mathrm{sz}}\,\dot{z}_s - k_{\mathrm{cfz}}\,z_c - k_{\mathrm{crz}}\,z_c - k_{\mathrm{sz}}\,z_c + k_{\mathrm{cfz}}\,z_{\mathrm{tr}} + k_{\mathrm{crz}}\,z_{\mathrm{tr}} + k_{\mathrm{sz}}\,z_s + \\ b_{\mathrm{cfz}}\,l_{\mathrm{cf}}\,\ddot{\theta}_c + b_{\mathrm{crz}}\,l_{\mathrm{cr}}\,\ddot{\theta}_c + b_{\mathrm{sz}}\,l_{\mathrm{cs}}\,\ddot{\theta}_c - b_{\mathrm{cfz}}\,l_{\mathrm{trfc}}\,\ddot{\theta}_{\mathrm{tr}} - b_{\mathrm{crz}}\,l_{\mathrm{trrc}}\,\ddot{\theta}_{\mathrm{tr}} + \\ c_{\mathrm{cfz}}\,l_{\mathrm{cf}}\,\dot{\theta}_c + c_{\mathrm{crz}}\,l_{\mathrm{cr}}\,\dot{\theta}_c + c_{\mathrm{sz}}\,l_{\mathrm{cs}}\,\dot{\theta}_c - c_{\mathrm{cfz}}\,l_{\mathrm{trfc}}\,\dot{\theta}_{\mathrm{tr}} - \\ c_{\mathrm{crz}}\,l_{\mathrm{trrc}}\,\dot{\theta}_{\mathrm{tr}} + k_{\mathrm{cfz}}\,l_{\mathrm{cf}}\,\theta_c + k_{\mathrm{crz}}\,l_{\mathrm{cr}}\,\theta_c + k_{\mathrm{sz}}\,l_{\mathrm{cs}}\,\theta_c - k_{\mathrm{cfz}}\,l_{\mathrm{trfc}}\,\theta_{\mathrm{tr}} - k_{\mathrm{crz}}\,l_{\mathrm{trrc}}\,\theta_{\mathrm{tr}}\end{aligned} \tag{35}$$

$$\ddot{\theta}_c \left(b_{\mathrm{cfx}} {h_{\mathrm{cf}}}^2 + b_{\mathrm{sx}} {h_{\mathrm{cs}}}^2 + b_{\mathrm{cfz}} {l_{\mathrm{cf}}}^2 + b_{\mathrm{crz}} {l_{\mathrm{cr}}}^2 + b_{\mathrm{sz}} {l_{\mathrm{cs}}}^2 + I_c\right) = b_{\mathrm{cfx}} h_{\mathrm{cf}} \ddot{x}_{\mathrm{tr}} -$$
$$c_{\mathrm{crz}} {l_{\mathrm{cr}}}^2 \dot{\theta}_c - c_{\mathrm{sz}} {l_{\mathrm{cs}}}^2 \dot{\theta}_c - {h_{\mathrm{cf}}}^2 k_{\mathrm{cfx}} \theta_c - {h_{\mathrm{cs}}}^2 k_{\mathrm{sx}} \theta_c - k_{\mathrm{cfz}} {l_{\mathrm{cf}}}^2 \theta_c - k_{\mathrm{crz}} {l_{\mathrm{cr}}}^2 \theta_c -$$
$$k_{\mathrm{sz}} {l_{\mathrm{cs}}}^2 \theta_c - b_{\mathrm{cfx}} h_{\mathrm{cf}} \ddot{x}_c - c_{\mathrm{cfz}} {l_{\mathrm{cf}}}^2 \dot{\theta}_c - b_{\mathrm{sx}} h_{\mathrm{cs}} \ddot{x}_c + b_{\mathrm{sx}} h_{\mathrm{cs}} \ddot{x}_s - c_{\mathrm{cfx}} h_{\mathrm{cf}} \dot{x}_c +$$
$$c_{\mathrm{cfx}} h_{\mathrm{cf}} \dot{x}_{\mathrm{tr}} - c_{\mathrm{sx}} h_{\mathrm{cs}} \dot{x}_c + c_{\mathrm{sx}} h_{\mathrm{cs}} \dot{x}_s + b_{\mathrm{cfz}} l_{\mathrm{cf}} \ddot{z}_c + b_{\mathrm{crz}} l_{\mathrm{cr}} \ddot{z}_c - b_{\mathrm{cfz}} l_{\mathrm{cf}} \ddot{z}_{\mathrm{tr}} -$$
$$b_{\mathrm{crz}} l_{\mathrm{cr}} \ddot{z}_{\mathrm{tr}} + b_{\mathrm{sz}} l_{\mathrm{cs}} \ddot{z}_c - b_{\mathrm{sz}} l_{\mathrm{cs}} \ddot{z}_s + c_{\mathrm{cfz}} l_{\mathrm{cf}} \dot{z}_c + c_{\mathrm{crz}} l_{\mathrm{cr}} \dot{z}_c - c_{\mathrm{cfz}} l_{\mathrm{cf}} \dot{z}_{\mathrm{tr}} - \tag{36}$$
$$c_{\mathrm{crz}} l_{\mathrm{cr}} \dot{z}_{\mathrm{tr}} + c_{\mathrm{sz}} l_{\mathrm{cs}} \dot{z}_c - c_{\mathrm{sz}} l_{\mathrm{cs}} \dot{z}_s - h_{\mathrm{cf}} k_{\mathrm{cfx}} x_c - h_{\mathrm{cs}} k_{\mathrm{sx}} x_c + h_{\mathrm{cf}} k_{\mathrm{cfx}} x_{\mathrm{tr}} +$$
$$h_{\mathrm{cs}} k_{\mathrm{sx}} x_s + k_{\mathrm{cfz}} l_{\mathrm{cf}} z_c + k_{\mathrm{crz}} l_{\mathrm{cr}} z_c + k_{\mathrm{sz}} l_{\mathrm{cs}} z_c - k_{\mathrm{cfz}} l_{\mathrm{cf}} z_{\mathrm{tr}} - k_{\mathrm{crz}} l_{\mathrm{cr}} z_{\mathrm{tr}} -$$
$$k_{\mathrm{sz}} l_{\mathrm{cs}} z_s - c_{\mathrm{cfx}} {h_{\mathrm{cf}}}^2 \dot{\theta}_c - c_{\mathrm{sx}} {h_{\mathrm{cs}}}^2 \dot{\theta}_c + b_{\mathrm{cfz}} l_{\mathrm{cf}} l_{\mathrm{trfc}} \ddot{\theta}_{\mathrm{tr}} + b_{\mathrm{crz}} l_{\mathrm{cr}} l_{\mathrm{trrc}} \ddot{\theta}_{\mathrm{tr}} +$$
$$c_{\mathrm{cfz}} l_{\mathrm{cf}} l_{\mathrm{trfc}} \dot{\theta}_{\mathrm{tr}} + c_{\mathrm{crz}} l_{\mathrm{cr}} l_{\mathrm{trrc}} \dot{\theta}_{\mathrm{tr}} + k_{\mathrm{cfz}} l_{\mathrm{cf}} l_{\mathrm{trfc}} \theta_{\mathrm{tr}} + k_{\mathrm{crz}} l_{\mathrm{cr}} l_{\mathrm{trrc}} \theta_{\mathrm{tr}}$$

$$\ddot{x}_{\mathrm{tr}} \left(b_{\mathrm{cfx}} + m_{\mathrm{st}} + m_{\mathrm{tr}}\right) = b_{\mathrm{cfx}} \ddot{x}_c + c_{\mathrm{cfx}} \dot{x}_c - c_{\mathrm{cfx}} \dot{x}_{\mathrm{tr}} + k_{\mathrm{cfx}} x_c -$$
$$k_{\mathrm{cfx}} x_{\mathrm{tr}} + b_{\mathrm{cfx}} h_{\mathrm{cf}} \ddot{\theta}_c + c_{\mathrm{cfx}} h_{\mathrm{cf}} \dot{\theta}_c + h_{\mathrm{cf}} k_{\mathrm{cfx}} \theta_c - h_{5\mathrm{st}} m_{\mathrm{st}} \ddot{\theta}_{\mathrm{st}} - h_{\mathrm{tr5}} m_{\mathrm{st}} \ddot{\theta}_{\mathrm{tr}} \tag{37}$$

$$\ddot{z}_{\mathrm{tr}} \left(b_{\mathrm{cfz}} + b_{\mathrm{crz}} + m_{\mathrm{st}} + m_{\mathrm{tr}}\right) = b_{\mathrm{cfz}} \ddot{z}_c + b_{\mathrm{crz}} \ddot{z}_c + c_{\mathrm{cfz}} \dot{z}_c + c_{\mathrm{crz}} \dot{z}_c - c_{\mathrm{cfz}} \dot{z}_{\mathrm{tr}} -$$
$$c_{\mathrm{crz}} \dot{z}_{\mathrm{tr}} + c_{\mathrm{st1}} \dot{z}_3 + c_{\mathrm{st2}} \dot{z}_4 + c_{\mathrm{st3}} \dot{z}_5 - c_{\mathrm{st1}} \dot{z}_{\mathrm{tr}} - c_{\mathrm{st2}} \dot{z}_{\mathrm{tr}} - c_{\mathrm{st3}} \dot{z}_{\mathrm{tr}} + c_{\mathrm{trf}} \dot{z}_1 +$$
$$c_{\mathrm{trr}} \dot{z}_2 - c_{\mathrm{trf}} \dot{z}_{\mathrm{tr}} - c_{\mathrm{trr}} \dot{z}_{\mathrm{tr}} + k_{\mathrm{st1}} z_3 + k_{\mathrm{st2}} z_4 + k_{\mathrm{st3}} z_5 + k_{\mathrm{trf}} z_1 + k_{\mathrm{trr}} z_2 +$$
$$k_{\mathrm{cfz}} z_c + k_{\mathrm{crz}} z_c - k_{\mathrm{cfz}} z_{\mathrm{tr}} - k_{\mathrm{crz}} z_{\mathrm{tr}} - k_{\mathrm{st1}} z_{\mathrm{tr}} - k_{\mathrm{st2}} z_{\mathrm{tr}} - k_{\mathrm{st3}} z_{\mathrm{tr}} - k_{\mathrm{trf}} z_{\mathrm{tr}} - k_{\mathrm{trr}} z_{\mathrm{tr}} -$$
$$b_{\mathrm{cfz}} l_{\mathrm{cf}} \ddot{\theta}_c - b_{\mathrm{crz}} l_{\mathrm{cr}} \ddot{\theta}_c + b_{\mathrm{cfz}} l_{\mathrm{trfc}} \ddot{\theta}_{\mathrm{tr}} + b_{\mathrm{crz}} l_{\mathrm{trrc}} \ddot{\theta}_{\mathrm{tr}} - c_{\mathrm{cfz}} l_{\mathrm{cf}} \dot{\theta}_c - c_{\mathrm{crz}} l_{\mathrm{cr}} \dot{\theta}_c +$$
$$c_{\mathrm{cfz}} l_{\mathrm{trfc}} \dot{\theta}_{\mathrm{tr}} + c_{\mathrm{crz}} l_{\mathrm{trrc}} \dot{\theta}_{\mathrm{tr}} + c_{\mathrm{st1}} l_{\mathrm{st1}} \dot{\theta}_{\mathrm{st}} + c_{\mathrm{st2}} l_{\mathrm{st2}} \dot{\theta}_{\mathrm{st}} + c_{\mathrm{st3}} l_{\mathrm{st3}} \dot{\theta}_{\mathrm{st}} + \tag{38}$$
$$c_{\mathrm{st1}} l_{\mathrm{tr5}} \dot{\theta}_{\mathrm{tr}} + c_{\mathrm{st2}} l_{\mathrm{tr5}} \dot{\theta}_{\mathrm{tr}} + c_{\mathrm{st3}} l_{\mathrm{tr5}} \dot{\theta}_{\mathrm{tr}} + c_{\mathrm{trf}} l_{\mathrm{trfa}} \dot{\theta}_{\mathrm{tr}} + c_{\mathrm{trr}} l_{\mathrm{trra}} \dot{\theta}_{\mathrm{tr}} -$$
$$k_{\mathrm{cfz}} l_{\mathrm{cf}} \theta_c - k_{\mathrm{crz}} l_{\mathrm{cr}} \theta_c + k_{\mathrm{cfz}} l_{\mathrm{trfc}} \theta_{\mathrm{tr}} +$$
$$k_{\mathrm{crz}} l_{\mathrm{trrc}} \theta_{\mathrm{tr}} + k_{\mathrm{st1}} l_{\mathrm{st1}} \theta_{\mathrm{st}} + k_{\mathrm{st2}} l_{\mathrm{st2}} \theta_{\mathrm{st}} + k_{\mathrm{st3}} l_{\mathrm{st3}} \theta_{\mathrm{st}} + k_{\mathrm{st1}} l_{\mathrm{tr5}} \theta_{\mathrm{tr}} +$$
$$k_{\mathrm{st2}} l_{\mathrm{tr5}} \theta_{\mathrm{tr}} + k_{\mathrm{st3}} l_{\mathrm{tr5}} \theta_{\mathrm{tr}} + k_{\mathrm{trf}} l_{\mathrm{trfa}} \theta_{\mathrm{tr}} + k_{\mathrm{trr}} l_{\mathrm{trra}} \theta_{\mathrm{tr}} + l_{5\mathrm{st}} m_{\mathrm{st}} \ddot{\theta}_{\mathrm{st}} + l_{\mathrm{tr5}} m_{\mathrm{st}} \ddot{\theta}_{\mathrm{tr}}$$

$$\ddot{\theta}_{\mathrm{tr}}\left(m_{\mathrm{st}}\,{h_{\mathrm{tr5}}}^2+m_{\mathrm{st}}\,{l_{\mathrm{tr5}}}^2+b_{\mathrm{cfz}}\,{l_{\mathrm{trfc}}}^2+b_{\mathrm{crz}}\,{l_{\mathrm{trrc}}}^2+I_{\mathrm{tr}}\right)=b_{\mathrm{cfz}}\,l_{\mathrm{trfc}}\,\ddot{z}_{\mathrm{tr}}-c_{\mathrm{crz}}\,{l_{\mathrm{trrc}}}^2\,\dot{\theta}_{\mathrm{tr}}-$$
$$c_{\mathrm{st1}}\,{l_{\mathrm{tr5}}}^2\,\dot{\theta}_{\mathrm{tr}}-c_{\mathrm{st2}}\,{l_{\mathrm{tr5}}}^2\,\dot{\theta}_{\mathrm{tr}}-c_{\mathrm{st3}}\,{l_{\mathrm{tr5}}}^2\,\dot{\theta}_{\mathrm{tr}}-c_{\mathrm{trf}}\,{l_{\mathrm{trfa}}}^2\,\dot{\theta}_{\mathrm{tr}}-c_{\mathrm{trr}}\,{l_{\mathrm{trra}}}^2\,\dot{\theta}_{\mathrm{tr}}-$$
$$k_{\mathrm{cfz}}\,{l_{\mathrm{trfc}}}^2\,\theta_{\mathrm{tr}}-k_{\mathrm{crz}}\,{l_{\mathrm{trrc}}}^2\,\theta_{\mathrm{tr}}-k_{\mathrm{st1}}\,{l_{\mathrm{tr5}}}^2\,\theta_{\mathrm{tr}}-k_{\mathrm{st2}}\,{l_{\mathrm{tr5}}}^2\,\theta_{\mathrm{tr}}-k_{\mathrm{st3}}\,{l_{\mathrm{tr5}}}^2\,\theta_{\mathrm{tr}}-$$
$$k_{\mathrm{trf}}\,{l_{\mathrm{trfa}}}^2\,\theta_{\mathrm{tr}}-k_{\mathrm{trr}}\,{l_{\mathrm{trra}}}^2\,\theta_{\mathrm{tr}}-b_{\mathrm{cfz}}\,l_{\mathrm{trfc}}\,\ddot{z}_c-b_{\mathrm{crz}}\,l_{\mathrm{trrc}}\,\ddot{z}_c-c_{\mathrm{cfz}}\,{l_{\mathrm{trfc}}}^2\,\dot{\theta}_{\mathrm{tr}}+$$
$$b_{\mathrm{crz}}\,l_{\mathrm{trrc}}\,\ddot{z}_{\mathrm{tr}}-c_{\mathrm{cfz}}\,l_{\mathrm{trfc}}\,\dot{z}_c-c_{\mathrm{crz}}\,l_{\mathrm{trrc}}\,\dot{z}_c+c_{\mathrm{cfz}}\,l_{\mathrm{trfc}}\,\dot{z}_{\mathrm{tr}}+c_{\mathrm{crz}}\,l_{\mathrm{trrc}}\,\dot{z}_{\mathrm{tr}}-c_{\mathrm{st1}}\,l_{\mathrm{tr5}}\,\dot{z}_3-$$
$$c_{\mathrm{st2}}\,l_{\mathrm{tr5}}\,\dot{z}_4-c_{\mathrm{st3}}\,l_{\mathrm{tr5}}\,\dot{z}_5+c_{\mathrm{st1}}\,l_{\mathrm{tr5}}\,\dot{z}_{\mathrm{tr}}+c_{\mathrm{st2}}\,l_{\mathrm{tr5}}\,\dot{z}_{\mathrm{tr}}+c_{\mathrm{st3}}\,l_{\mathrm{tr5}}\,\dot{z}_{\mathrm{tr}}-c_{\mathrm{trf}}\,l_{\mathrm{trfa}}\,\dot{z}_1-$$
$$c_{\mathrm{trr}}\,l_{\mathrm{trra}}\,\dot{z}_2+c_{\mathrm{trf}}\,l_{\mathrm{trfa}}\,\dot{z}_{\mathrm{tr}}+c_{\mathrm{trr}}\,l_{\mathrm{trra}}\,\dot{z}_{\mathrm{tr}}-h_{\mathrm{tr5}}\,m_{\mathrm{st}}\,\ddot{x}_{\mathrm{tr}}-k_{\mathrm{st1}}\,l_{\mathrm{tr5}}\,z_3- \tag{39}$$
$$k_{\mathrm{st2}}\,l_{\mathrm{tr5}}\,z_4-k_{\mathrm{st3}}\,l_{\mathrm{tr5}}\,z_5-k_{\mathrm{trf}}\,l_{\mathrm{trfa}}\,z_1-k_{\mathrm{trr}}\,l_{\mathrm{trra}}\,z_2-k_{\mathrm{cfz}}\,l_{\mathrm{trfc}}\,z_c-$$
$$k_{\mathrm{crz}}\,l_{\mathrm{trrc}}\,z_c+k_{\mathrm{cfz}}\,l_{\mathrm{trfc}}\,z_{\mathrm{tr}}+k_{\mathrm{crz}}\,l_{\mathrm{trrc}}\,z_{\mathrm{tr}}+k_{\mathrm{st1}}\,l_{\mathrm{tr5}}\,z_{\mathrm{tr}}+k_{\mathrm{st2}}\,l_{\mathrm{tr5}}\,z_{\mathrm{tr}}+$$
$$k_{\mathrm{st3}}\,l_{\mathrm{tr5}}\,z_{\mathrm{tr}}+k_{\mathrm{trf}}\,l_{\mathrm{trfa}}\,z_{\mathrm{tr}}+k_{\mathrm{trr}}\,l_{\mathrm{trra}}\,z_{\mathrm{tr}}+l_{\mathrm{tr5}}\,m_{\mathrm{st}}\,\ddot{z}_{\mathrm{tr}}+b_{\mathrm{cfz}}\,l_{\mathrm{cf}}\,l_{\mathrm{trfc}}\,\ddot{\theta}_c+$$
$$b_{\mathrm{crz}}\,l_{\mathrm{cr}}\,l_{\mathrm{trrc}}\,\ddot{\theta}_c+c_{\mathrm{cfz}}\,l_{\mathrm{cf}}\,l_{\mathrm{trfc}}\,\dot{\theta}_c+c_{\mathrm{crz}}\,l_{\mathrm{cr}}\,l_{\mathrm{trrc}}\,\dot{\theta}_c-c_{\mathrm{st1}}\,l_{\mathrm{st1}}\,l_{\mathrm{tr5}}\,\dot{\theta}_{\mathrm{st}}-c_{\mathrm{st2}}\,l_{\mathrm{st2}}\,l_{\mathrm{tr5}}\,\dot{\theta}_{\mathrm{st}}-$$
$$c_{\mathrm{st3}}\,l_{\mathrm{st3}}\,l_{\mathrm{tr5}}\,\dot{\theta}_{\mathrm{st}}-h_{\mathrm{5st}}\,h_{\mathrm{tr5}}\,m_{\mathrm{st}}\,\ddot{\theta}_{\mathrm{st}}+k_{\mathrm{cfz}}\,l_{\mathrm{cf}}\,l_{\mathrm{trfc}}\,\theta_c+k_{\mathrm{crz}}\,l_{\mathrm{cr}}\,l_{\mathrm{trrc}}\,\theta_c-k_{\mathrm{st1}}\,l_{\mathrm{st1}}\,l_{\mathrm{tr5}}\,\theta_{\mathrm{st}}-$$
$$k_{\mathrm{st2}}\,l_{\mathrm{st2}}\,l_{\mathrm{tr5}}\,\theta_{\mathrm{st}}-k_{\mathrm{st3}}\,l_{\mathrm{st3}}\,l_{\mathrm{tr5}}\,\theta_{\mathrm{st}}-l_{\mathrm{5st}}\,l_{\mathrm{tr5}}\,m_{\mathrm{st}}\,\ddot{\theta}_{\mathrm{st}}$$

$$\ddot{\theta}_{\mathrm{st}}\left(m_{\mathrm{st}}\,{h_{\mathrm{5st}}}^2+m_{\mathrm{st}}\,{l_{\mathrm{5st}}}^2+I_{\mathrm{st}}\right)=c_{\mathrm{st1}}\,l_{\mathrm{st1}}\,\dot{z}_{\mathrm{tr}}-c_{\mathrm{st2}}\,{l_{\mathrm{st2}}}^2\,\dot{\theta}_{\mathrm{st}}-c_{\mathrm{st3}}\,{l_{\mathrm{st3}}}^2\,\dot{\theta}_{\mathrm{st}}-$$
$$k_{\mathrm{st1}}\,{l_{\mathrm{st1}}}^2\,\theta_{\mathrm{st}}-k_{\mathrm{st2}}\,{l_{\mathrm{st2}}}^2\,\theta_{\mathrm{st}}-k_{\mathrm{st3}}\,{l_{\mathrm{st3}}}^2\,\theta_{\mathrm{st}}-c_{\mathrm{st1}}\,l_{\mathrm{st1}}\,\dot{z}_3-c_{\mathrm{st2}}\,l_{\mathrm{st2}}\,\dot{z}_4-$$
$$c_{\mathrm{st3}}\,l_{\mathrm{st3}}\,\dot{z}_5-c_{\mathrm{st1}}\,{l_{\mathrm{st1}}}^2\,\dot{\theta}_{\mathrm{st}}+c_{\mathrm{st2}}\,l_{\mathrm{st2}}\,\dot{z}_{\mathrm{tr}}+c_{\mathrm{st3}}\,l_{\mathrm{st3}}\,\dot{z}_{\mathrm{tr}}-h_{\mathrm{5st}}\,m_{\mathrm{st}}\,\ddot{x}_{\mathrm{tr}}- \tag{40}$$
$$k_{\mathrm{st1}}\,l_{\mathrm{st1}}\,z_3-k_{\mathrm{st2}}\,l_{\mathrm{st2}}\,z_4-k_{\mathrm{st3}}\,l_{\mathrm{st3}}\,z_5+k_{\mathrm{st1}}\,l_{\mathrm{st1}}\,z_{\mathrm{tr}}+k_{\mathrm{st2}}\,l_{\mathrm{st2}}\,z_{\mathrm{tr}}+k_{\mathrm{st3}}\,l_{\mathrm{st3}}\,z_{\mathrm{tr}}+$$
$$l_{\mathrm{5st}}\,m_{\mathrm{st}}\,\ddot{z}_{\mathrm{tr}}-c_{\mathrm{st1}}\,l_{\mathrm{st1}}\,l_{\mathrm{tr5}}\,\dot{\theta}_{\mathrm{tr}}-c_{\mathrm{st2}}\,l_{\mathrm{st2}}\,l_{\mathrm{tr5}}\,\dot{\theta}_{\mathrm{tr}}-c_{\mathrm{st3}}\,l_{\mathrm{st3}}\,l_{\mathrm{tr5}}\,\dot{\theta}_{\mathrm{tr}}-h_{\mathrm{5st}}\,h_{\mathrm{tr5}}\,m_{\mathrm{st}}\,\ddot{\theta}_{\mathrm{tr}}-$$
$$k_{\mathrm{st1}}\,l_{\mathrm{st1}}\,l_{\mathrm{tr5}}\,\theta_{\mathrm{tr}}-k_{\mathrm{st2}}\,l_{\mathrm{st2}}\,l_{\mathrm{tr5}}\,\theta_{\mathrm{tr}}-k_{\mathrm{st3}}\,l_{\mathrm{st3}}\,l_{\mathrm{tr5}}\,\theta_{\mathrm{tr}}-l_{\mathrm{5st}}\,l_{\mathrm{tr5}}\,m_{\mathrm{st}}\,\ddot{\theta}_{\mathrm{tr}}$$

$$m_1\,\ddot{z}_1=c_{\mathrm{trf}}\,\dot{z}_{\mathrm{tr}}-c_{\mathrm{trf}}\,\dot{z}_1+k_1\,u_1-k_1\,z_1-k_{\mathrm{trf}}\,z_1+ \tag{41}$$
$$k_{\mathrm{trf}}\,z_{\mathrm{tr}}-c_{\mathrm{trf}}\,l_{\mathrm{trfa}}\,\dot{\theta}_{\mathrm{tr}}-k_{\mathrm{trf}}\,l_{\mathrm{trfa}}\,\theta_{\mathrm{tr}}$$

$$m_2\,\ddot{z}_2 = c_{\mathrm{trr}}\,\dot{z}_{\mathrm{tr}} - c_{\mathrm{trr}}\,\dot{z}_2 + k_2\,u_2 - k_2\,z_2 - k_{\mathrm{trr}}\,z_2 + k_{\mathrm{trr}}\,z_{\mathrm{tr}} - c_{\mathrm{trr}}\,l_{\mathrm{trra}}\,\dot{\theta}_{\mathrm{tr}} - k_{\mathrm{trr}}\,l_{\mathrm{trra}}\,\theta_{\mathrm{tr}} \tag{42}$$

$$m_3\,\ddot{z}_3 = c_{\mathrm{st1}}\,\dot{z}_{\mathrm{tr}} - c_{\mathrm{st1}}\,\dot{z}_3 + k_3\,u_3 - k_3\,z_3 - k_{\mathrm{st1}}\,z_3 + k_{\mathrm{st1}}\,z_{\mathrm{tr}} - c_{\mathrm{st1}}\,l_{\mathrm{st1}}\,\dot{\theta}_{\mathrm{st}} - c_{\mathrm{st1}}\,l_{\mathrm{tr5}}\,\dot{\theta}_{\mathrm{tr}} - k_{\mathrm{st1}}\,l_{\mathrm{st1}}\,\theta_{\mathrm{st}} - k_{\mathrm{st1}}\,l_{\mathrm{tr5}}\,\theta_{\mathrm{tr}} \tag{43}$$

$$m_4\,\ddot{z}_4 = c_{\mathrm{st2}}\,\dot{z}_{\mathrm{tr}} - c_{\mathrm{st2}}\,\dot{z}_4 + k_4\,u_4 - k_4\,z_4 - k_{\mathrm{st2}}\,z_4 + k_{\mathrm{st2}}\,z_{\mathrm{tr}} - c_{\mathrm{st2}}\,l_{\mathrm{st2}}\,\dot{\theta}_{\mathrm{st}} - c_{\mathrm{st2}}\,l_{\mathrm{tr5}}\,\dot{\theta}_{\mathrm{tr}} - k_{\mathrm{st2}}\,l_{\mathrm{st2}}\,\theta_{\mathrm{st}} - k_{\mathrm{st2}}\,l_{\mathrm{tr5}}\,\theta_{\mathrm{tr}} \tag{44}$$

$$m_5\,\ddot{z}_5 = c_{\mathrm{st3}}\,\dot{z}_{\mathrm{tr}} - c_{\mathrm{st3}}\,\dot{z}_5 + k_5\,u_5 - k_5\,z_5 - k_{\mathrm{st3}}\,z_5 + k_{\mathrm{st3}}\,z_{\mathrm{tr}} - c_{\mathrm{st3}}\,l_{\mathrm{st3}}\,\dot{\theta}_{\mathrm{st}} - c_{\mathrm{st3}}\,l_{\mathrm{tr5}}\,\dot{\theta}_{\mathrm{tr}} - k_{\mathrm{st3}}\,l_{\mathrm{st3}}\,\theta_{\mathrm{st}} - k_{\mathrm{st3}}\,l_{\mathrm{tr5}}\,\theta_{\mathrm{tr}} \tag{45}$$

These equations of motion can be converted into matrix form given in the equation 46.

$$M\ddot{q} + C\dot{q} + Kq = K_f u \tag{46}$$

where M is the mass matrix, C is damping matrix, K is stiffness matrix, K_f is the forcing stiffness matrix and u is the kinematic input given as $u = (\ u_1 \quad u_2 \quad u_3 \quad u_4 \quad u_5\ )$, u_{1-5} are the road inputs to the tyres as shown in model figure 3.4.

Mass matrix obtained as,

$$M = \begin{pmatrix} M_1 & M_2 & M_3 & M_4 \end{pmatrix} \tag{47}$$

where submatrices are;

$$M_1 = \begin{pmatrix} b_{\text{sx}} + m_s & 0 & -b_{\text{sx}} & 0 \\ 0 & b_{\text{sz}} + m_s & 0 & -b_{\text{sz}} \\ -b_{\text{sx}} & 0 & b_{\text{cfx}} + b_{\text{sx}} + m_c & 0 \\ 0 & -b_{\text{sz}} & 0 & b_{\text{cfz}} + b_{\text{crz}} + b_{\text{sz}} + m_c \\ -b_{\text{sx}}\, h_{\text{cs}} & b_{\text{sz}}\, l_{\text{cs}} & b_{\text{cfx}}\, h_{\text{cf}} + b_{\text{sx}}\, h_{\text{cs}} & -b_{\text{cfz}}\, l_{\text{cf}} - b_{\text{crz}}\, l_{\text{cr}} - b_{\text{sz}}\, l_{\text{cs}} \\ 0 & 0 & -b_{\text{cfx}} & 0 \\ 0 & 0 & 0 & -b_{\text{cfz}} - b_{\text{crz}} \\ 0 & 0 & 0 & b_{\text{cfz}}\, l_{\text{trfc}} + b_{\text{crz}}\, l_{\text{trrc}} \\ 0 & 0 & 0 & 0 \\ 0 & 0 & 0 & 0 \\ 0 & 0 & 0 & 0 \\ 0 & 0 & 0 & 0 \\ 0 & 0 & 0 & 0 \\ 0 & 0 & 0 & 0 \end{pmatrix}$$

$$M_2 = \begin{pmatrix} -b_{\text{sx}}\, h_{\text{cs}} & 0 \\ b_{\text{sz}}\, l_{\text{cs}} & 0 \\ b_{\text{cfx}}\, h_{\text{cf}} + b_{\text{sx}}\, h_{\text{cs}} & -b_{\text{cfx}} \\ -b_{\text{cfz}}\, l_{\text{cf}} - b_{\text{crz}}\, l_{\text{cr}} - b_{\text{sz}}\, l_{\text{cs}} & 0 \\ b_{\text{cfx}}\, {h_{\text{cf}}}^2 + b_{\text{sx}}\, {h_{\text{cs}}}^2 + b_{\text{cfz}}\, {l_{\text{cf}}}^2 + b_{\text{crz}}\, {l_{\text{cr}}}^2 + b_{\text{sz}}\, {l_{\text{cs}}}^2 + I_c & -b_{\text{cfx}}\, h_{\text{cf}} \\ -b_{\text{cfx}}\, h_{\text{cf}} & b_{\text{cfx}} + m_{\text{st}} + m_{\text{tr}} \\ b_{\text{cfz}}\, l_{\text{cf}} + b_{\text{crz}}\, l_{\text{cr}} & 0 \\ -b_{\text{cfz}}\, l_{\text{cf}}\, l_{\text{trfc}} - b_{\text{crz}}\, l_{\text{cr}}\, l_{\text{trrc}} & h_{\text{tr5}}\, m_{\text{st}} \\ 0 & h_{\text{5st}}\, m_{\text{st}} \\ 0 & 0 \\ 0 & 0 \\ 0 & 0 \\ 0 & 0 \\ 0 & 0 \end{pmatrix}$$

$$M_3 = \begin{pmatrix} 0 & 0 \\ 0 & 0 \\ 0 & 0 \\ -b_{\text{cfz}} - b_{\text{crz}} & b_{\text{cfz}}\, l_{\text{trfc}} + b_{\text{crz}}\, l_{\text{trrc}} \\ b_{\text{cfz}}\, l_{\text{cf}} + b_{\text{crz}}\, l_{\text{cr}} & -b_{\text{cfz}}\, l_{\text{cf}}\, l_{\text{trfc}} - b_{\text{crz}}\, l_{\text{cr}}\, l_{\text{trrc}} \\ 0 & h_{\text{tr5}}\, m_{\text{st}} \\ b_{\text{cfz}} + b_{\text{crz}} + m_{\text{st}} + m_{\text{tr}} & -b_{\text{cfz}}\, l_{\text{trfc}} - b_{\text{crz}}\, l_{\text{trrc}} - l_{\text{tr5}}\, m_{\text{st}} \\ -b_{\text{cfz}}\, l_{\text{trfc}} - b_{\text{crz}}\, l_{\text{trrc}} - l_{\text{tr5}}\, m_{\text{st}} & m_{\text{st}}\, {h_{\text{tr5}}}^2 + m_{\text{st}}\, {l_{\text{tr5}}}^2 + b_{\text{cfz}}\, {l_{\text{trfc}}}^2 + b_{\text{crz}}\, {l_{\text{trrc}}}^2 + I_{\text{tr}} \\ -l_{\text{5st}}\, m_{\text{st}} & h_{\text{5st}}\, h_{\text{tr5}}\, m_{\text{st}} + l_{\text{5st}}\, l_{\text{tr5}}\, m_{\text{st}} \\ 0 & 0 \\ 0 & 0 \\ 0 & 0 \\ 0 & 0 \\ 0 & 0 \end{pmatrix}$$

$$M_4 = \begin{pmatrix} 0 & 0 & 0 & 0 & 0 & 0 \\ 0 & 0 & 0 & 0 & 0 & 0 \\ 0 & 0 & 0 & 0 & 0 & 0 \\ 0 & 0 & 0 & 0 & 0 & 0 \\ 0 & 0 & 0 & 0 & 0 & 0 \\ h_{\text{5st}}\, m_{\text{st}} & 0 & 0 & 0 & 0 & 0 \\ -l_{\text{5st}}\, m_{\text{st}} & 0 & 0 & 0 & 0 & 0 \\ h_{\text{5st}}\, h_{\text{tr5}}\, m_{\text{st}} + l_{\text{5st}}\, l_{\text{tr5}}\, m_{\text{st}} & 0 & 0 & 0 & 0 & 0 \\ m_{\text{st}}\, {h_{\text{5st}}}^2 + m_{\text{st}}\, {l_{\text{5st}}}^2 + I_{\text{st}} & 0 & 0 & 0 & 0 & 0 \\ 0 & m_1 & 0 & 0 & 0 & 0 \\ 0 & 0 & m_2 & 0 & 0 & 0 \\ 0 & 0 & 0 & m_3 & 0 & 0 \\ 0 & 0 & 0 & 0 & m_4 & 0 \\ 0 & 0 & 0 & 0 & 0 & m_5 \end{pmatrix}$$

The damping matrix is given below,

$$C = \begin{pmatrix} C_1 & C_2 & C_3 & C_4 & C_5 \end{pmatrix} \tag{48}$$

where submatrices C_1, C_2, C_3, C_4, C_5 are,

$$C_1 = \begin{pmatrix} c_{\text{sx}} & 0 & -c_{\text{sx}} & 0 \\ 0 & c_{\text{sz}} & 0 & -c_{\text{sz}} \\ -c_{\text{sx}} & 0 & c_{\text{cfx}} + c_{\text{sx}} & 0 \\ 0 & -c_{\text{sz}} & 0 & c_{\text{cfz}} + c_{\text{crz}} + c_{\text{sz}} \\ -c_{\text{sx}}\, h_{\text{cs}} & c_{\text{sz}}\, l_{\text{cs}} & c_{\text{cfx}}\, h_{\text{cf}} + c_{\text{sx}}\, h_{\text{cs}} & -c_{\text{cfz}}\, l_{\text{cf}} - c_{\text{crz}}\, l_{\text{cr}} - c_{\text{sz}}\, l_{\text{cs}} \\ 0 & 0 & -c_{\text{cfx}} & 0 \\ 0 & 0 & 0 & -c_{\text{cfz}} - c_{\text{crz}} \\ 0 & 0 & 0 & c_{\text{cfz}}\, l_{\text{trfc}} + c_{\text{crz}}\, l_{\text{trrc}} \\ 0 & 0 & 0 & 0 \\ 0 & 0 & 0 & 0 \\ 0 & 0 & 0 & 0 \\ 0 & 0 & 0 & 0 \\ 0 & 0 & 0 & 0 \\ 0 & 0 & 0 & 0 \end{pmatrix}$$

$$C_2 = \begin{pmatrix} -c_{\mathrm{sx}}\, h_{\mathrm{cs}} & 0 \\ c_{\mathrm{sz}}\, l_{\mathrm{cs}} & 0 \\ c_{\mathrm{cfx}}\, h_{\mathrm{cf}} + c_{\mathrm{sx}}\, h_{\mathrm{cs}} & -c_{\mathrm{cfx}} \\ -c_{\mathrm{cfz}}\, l_{\mathrm{cf}} - c_{\mathrm{crz}}\, l_{\mathrm{cr}} - c_{\mathrm{sz}}\, l_{\mathrm{cs}} & 0 \\ c_{\mathrm{cfx}}\, {h_{\mathrm{cf}}}^2 + c_{\mathrm{sx}}\, {h_{\mathrm{cs}}}^2 + c_{\mathrm{cfz}}\, {l_{\mathrm{cf}}}^2 + c_{\mathrm{crz}}\, {l_{\mathrm{cr}}}^2 + c_{\mathrm{sz}}\, {l_{\mathrm{cs}}}^2 & -c_{\mathrm{cfx}}\, h_{\mathrm{cf}} \\ -c_{\mathrm{cfx}}\, h_{\mathrm{cf}} & c_{\mathrm{cfx}} \\ c_{\mathrm{cfz}}\, l_{\mathrm{cf}} + c_{\mathrm{crz}}\, l_{\mathrm{cr}} & 0 \\ -c_{\mathrm{cfz}}\, l_{\mathrm{cf}}\, l_{\mathrm{trfc}} - c_{\mathrm{crz}}\, l_{\mathrm{cr}}\, l_{\mathrm{trrc}} & 0 \\ 0 & 0 \\ 0 & 0 \\ 0 & 0 \\ 0 & 0 \\ 0 & 0 \\ 0 & 0 \end{pmatrix}$$

$$C_3 = \begin{pmatrix} 0 \\ 0 \\ 0 \\ -c_{\mathrm{cfz}} - c_{\mathrm{crz}} \\ c_{\mathrm{cfz}}\, l_{\mathrm{cf}} + c_{\mathrm{crz}}\, l_{\mathrm{cr}} \\ 0 \\ c_{\mathrm{cfz}} + c_{\mathrm{crz}} + c_{\mathrm{st1}} + c_{\mathrm{st2}} + c_{\mathrm{st3}} + c_{\mathrm{trf}} + c_{\mathrm{trr}} \\ -c_{\mathrm{cfz}}\, l_{\mathrm{trfc}} - c_{\mathrm{crz}}\, l_{\mathrm{trrc}} - c_{\mathrm{st1}}\, l_{\mathrm{tr5}} - c_{\mathrm{st2}}\, l_{\mathrm{tr5}} - c_{\mathrm{st3}}\, l_{\mathrm{tr5}} - c_{\mathrm{trf}}\, l_{\mathrm{trfa}} - c_{\mathrm{trr}}\, l_{\mathrm{trra}} \\ -c_{\mathrm{st1}}\, l_{\mathrm{st1}} - c_{\mathrm{st2}}\, l_{\mathrm{st2}} - c_{\mathrm{st3}}\, l_{\mathrm{st3}} \\ -c_{\mathrm{trf}} \\ -c_{\mathrm{trr}} \\ -c_{\mathrm{st1}} \\ -c_{\mathrm{st2}} \\ -c_{\mathrm{st3}} \end{pmatrix}$$

$$C_4 = \begin{pmatrix} 0 \\ 0 \\ 0 \\ c_{\text{cfz}}\, l_{\text{trfc}} + c_{\text{crz}}\, l_{\text{trrc}} \\ -c_{\text{cfz}}\, l_{\text{cf}}\, l_{\text{trfc}} - c_{\text{crz}}\, l_{\text{cr}}\, l_{\text{trrc}} \\ 0 \\ -c_{\text{cfz}}\, l_{\text{trfc}} - c_{\text{crz}}\, l_{\text{trrc}} - c_{\text{st1}}\, l_{\text{tr5}} - c_{\text{st2}}\, l_{\text{tr5}} - c_{\text{st3}}\, l_{\text{tr5}} - c_{\text{trf}}\, l_{\text{trfa}} - c_{\text{trr}}\, l_{\text{trra}} \\ c_{\text{cfz}}\, {l_{\text{trfc}}}^2 + c_{\text{crz}}\, {l_{\text{trrc}}}^2 + c_{\text{st1}}\, {l_{\text{tr5}}}^2 + c_{\text{st2}}\, {l_{\text{tr5}}}^2 + c_{\text{st3}}\, {l_{\text{tr5}}}^2 + c_{\text{trf}}\, {l_{\text{trfa}}}^2 + c_{\text{trr}}\, {l_{\text{trra}}}^2 \\ c_{\text{st1}}\, l_{\text{st1}}\, l_{\text{tr5}} + c_{\text{st2}}\, l_{\text{st2}}\, l_{\text{tr5}} + c_{\text{st3}}\, l_{\text{st3}}\, l_{\text{tr5}} \\ c_{\text{trf}}\, l_{\text{trfa}} \\ c_{\text{trr}}\, l_{\text{trra}} \\ c_{\text{st1}}\, l_{\text{tr5}} \\ c_{\text{st2}}\, l_{\text{tr5}} \\ c_{\text{st3}}\, l_{\text{tr5}} \end{pmatrix}$$

$$C_5 = \begin{pmatrix} 0 & 0 & 0 & 0 & 0 & 0 \\ 0 & 0 & 0 & 0 & 0 & 0 \\ 0 & 0 & 0 & 0 & 0 & 0 \\ 0 & 0 & 0 & 0 & 0 & 0 \\ 0 & 0 & 0 & 0 & 0 & 0 \\ 0 & 0 & 0 & 0 & 0 & 0 \\ -c_{\text{st1}}\, l_{\text{st1}} - c_{\text{st2}}\, l_{\text{st2}} - c_{\text{st3}}\, l_{\text{st3}} & -c_{\text{trf}} & -c_{\text{trr}} & -c_{\text{st1}} & -c_{\text{st2}} & -c_{\text{st3}} \\ c_{\text{st1}}\, l_{\text{st1}}\, l_{\text{tr5}} + c_{\text{st2}}\, l_{\text{st2}}\, l_{\text{tr5}} + c_{\text{st3}}\, l_{\text{st3}}\, l_{\text{tr5}} & c_{\text{trf}}\, l_{\text{trfa}} & c_{\text{trr}}\, l_{\text{trra}} & c_{\text{st1}}\, l_{\text{tr5}} & c_{\text{st2}}\, l_{\text{tr5}} & c_{\text{st3}}\, l_{\text{tr5}} \\ c_{\text{st1}}\, {l_{\text{st1}}}^2 + c_{\text{st2}}\, {l_{\text{st2}}}^2 + c_{\text{st3}}\, {l_{\text{st3}}}^2 & 0 & 0 & c_{\text{st1}}\, l_{\text{st1}} & c_{\text{st2}}\, l_{\text{st2}} & c_{\text{st3}}\, l_{\text{st3}} \\ 0 & c_{\text{trf}} & 0 & 0 & 0 & 0 \\ 0 & 0 & c_{\text{trr}} & 0 & 0 & 0 \\ c_{\text{st1}}\, l_{\text{st1}} & 0 & 0 & c_{\text{st1}} & 0 & 0 \\ c_{\text{st2}}\, l_{\text{st2}} & 0 & 0 & 0 & c_{\text{st2}} & 0 \\ c_{\text{st3}}\, l_{\text{st3}} & 0 & 0 & 0 & 0 & c_{\text{st3}} \end{pmatrix}$$

The stiffness matrix K can be obtained as,

$$K = \begin{pmatrix} K_1 & K_2 & K_3 & K_4 & K_5 & K_6 \end{pmatrix} \tag{49}$$

$$K_1 = \begin{pmatrix} k_{\text{sx}} & 0 & -k_{\text{sx}} & 0 \\ 0 & k_{\text{sz}} & 0 & -k_{\text{sz}} \\ -k_{\text{sx}} & 0 & k_{\text{cfx}} + k_{\text{sx}} & 0 \\ 0 & -k_{\text{sz}} & 0 & k_{\text{cfz}} + k_{\text{crz}} + k_{\text{sz}} \\ -h_{\text{cs}}\, k_{\text{sx}} & k_{\text{sz}}\, l_{\text{cs}} & h_{\text{cf}}\, k_{\text{cfx}} + h_{\text{cs}}\, k_{\text{sx}} & -k_{\text{cfz}}\, l_{\text{cf}} - k_{\text{crz}}\, l_{\text{cr}} - k_{\text{sz}}\, l_{\text{cs}} \\ 0 & 0 & -k_{\text{cfx}} & 0 \\ 0 & 0 & 0 & -k_{\text{cfz}} - k_{\text{crz}} \\ 0 & 0 & 0 & k_{\text{cfz}}\, l_{\text{trfc}} + k_{\text{crz}}\, l_{\text{trrc}} \\ 0 & 0 & 0 & 0 \\ 0 & 0 & 0 & 0 \\ 0 & 0 & 0 & 0 \\ 0 & 0 & 0 & 0 \\ 0 & 0 & 0 & 0 \\ 0 & 0 & 0 & 0 \end{pmatrix}$$

$$K_2 = \begin{pmatrix} -h_{\mathrm{cs}}\, k_{\mathrm{sx}} & 0 \\ k_{\mathrm{sz}}\, l_{\mathrm{cs}} & 0 \\ h_{\mathrm{cf}}\, k_{\mathrm{cfx}} + h_{\mathrm{cs}}\, k_{\mathrm{sx}} & -k_{\mathrm{cfx}} \\ -k_{\mathrm{cfz}}\, l_{\mathrm{cf}} - k_{\mathrm{crz}}\, l_{\mathrm{cr}} - k_{\mathrm{sz}}\, l_{\mathrm{cs}} & 0 \\ k_{\mathrm{cfx}}\, {h_{\mathrm{cf}}}^2 + k_{\mathrm{sx}}\, {h_{\mathrm{cs}}}^2 + k_{\mathrm{cfz}}\, {l_{\mathrm{cf}}}^2 + k_{\mathrm{crz}}\, {l_{\mathrm{cr}}}^2 + k_{\mathrm{sz}}\, {l_{\mathrm{cs}}}^2 & -h_{\mathrm{cf}}\, k_{\mathrm{cfx}} \\ -h_{\mathrm{cf}}\, k_{\mathrm{cfx}} & k_{\mathrm{cfx}} \\ k_{\mathrm{cfz}}\, l_{\mathrm{cf}} + k_{\mathrm{crz}}\, l_{\mathrm{cr}} & 0 \\ -k_{\mathrm{cfz}}\, l_{\mathrm{cf}}\, l_{\mathrm{trfc}} - k_{\mathrm{crz}}\, l_{\mathrm{cr}}\, l_{\mathrm{trrc}} & 0 \\ 0 & 0 \\ 0 & 0 \\ 0 & 0 \\ 0 & 0 \\ 0 & 0 \\ 0 & 0 \end{pmatrix}$$

$$K_3 = \begin{pmatrix} 0 \\ 0 \\ 0 \\ -k_{\mathrm{cfz}} - k_{\mathrm{crz}} \\ k_{\mathrm{cfz}}\, l_{\mathrm{cf}} + k_{\mathrm{crz}}\, l_{\mathrm{cr}} \\ 0 \\ k_{\mathrm{cfz}} + k_{\mathrm{crz}} + k_{\mathrm{st1}} + k_{\mathrm{st2}} + k_{\mathrm{st3}} + k_{\mathrm{trf}} + k_{\mathrm{trr}} \\ -k_{\mathrm{cfz}}\, l_{\mathrm{trfc}} - k_{\mathrm{crz}}\, l_{\mathrm{trrc}} - k_{\mathrm{st1}}\, l_{\mathrm{tr5}} - k_{\mathrm{st2}}\, l_{\mathrm{tr5}} - k_{\mathrm{st3}}\, l_{\mathrm{tr5}} - k_{\mathrm{trf}}\, l_{\mathrm{trfa}} - k_{\mathrm{trr}}\, l_{\mathrm{trra}} \\ -k_{\mathrm{st1}}\, l_{\mathrm{st1}} - k_{\mathrm{st2}}\, l_{\mathrm{st2}} - k_{\mathrm{st3}}\, l_{\mathrm{st3}} \\ -k_{\mathrm{trf}} \\ -k_{\mathrm{trr}} \\ -k_{\mathrm{st1}} \\ -k_{\mathrm{st2}} \\ -k_{\mathrm{st3}} \end{pmatrix}$$

$$K_4 = \begin{pmatrix} 0 \\ 0 \\ 0 \\ k_{\text{cfz}}\, l_{\text{trfc}} + k_{\text{crz}}\, l_{\text{trrc}} \\ -k_{\text{cfz}}\, l_{\text{cf}}\, l_{\text{trfc}} - k_{\text{crz}}\, l_{\text{cr}}\, l_{\text{trrc}} \\ 0 \\ -k_{\text{cfz}}\, l_{\text{trfc}} - k_{\text{crz}}\, l_{\text{trrc}} - k_{\text{st1}}\, l_{\text{tr5}} - k_{\text{st2}}\, l_{\text{tr5}} - k_{\text{st3}}\, l_{\text{tr5}} - k_{\text{trf}}\, l_{\text{trfa}} - k_{\text{trr}}\, l_{\text{trra}} \\ k_{\text{cfz}}\, {l_{\text{trfc}}}^2 + k_{\text{crz}}\, {l_{\text{trrc}}}^2 + k_{\text{st1}}\, {l_{\text{tr5}}}^2 + k_{\text{st2}}\, {l_{\text{tr5}}}^2 + k_{\text{st3}}\, {l_{\text{tr5}}}^2 + k_{\text{trf}}\, {l_{\text{trfa}}}^2 + k_{\text{trr}}\, {l_{\text{trra}}}^2 \\ k_{\text{st1}}\, l_{\text{st1}}\, l_{\text{tr5}} + k_{\text{st2}}\, l_{\text{st2}}\, l_{\text{tr5}} + k_{\text{st3}}\, l_{\text{st3}}\, l_{\text{tr5}} \\ k_{\text{trf}}\, l_{\text{trfa}} \\ k_{\text{trr}}\, l_{\text{trra}} \\ k_{\text{st1}}\, l_{\text{tr5}} \\ k_{\text{st2}}\, l_{\text{tr5}} \\ k_{\text{st3}}\, l_{\text{tr5}} \end{pmatrix}$$

$$K_5 = \begin{pmatrix} 0 & 0 \\ 0 & 0 \\ 0 & 0 \\ 0 & 0 \\ 0 & 0 \\ 0 & 0 \\ -k_{\text{st1}}\, l_{\text{st1}} - k_{\text{st2}}\, l_{\text{st2}} - k_{\text{st3}}\, l_{\text{st3}} & -k_{\text{trf}} \\ k_{\text{st1}}\, l_{\text{st1}}\, l_{\text{tr5}} + k_{\text{st2}}\, l_{\text{st2}}\, l_{\text{tr5}} + k_{\text{st3}}\, l_{\text{st3}}\, l_{\text{tr5}} & k_{\text{trf}}\, l_{\text{trfa}} \\ k_{\text{st1}}\, {l_{\text{st1}}}^2 + k_{\text{st2}}\, {l_{\text{st2}}}^2 + k_{\text{st3}}\, {l_{\text{st3}}}^2 & 0 \\ 0 & k_1 + k_{\text{trf}} \\ 0 & 0 \\ k_{\text{st1}}\, l_{\text{st1}} & 0 \\ k_{\text{st2}}\, l_{\text{st2}} & 0 \\ k_{\text{st3}}\, l_{\text{st3}} & 0 \end{pmatrix}$$

$$K_6 = \begin{pmatrix} 0 & 0 & 0 & 0 \\ 0 & 0 & 0 & 0 \\ 0 & 0 & 0 & 0 \\ 0 & 0 & 0 & 0 \\ 0 & 0 & 0 & 0 \\ 0 & 0 & 0 & 0 \\ -k_{\text{trr}} & -k_{\text{st1}} & -k_{\text{st2}} & -k_{\text{st3}} \\ k_{\text{trr}}\, l_{\text{trra}} & k_{\text{st1}}\, l_{\text{tr5}} & k_{\text{st2}}\, l_{\text{tr5}} & k_{\text{st3}}\, l_{\text{tr5}} \\ 0 & k_{\text{st1}}\, l_{\text{st1}} & k_{\text{st2}}\, l_{\text{st2}} & k_{\text{st3}}\, l_{\text{st3}} \\ 0 & 0 & 0 & 0 \\ k_2 + k_{\text{trr}} & 0 & 0 & 0 \\ 0 & k_3 + k_{\text{st1}} & 0 & 0 \\ 0 & 0 & k_4 + k_{\text{st2}} & 0 \\ 0 & 0 & 0 & k_5 + k_{\text{st3}} \end{pmatrix}$$

And the forcing stiffness matrix K_f is obtained as,

$$K_f = \begin{pmatrix} 0 & 0 & 0 & 0 & 0 \\ 0 & 0 & 0 & 0 & 0 \\ 0 & 0 & 0 & 0 & 0 \\ 0 & 0 & 0 & 0 & 0 \\ 0 & 0 & 0 & 0 & 0 \\ 0 & 0 & 0 & 0 & 0 \\ 0 & 0 & 0 & 0 & 0 \\ 0 & 0 & 0 & 0 & 0 \\ 0 & 0 & 0 & 0 & 0 \\ 0 & 0 & 0 & 0 & 0 \\ -k_1 & 0 & 0 & 0 & 0 \\ 0 & -k_2 & 0 & 0 & 0 \\ 0 & 0 & -k_3 & 0 & 0 \\ 0 & 0 & 0 & -k_4 & 0 \\ 0 & 0 & 0 & 0 & -k_5 \end{pmatrix}$$

The transfer functions of the system can be obtained in various ways. In this thesis, a state-space representation of the system is obtained. Then the necessary transfer functions obtained using Matlab's "ss2tf" command. This procedure provided followed for its convenient during the calculations which are done in the Matlab environment. Having a state-space representation enabled easier system verification in Simulink-Simscape simulation software.

The general form of the state-space representation is given in the equations 50 and 51.

$$\dot{x} = \mathbf{A}x + \mathbf{B}z \tag{50}$$

$$y = \mathbf{C}x + \mathbf{D}z \tag{51}$$

where:

x : state vector

y : output vector

z : input vector

A : state matrix

B : input-to-state matrix

C : state-to-output matrix

D : feed-through matrix

The matrix form of the equations of motion was given in the equation 46 can be used to construct the state-space matrices **A** and **B** using the relationship given in the equation 52.

$$\dot{x} = \begin{pmatrix} 0 & I \\ -\frac{K}{M} & -\frac{C}{M} \end{pmatrix} x + \begin{pmatrix} 0 \\ -\frac{K_f}{M} \end{pmatrix} z \tag{52}$$

Then, **A** and **B** matrices becomes,

$$\mathbf{A} = \begin{pmatrix} 0 & I \\ -\frac{K}{M} & -\frac{C}{M} \end{pmatrix}$$

$$\mathbf{B} = \begin{pmatrix} 0 \\ -\frac{K_f}{M} \end{pmatrix}$$

C can be constructed so that equation 51 yields to to the desired outputs and it is given below,

$$\mathbf{C} = \begin{pmatrix} \mathbf{C}_1 & \mathbf{C}_2 \\ \mathbf{C}_3 & \mathbf{C}_4 \end{pmatrix} \tag{53}$$

where,

$$\mathbf{C}_1 = \begin{pmatrix} 1 & 0 & 0 & 0 & 0 & 0 & 0 & 0 \\ 0 & 1 & 0 & 0 & 0 & 0 & 0 & 0 \\ 1 & 0 & -1 & 0 & -h_{\text{cs}} & 0 & 0 & 0 \\ 0 & 1 & 0 & -1 & l_{\text{cs}} & 0 & 0 & 0 \\ 0 & 0 & 0 & 1 & 0 & 0 & -1 & -l_{\text{cr}} - l_{\text{trrc}} \\ 0 & 0 & 0 & 0 & 0 & 1 & 0 & 0 \\ 0 & 0 & 0 & 0 & 0 & 0 & 1 & 0 \\ 0 & 0 & 0 & 0 & 0 & 0 & 0 & 1 \end{pmatrix}$$

and $\mathbf{C}_2$ and $\mathbf{C}_3$ are 20 by 20 zero matrices and $\mathbf{C}_4$ is a 20 by 20 identity matrix. With this definition of **C**, the outputs of the state-space representation becomes the state variables

Table 3.5 Description of the first 5 state-space model output

Output Number	Description
1	Seat fore-aft position
2	Seat vertical position
3	Seat suspension fore-aft deflection
4	Seat suspension vertical deflection
5	Cab CoG-Chassis distance

theirselves except for the 3rd, 4th and 5th outputs and their descriptions are given in the table 3.5.

Feed-through matrix **D** is simply zero as there is no direct transition between input and output.

State variables are chosen based on the generalized vectors with which the equations of motion obtained and given as,

$$x = \begin{pmatrix} q \\ \dot{q} \end{pmatrix} \tag{54}$$

and the input vector is given below.

$$z = u \tag{55}$$

To calculate the **A** and **B** the inverse of M is required. With the model utilized in this thesis, M is a 14 by 14 matrix and it is not viable to calculate the parametric version. So, rather

numerical version is provided below which is calculated with the numerical values of the model parameters given in the section 3.2.4..

$$M^{-1} = \begin{pmatrix} M_{inv1} & M_{inv2} \end{pmatrix} \tag{56}$$

When all the inertances are set to zero, the submatices found as,

$$M_{inv1} = \begin{pmatrix} 0.00949 & 0 & 0 & 0 & 0 & 0 & 0 \\ 0 & 0.00949 & 0 & 0 & 0 & 0 & 0 \\ 0 & 0 & 0.00154 & 0 & 0 & 0 & 0 \\ 0 & 0 & 0 & 0.00154 & 0 & 0 & 0 \\ 0 & 0 & 0 & 0 & 0.00182 & 0 & 0 \\ 0 & 0 & 0 & 0 & 0 & 6.0\text{e-}5 & 1.95\text{e-}5 \\ 0 & 0 & 0 & 0 & 0 & 1.95\text{e-}5 & 2.46\text{e-}4 \\ 0 & 0 & 0 & 0 & 0 & -6.08\text{e-}6 & -3.65\text{e-}5 \\ 0 & 0 & 0 & 0 & 0 & -2.01\text{e-}6 & -2.64\text{e-}5 \\ 0 & 0 & 0 & 0 & 0 & 0 & 0 \\ 0 & 0 & 0 & 0 & 0 & 0 & 0 \\ 0 & 0 & 0 & 0 & 0 & 0 & 0 \\ 0 & 0 & 0 & 0 & 0 & 0 & 0 \\ 0 & 0 & 0 & 0 & 0 & 0 & 0 \end{pmatrix}$$

$$M_{inv2} = \begin{pmatrix} 0 & 0 & 0 & 0 & 0 & 0 & 0 \\ 0 & 0 & 0 & 0 & 0 & 0 & 0 \\ 0 & 0 & 0 & 0 & 0 & 0 & 0 \\ 0 & 0 & 0 & 0 & 0 & 0 & 0 \\ 0 & 0 & 0 & 0 & 0 & 0 & 0 \\ -6.08\text{e-}6 & -2.01\text{e-}6 & 0 & 0 & 0 & 0 & 0 \\ -3.65\text{e-}5 & -2.64\text{e-}5 & 0 & 0 & 0 & 0 & 0 \\ 3.67\text{e-}5 & -4.46\text{e-}6 & 0 & 0 & 0 & 0 & 0 \\ -4.46\text{e-}6 & 6.81\text{e-}6 & 0 & 0 & 0 & 0 & 0 \\ 0 & 0 & 0.00286 & 0 & 0 & 0 & 0 \\ 0 & 0 & 0 & 0.00161 & 0 & 0 & 0 \\ 0 & 0 & 0 & 0 & 0.00222 & 0 & 0 \\ 0 & 0 & 0 & 0 & 0 & 0.00222 & 0 \\ 0 & 0 & 0 & 0 & 0 & 0 & 0.00222 \end{pmatrix}$$

and when all inertances set to 10 kg the submatrices found as,

$$M_{inv1} = \begin{pmatrix} 0.00868 & 1.85\text{e-}6 & 1.27\text{e-}4 & -8.91\text{e-}9 & -9.28\text{e-}5 & 1.37\text{e-}7 & 5.88\text{e-}8 \\ 1.85\text{e-}6 & 0.00868 & -7.94\text{e-}7 & 1.28\text{e-}4 & -3.4\text{e-}5 & 9.47\text{e-}8 & 7.75\text{e-}7 \\ 1.27\text{e-}4 & -7.94\text{e-}7 & 0.0015 & 1.69\text{e-}8 & 3.99\text{e-}5 & 8.7\text{e-}7 & 2.75\text{e-}7 \\ -8.91\text{e-}9 & 1.28\text{e-}4 & 1.69\text{e-}8 & 0.00147 & 1.84\text{e-}7 & 8.41\text{e-}7 & 8.8\text{e-}6 \\ -9.28\text{e-}5 & -3.4\text{e-}5 & 3.99\text{e-}5 & 1.84\text{e-}7 & 0.00171 & -1.09\text{e-}6 & -6.2\text{e-}7 \\ 1.37\text{e-}7 & 9.47\text{e-}8 & 8.7\text{e-}7 & 8.41\text{e-}7 & -1.09\text{e-}6 & 5.99\text{e-}5 & 1.94\text{e-}5 \\ 5.88\text{e-}8 & 7.75\text{e-}7 & 2.75\text{e-}7 & 8.8\text{e-}6 & -6.2\text{e-}7 & 1.94\text{e-}5 & 2.44\text{e-}4 \\ -6.92\text{e-}8 & -2.57\text{e-}7 & -6.35\text{e-}8 & -2.7\text{e-}6 & 1.13\text{e-}6 & -6.02\text{e-}6 & -3.6\text{e-}5 \\ 8.28\text{e-}9 & -4.54\text{e-}8 & -3.45\text{e-}8 & -5.7\text{e-}7 & -2.0\text{e-}7 & -1.99\text{e-}6 & -2.62\text{e-}5 \\ 0 & 0 & 0 & 0 & 0 & 0 & 0 \\ 0 & 0 & 0 & 0 & 0 & 0 & 0 \\ 0 & 0 & 0 & 0 & 0 & 0 & 0 \\ 0 & 0 & 0 & 0 & 0 & 0 & 0 \\ 0 & 0 & 0 & 0 & 0 & 0 & 0 \end{pmatrix}$$

$$M_{inv2} = \begin{pmatrix} -6.92\text{e-}8 & 8.28\text{e-}9 & 0 & 0 & 0 & 0 & 0 \\ -2.57\text{e-}7 & -4.54\text{e-}8 & 0 & 0 & 0 & 0 & 0 \\ -6.35\text{e-}8 & -3.45\text{e-}8 & 0 & 0 & 0 & 0 & 0 \\ -2.7\text{e-}6 & -5.7\text{e-}7 & 0 & 0 & 0 & 0 & 0 \\ 1.13\text{e-}6 & -2.0\text{e-}7 & 0 & 0 & 0 & 0 & 0 \\ -6.02\text{e-}6 & -1.99\text{e-}6 & 0 & 0 & 0 & 0 & 0 \\ -3.6\text{e-}5 & -2.62\text{e-}5 & 0 & 0 & 0 & 0 & 0 \\ 3.65\text{e-}5 & -4.49\text{e-}6 & 0 & 0 & 0 & 0 & 0 \\ -4.49\text{e-}6 & 6.8\text{e-}6 & 0 & 0 & 0 & 0 & 0 \\ 0 & 0 & 0.00286 & 0 & 0 & 0 & 0 \\ 0 & 0 & 0 & 0.00161 & 0 & 0 & 0 \\ 0 & 0 & 0 & 0 & 0.00222 & 0 & 0 \\ 0 & 0 & 0 & 0 & 0 & 0.00222 & 0 \\ 0 & 0 & 0 & 0 & 0 & 0 & 0.00222 \end{pmatrix}$$

A state-space representation can be converted to transfer function. This transformation realized with Matlab by using "ss2tf" command. As the vehicle model features 5 axles excited by the same road profile but with time delays based on both velocity and longitudinal distances between them, the resulting transfer functions are related by a transport delay. This is achieved using Equation 57.

$$H(s) = e^{-\tau_1} H_1(s) + e^{-\tau_2} H_2(s) + e^{-\tau_3} H_3(s) + e^{-\tau_4} H_4(s) + e^{-\tau_5} H_5(s) \tag{57}$$

where:

$H(s)$: resulting transfer function

$H_{1,5}$: transfer functions of the same output for the first to last inputs

$\tau_{1,5}$: time delays for the inputs

Time delays are calculated using Equation 58.

$$\tau_n = \frac{l_n}{V} \tag{58}$$

where:

l_n : distance from the first input in meters (e.g., distances of axles from tractor front axle)

n : axle index from 1 to 5

V : vehicle velocity in meters/second

Note that τ_1 is zero, as it corresponds to the first axle.

3.2.6. Model Verification

Obtained system model verified against a non-linear Simscape multi-body model. The exact same system was built using mass, rigid transformation and different joints. For comparison, the state-space model is also included within the Simscape model and the supplied with the same inputs. Both models uses the parameters presented in the section 3.2.4. with 30 kg inertances at the seat suspensions and 300 kg of inertances at the cab suspensions execpt the cab front longitudinal direction. Then, the equivalent signals for the outputs defined in the table 3.5 are obtained and compared. Complete Simscape model provided in the appendix.

As the excitation, a random, hundred meter long, ISO-8608:2016 A class road profile generated using the method described in the section 3.1.. Road profile is given to each tyres by introducing shifts in order to satisfy that each tyre receives the same inputs with a time delay. Time delays are calculated using the equation 58 and velocity is chosen as 60 km/h. In figure 3.7 only the tractor front tyre and trailer rear tyre inputs are shown for clarity. The shifts in the inputs are visible. It should be noted that due to the wheelbase, some portions of the road do not excite all the tyres. Tractor first axle, for example, is not excited by the first 12,21 meters of the road and the last 12,21 meters of the road do not excite the trailer rear tyre.

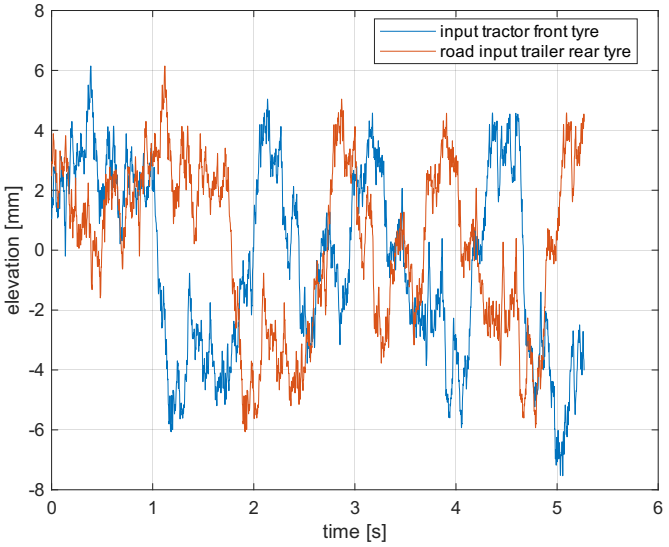

Figure 3.7 Inputs for tractor front tyre and trailer rear axle

The outputs obtained by both Simscape and state-space models are presented in figures 3.8 - 3.12. It is seen that the results for the vertical direction are more well-matched than the longitudinal results. This is because the longitudinal motions occur due to pitching motions and during the linearization, longitudinal motions are more affected. However, it is also seen that the general behaviour of the state-space results in figures 3.8 and 3.10 are similar and assumed to be acceptable. Vertical motion results, on the other hand, are seen to be well-matching. Cab deflection results presented in 3.12 has the best match with non-linear Simscape solution compared to others.

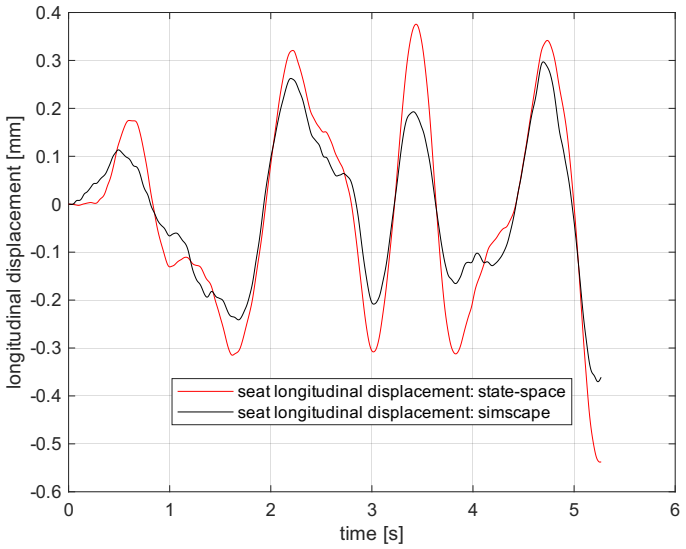

Figure 3.8 Seat longitudinal displacements obtained by state-space and simscape models

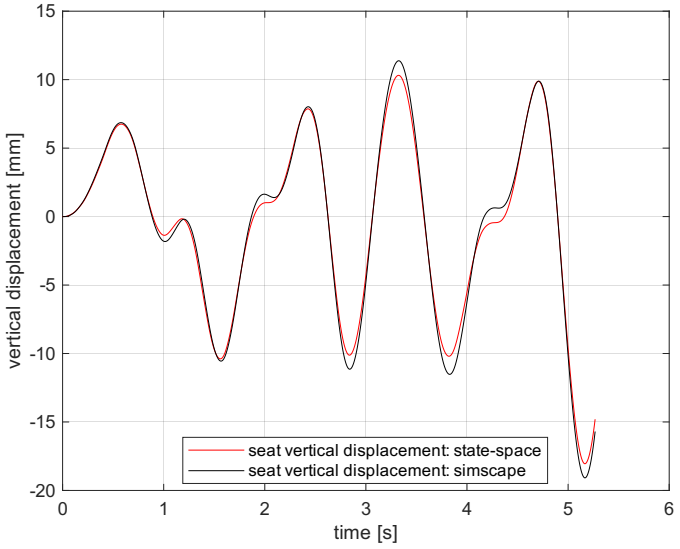

Figure 3.9 Seat vertical displacements obtained by state-space and simscape models

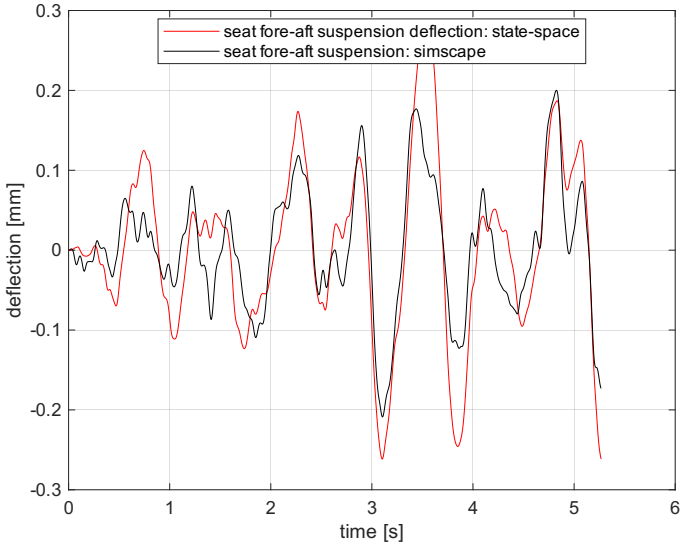

Figure 3.10 Seat fore-aft suspension deflections obtained by state-space and simscape models

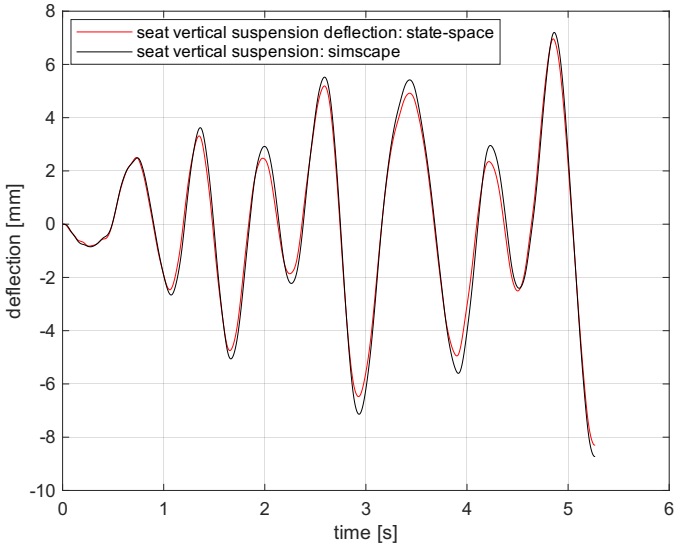

Figure 3.11 Seat vertical suspension deflections obtained by state-space and simscape models

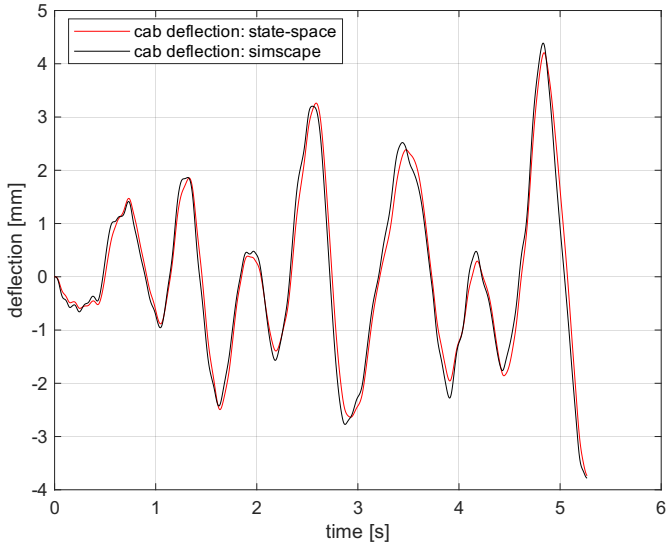

Figure 3.12 Cab deflections obtained by state-space and simscape models

3.3. Frequency Domain Calculations

As discussed in Section 2.2., the ISO-2631 standard uses RMS vibrations for assessing ride comfort. One method involves running time-domain simulations to obtain vibration data in the time domain, from which the RMS vibration can be easily calculated using Equation 59.

$$a_w = \left[\sum_i (W_i a_i)^2 \right]^{\frac{1}{2}} \tag{59}$$

where:

a_w : frequency-weighted acceleration

W_i : weighting factor for the ith one-third octave band defined by ISO-2631

a_i : RMS acceleration for the ith one-third octave band

However, performing time-domain simulations involves several steps:

- Synthesize a road profile

- Calculate initial conditions for the model based on the random road profile
- Run the simulation and collect results in the time domain
- Apply frequency weightings
- Calculate RMS values

This process is complex, susceptible to numerical difficulties, computationally expensive, and may be avoided by employing frequency domain calculations when RMS values suffice. Time-domain results become necessary when crest factor is significant or when the input PSD function is unknown.

The area under the PSD curve yields to the RMS value. Given the acceleration PSD, the RMS acceleration value can be determined using the relationship provided by Equation 60.

$$S_r(f) = H^2(f)S(f) \tag{60}$$

where:

$S_r(f)$: PSD function of the response

$H(f)$: frequency response function of the system

$S(f)$: PSD function of the excitation input

The RMS value of the response can be obtained by taking the square root of the integral of the response, as given by Equation 61 [4], [10].

$$a_{rms} = \sqrt{\int_{f_1}^{f_2} S_r(f)df} \tag{61}$$

where:

a_{rms} : RMS response (e.g., RMS acceleration)

The input excitation PSD function, replaced in Equation 60, is defined in Equation 1.

ISO-2631 mandates frequency-weighted accelerations. To this end, it defines filter transfer functions with parameters provided in Table 3.6.

Table 3.6 Transfer function parameters for ISO-2631 principle axes frequency weighting [1]

Weighting	**Band-limiting**		**Acceleration-velocity transition (a-v transition)**			**Upward step**			
	f_1 Hz	f_2 Hz	f_3 Hz	f_4 Hz	Q_4	f_5 Hz	Q_5	f_6 Hz	Q_6
W_k	0,4	100	12,5	12,5	0,63	2,37	0,91	3,35	0,91
W_d	0,4	100	2,0	2,0	0,63	∞	-	∞	-
W_f	0,08	0,63	∞	0,25	0,86	0,0625	0,80	0,1	0,80

The resulting weighting curves are presented in the figure 2.7. These weightings can be incorporated into Equation 60 as shown in equations 62 and 63 for the vertical and longitudinal axes, respectively.

$$S_r(f) = W_k^2 H^2(f) S(f) \tag{62}$$

$$S_r(f) = W_d^2 H^2(f) S(f) \tag{63}$$

Inserting Equations 62 and 63 into Equation 61 yields the weighted RMS responses of a system. The output is determined by the system transfer function definition. If acceleration is defined in the transfer function, the result is acceleration; if deflection is defined, then it is deflection.

3.4. Performance Investigation

The study investigates the impact of an inerter on vibration isolation performance at two key locations in a tractor-semitrailer combination: the cab suspension and seat suspension. Initially, inerters are utilized at the cab's vertical suspension using three distinct configurations: inerter placement at the cab front suspension, rear suspension, and both front and rear suspensions. To accommodate various design considerations, the spring and damper values of the cab suspension are varied for natural frequencies of 0.8, 1.4, and 1.6 Hz, and damping ratios of 0.2, 0.4, and 0.8. These parameter selections are based on the study by ElMadany [17]. Inertance values are increased from 0 kg to 300 kg for each combination of natural frequency and damping ratio pairs. The vehicle constant velocity is 90 km/h, while the seat suspension parameters remain unchanged as specified in Table 3.2. The fundamental properties of the cab suspension cases are summarized in Table 3.7.

Table 3.7 Fundamental properties of investigated cases for cab suspension

Case Number	Velocity [km/h]	Cab Undamped Natural Frequency [Hz]	Cab Damping Ratio	Cab Front Inerter [kg]	Cab Rear Inerter [kg]	Seat Suspension
1	90	0.8 , 1.2 , 1.6	0.2 , 0.4 , 0.8	0 - 300	0	base values
2	90	0.8 , 1.2 , 1.6	0.2 , 0.4 , 0.8	0	0 - 300	base values
3	90	0.8 , 1.2 , 1.6	0.2 , 0.4 , 0.8	0 - 300	0 - 300	base values

Undamped natural frequency and damping ratio are calculated using the following equations 64 and 65.

$$w_n = \frac{1}{2\pi}\sqrt{\frac{k_{cfz} + k_{crz}}{m_c}} \tag{64}$$

$$\zeta = \frac{c_{cfz} + c_{crz}}{2\sqrt{(k_{cfz} + k_{crz})m_c}} \tag{65}$$

where:

w_n : undamped natural frequency

ζ : damping ratio

At each case, the weighted RMS seat acceleration and RMS cab deflection for each natural frequency-damping ratio pair are calculated using the methods described in Section 3.3.. These results are then plotted on an RMS deflection versus weighted RMS acceleration graph. Each pair starts from a point and moves with increasing inertance, allowing for the visualization of inerter effects on a single plot for multiple natural frequencies and damping ratios.

In Figure 3.13, the results for each natural frequency-damping ratio pair with inertance values of 0 kg are presented. Subsequently, inertance values are increased up to 300 kg with steps of 20 kg. As the inertance values increase, the corresponding RMS results are depicted with red lines, as shown in Figure 3.14.

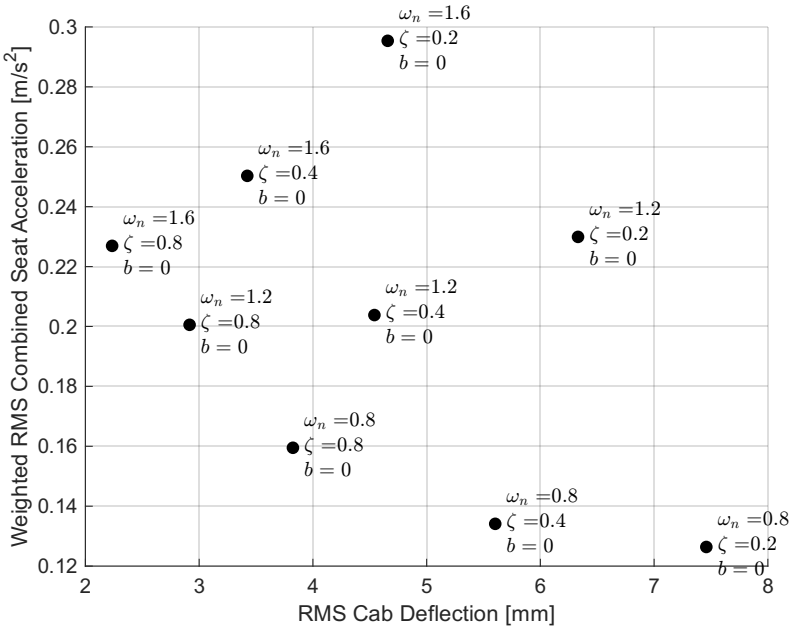

Figure 3.13 Supplementary Graph Illustrating Plotting Methodology

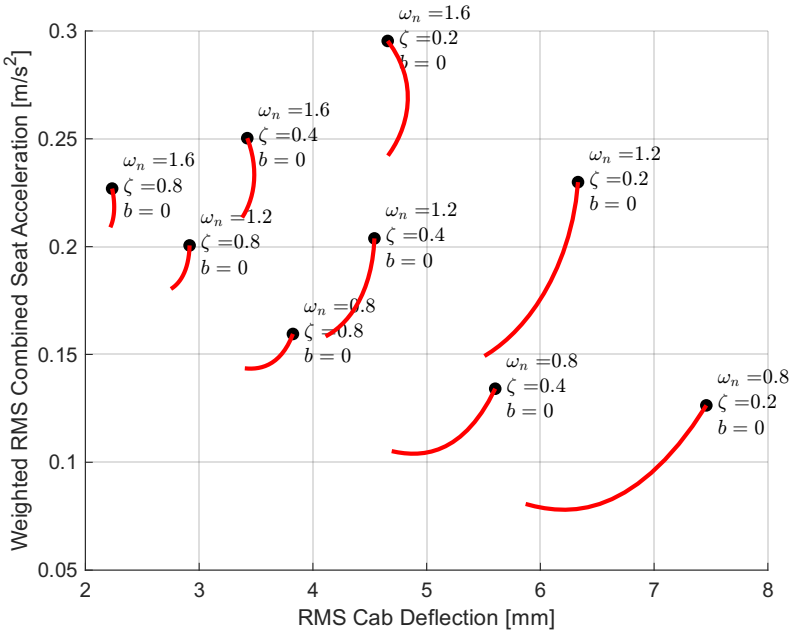

Figure 3.14 Supplementary Graph Illustrating Plotting Methodology

At the termination points of the red lines, the inertance values reach their maximum value for the respective case. This is visually demonstrated in Figure 3.15 for the maximum inertance

value of 300 kg.

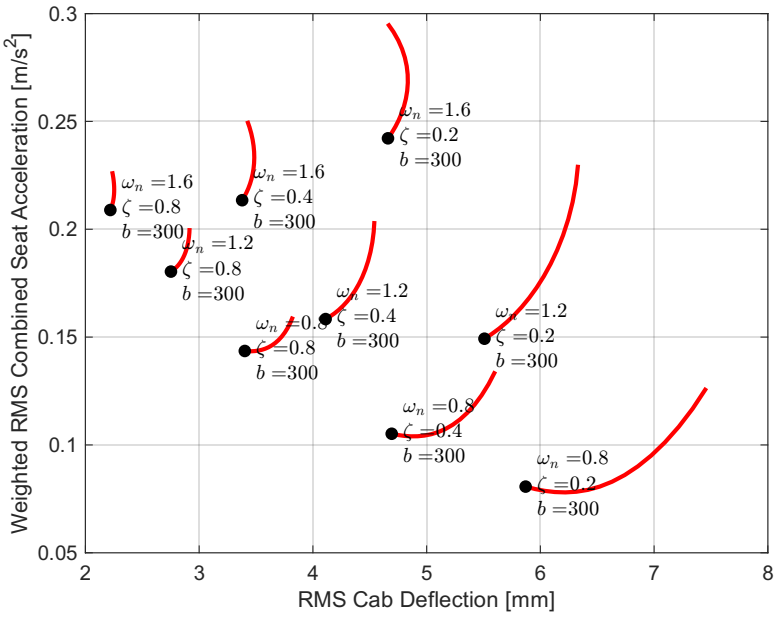

Figure 3.15 Supplementary Graph Illustrating Plotting Methodology

The results are displayed in a format where the constant natural frequency and damping ratios are connected at the 0 inertance points with dashed lines. The corresponding values are printed next to them, as depicted in Figure 3.16.

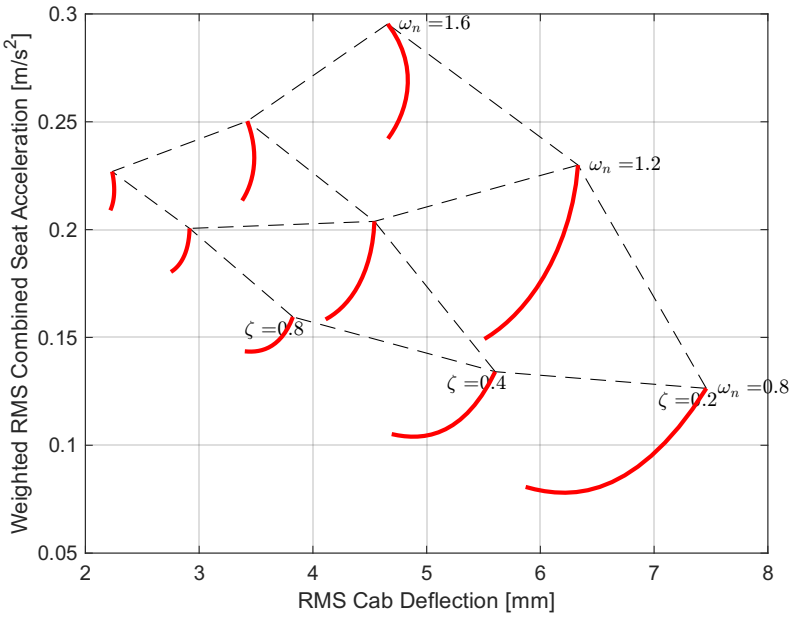

Figure 3.16 Supplementary Graph Illustrating Plotting Methodology

For each case, the best performing suspension is determined by introducing non-dimensional parameters J_1 and J_2. Both are obtained by applying normalization as defined in equations 66 and 67. For a well performing suspension, both parameters are expected to be as small as possible.

$$J_1 = \frac{a_v^2}{a_{v0}^2} \tag{66}$$

$$J_2 = \frac{\Delta_c^2}{\Delta_{c0}^2} \tag{67}$$

where:

J_1 : non-dimensional comfort parameter

J_2 : non-dimensional suspension deflection parameter

a_v : weighted combined seat acceleration

a_{v0} : reference value of weighted combined seat acceleration

Δ_c : cab deflection measured between cab center of gravity and its vertical projection onto tractor chassis

Δ_{c0} : reference deflection

Reference values are obtained for the original model parameters which are given in the table 3.2. The best-performing suspension is selected based on the minimum J, as defined in equation 68, which ideally approaches zero.

$$J = \sqrt{J_1^2 + J_2^2} \tag{68}$$

A similar methodology is applied to seat suspensions. The same suspension parameters, in terms of spring, damper, and inerter, are assumed for fore-aft and vertical directions. Natural frequencies are set to 1.2, 1.4, and 1.6 Hz, while damping ratios are set to 0.2, 0.3, and 0.4. Values are chosen based on the studies [13], [22] and [21]. Inerters are set between 0 and 30 kg, taking into account available space in the seat assembly. Velocity is again 90 km/h and with these properties, seat suspension is investigated with a single case. Seat suspension performance is evaluated based on weighted RMS accelerations and RMS deflections. Unlike the cab suspensions, as seat suspensions operate directly in the principal axes of the seat, cross-axial forces can be disregarded [21], and only principal axis accelerations and deflections (e.g., fore-aft acceleration and deflection for fore-aft suspension, and vertical acceleration and deflection for vertical suspension) are considered. Performance metrics are again normalized by their respective initial performances, obtained with initial spring and damper values and no inerter.

4. RESULTS

The calculation methods described in Section 3. are implemented through a series of MATLAB programs, with time-domain simulations realized using Simulink modules. All codes and models are provided in the appendix.

The presented results include Power Spectral Density (PSD) graphs, illustrating the frequencies at which the inerter effectively modifies the suspension's isolation behavior. According to the ISO2631-1997 standard, the 0.5 - 80 Hz band is crucial for ride comfort studies. Consequently, acceleration PSD graphs are confined within this range, with RMS values derived by integration over this frequency band. In contrast, suspension deflections are calculated and plotted across the entire excitation band. ISO8608:2016 recommends a spatial frequency band of 0.01 - 10 cycles/meter for representing road profiles. This corresponds to another frequency band, calculated by multiplying the band limits with the velocity. For a velocity of 90 km/h, this results in 0.25 - 250 Hz, thus deflection PSD graphs are delineated within this frequency band. The results for each case are presented in their respective sections.

Time history plots from the Simulink model are provided to compare and observe changes in the frequency domain. While time domain and PSD results represent the same system, their methods of acquisition render them incomparable in terms of back calculability. PSD plots are derived from analytical functions, whereas the Simulink model is based on a synthesized road profile.

Additionally, RMS values are tabulated for each $w_n - \zeta$ pair, both with and without inerters, for convenience.

4.1. Case 1: Inerter at front cab suspension, velocity is 90 km/h

The weighted RMS acceleration and RMS cab deflection results are illustrated in Figure 4.1. In general, it is observed that inerter has a positive effect on isolation performance.

For the lowest undamped natural frequency and damping pair, a significant decrease in RMS deflection is noticeable together with a high reduction in weighted combined RMS acceleration. Following the constant frequency path to the left side from 0.2 damping to 0.8 damping, the impact diminishes. Conversely, for values corresponding to the highest frequency-damping pair, while the weighted combined RMS acceleration decreases by 8%, deflection values remain relatively unchanged with only 1% change.

The results regarding to each pairs with 0 kg of inertance, e.g. no inerter, and with 300 kg of inertance are presented in the table 4.1. The relative changes are also calculated and listed in this table. Overall, it can be inferred that the impact of an inerter, when applied at the front cab suspension, is most pronounced with lower damping ratios.

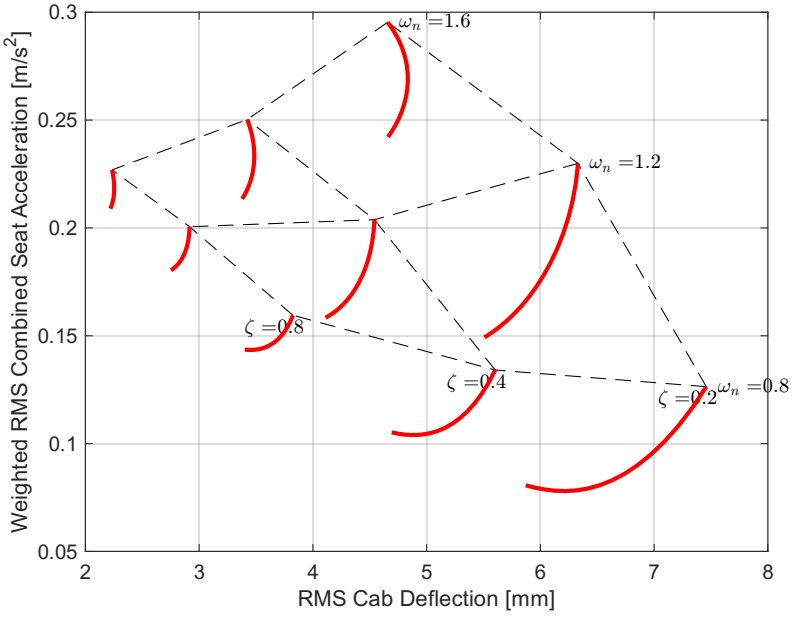

Figure 4.1 Illustration of RMS value changes with increasing inertance for all $w_n - \zeta$ pairs in Case 1

Table 4.1 Summarized RMS results for case-1.

w_n	ζ	Seat Weighted RMS Acceleration $[m/s^2]$									Cab RMS deflection $[mm]$		
		fore-aft			vertical			combined					
		b=0	b=300	relative change	b=0	b=300	relative change	b=0	b=300	change	b=0	b=300	relative change
0.8	0.2	0.0403	0.031	-23%	0.1198	0.0745	-38%	0.1264	0.0807	-36%	7.4591	5.8704	-21%
0.8	0.4	0.0403	0.0379	-6%	0.1279	0.0981	-23%	0.1341	0.1052	-22%	5.6031	4.6928	-16%
0.8	0.8	0.0426	0.0462	8%	0.1537	0.1359	-12%	0.1595	0.1436	-10%	3.8243	3.4013	-11%
1.2	0.2	0.0418	0.0658	57%	0.2261	0.134	-41%	0.2299	0.1493	-35%	6.331	5.5084	-13%
1.2	0.4	0.0432	0.0596	38%	0.1992	0.1467	-26%	0.2038	0.1584	-22%	4.5408	4.1117	-9%
1.2	0.8	0.0447	0.0551	23%	0.1955	0.1717	-12%	0.2006	0.1804	-10%	2.9158	2.7519	-6%
1.6	0.2	0.0624	0.1118	79%	0.2887	0.2148	-26%	0.2954	0.2422	-18%	4.6577	4.6601	0%
1.6	0.4	0.0508	0.0787	55%	0.2451	0.1984	-19%	0.2503	0.2135	-15%	3.423	3.378	-1%
1.6	0.8	0.0457	0.0578	26%	0.2223	0.2008	-10%	0.2269	0.2089	-8%	2.2347	2.2191	-1%

The non-dimensional parameter results are illustrated in figure 4.2. The more pronounced effect with lower damping ratio is very clear. However, due to high deflections, low damping ratio pairs perform considerable worse than the higher damping ratio counterparts. The best performing pair is pointed with a blue dashed line respecting to 1.6 Hz undamped natural frequency and 0.8 damping ration with 300 kg inertance.

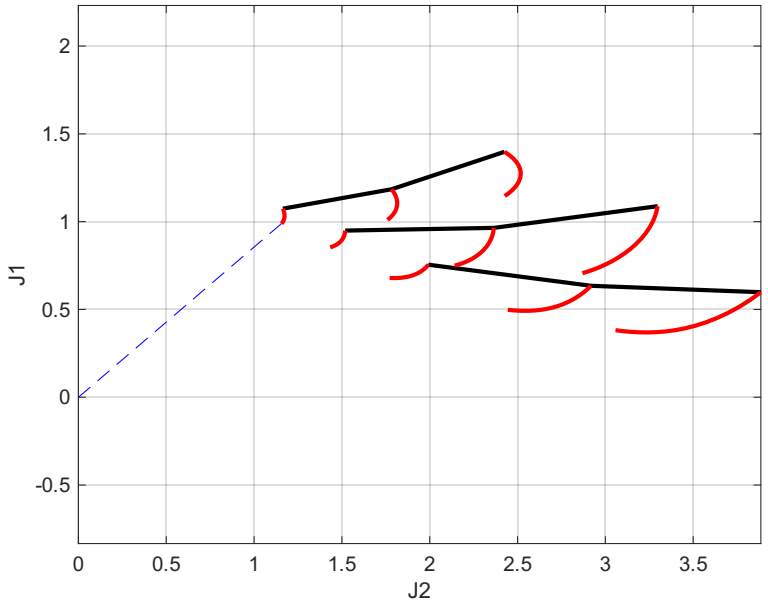

Figure 4.2 Illustration of non-dimensional parameter changes with increasing inertance for all $w_n - \zeta$ pairs in Case 1.

The analytically obtained seat wieghted fore-aft PSD functions are plotted for the highest and lowest frequency-damping pairs in Figure 4.3. As discussed in Section 2.4., it is expected that the isolation performance worsens with the inerter for higher frequencies. This trend is clearly visible after approximately 10 Hz.

The responses around 1.5 Hz are predominant for each pair. In this region, it is observed that the inerter causes a greater response with the high frequency-damping pair, indicating the deterioration also seen in the table 4.1 as 26% increase in acceleration. An improvement is noticeable for the low frequency-damping pair, black solid and dashed lines on the figures. Additionally, numerous anti-resonances are present, which are caused by the wheelbase filtering effect [23]

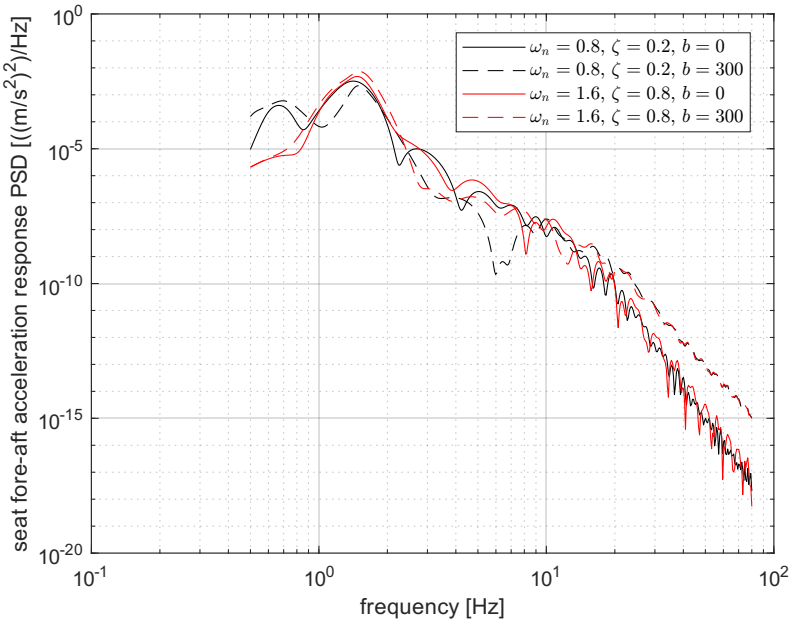

Figure 4.3 Seat fore-aft weighted acceleration PSD plots for the highest and lowest $w_n - \zeta$ pairs, comparing inerter and non-inerter versions, Case 1.

Figures 4.4 and 4.5 depict the seat fore-aft weighted acceleration response in the time domain. These graphs are obtained through time-domain simulations in a Simulink model.

In Figure 4.4, the improvement for the low frequency-damping pair is observable. The peaks are seen to be smaller with the inerter than without. Furthermore, the response is significantly dominated by frequencies around 1.5 Hz.

Conversely, in Figure 4.5, the deterioration in the acceleration isolation is evident. The response is greater with the inerter, indicating degraded performance.

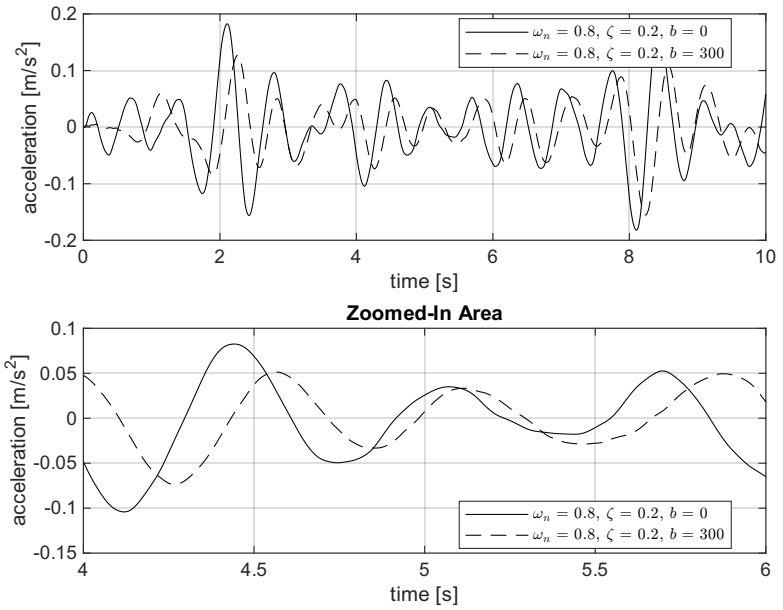

Figure 4.4 Seat fore-aft weighted acceleration plot for the lowest $w_n - \zeta$ pair with and without inerter from Simulink time domain simulation, case-1.

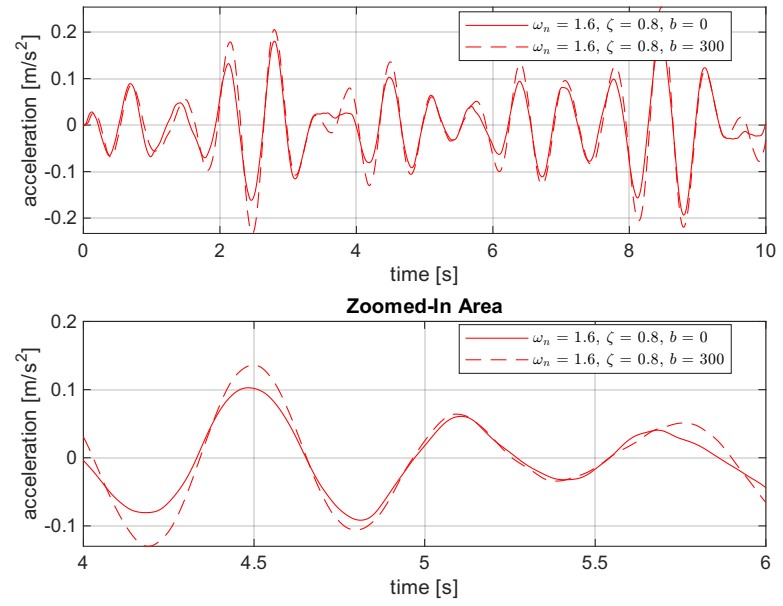

Figure 4.5 Seat fore-aft weighted acceleration plot for the highest $w_n - \zeta$ pair with and without inerter from Simulink time domain simulation, case-1.

The analytically obtained PSD functions of the seat vertical weighted acceleration are depicted in Figure 4.7. Decreased accelerations with inerter around 1 Hz are evident, while the degraded performance after approximately 2 Hz is also apparent. It should be noted that the magnitudes during the degraded performance are much lower than the range where the acceleration magnitude is suppressed with the inerter.

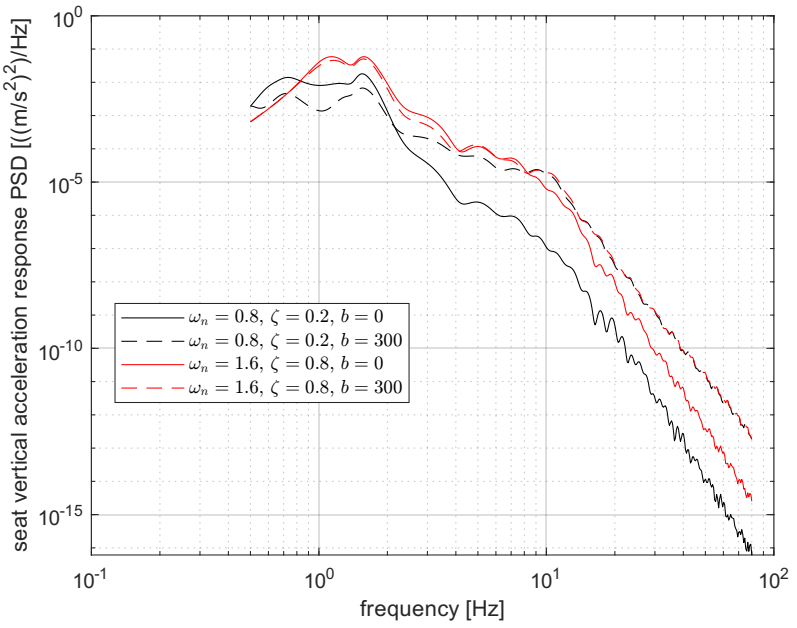

Figure 4.6 Seat vertical weighted acceleration PSD plots for the highest and lowest $w_n - \zeta$ pairs, comparing inerter and non-inerter versions, Case 1.

The time domain simulation results for seat vertical weighted acceleration are plotted in Figures 4.8 and 4.9.

In the first plot (Figure 4.8), the lower peaks with the inerter-based suspension are evident. However, as expected, higher frequency content is more pronounced with the inerter.

In the second figure (Figure 4.9), a slight decrease in the peaks is observed, and the higher frequency content is not as obvious. This is because, as shown in Figure 4.7, even though the isolation performance is degraded, the magnitudes are very low.

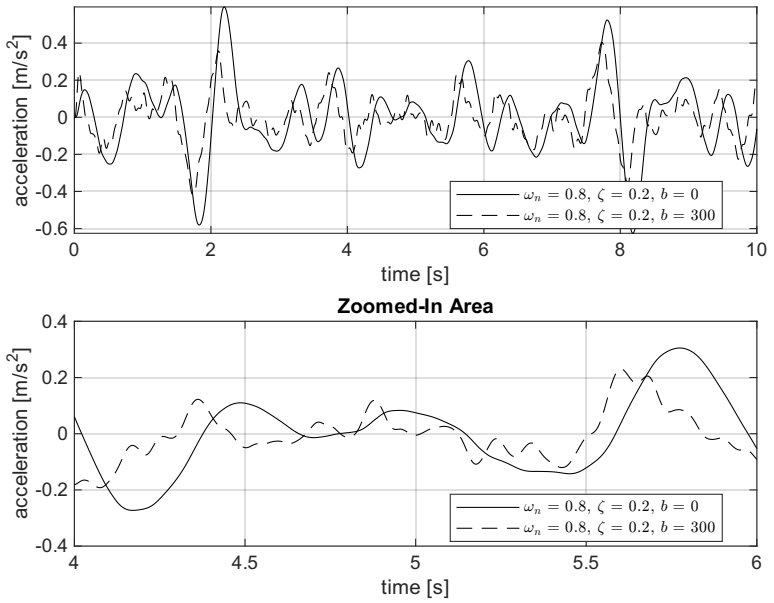

Figure 4.7 Seat vertical weighted acceleration plot for the lowest $w_n - \zeta$ pair with and without inerter from Simulink time domain simulation, case-1.

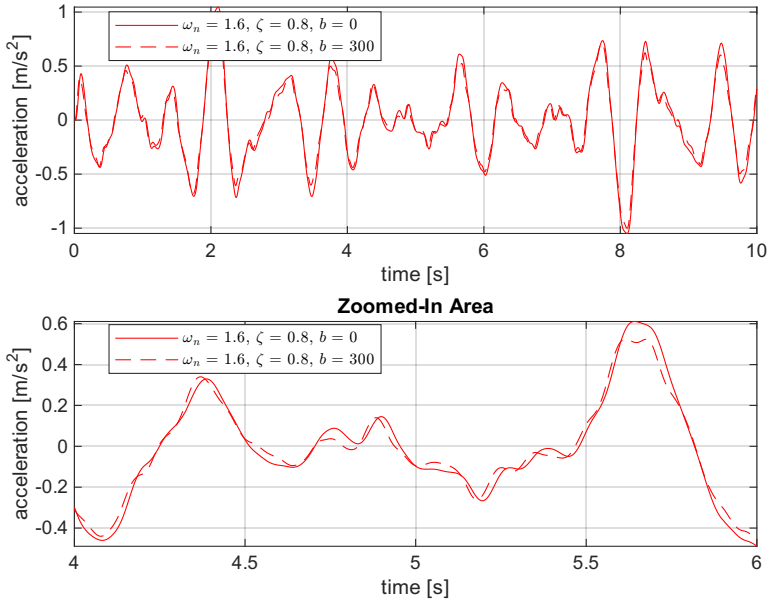

Figure 4.8 Seat fore-aft weighted acceleration plot for the highest $w_n - \zeta$ pair with and without inerter from Simulink time domain simulation, case-1.

The PSD plot for cab deflection is depicted in Figure 4.9, which is derived from its analytical definition.

For the high frequency-damping pair, the differences in magnitude are minimal up to 2 Hz. Afterward, there is a slight lower magnitude with the inerter, resulting in almost no effect on the RMS deflection, as seen in Figure 4.1. This is because the magnitudes are very low in the range where the magnitude is lower, and the contribution to the integral is minimal, considering the plots are in log scale.

On the other hand, the decrease for the low frequency-damping pair is more pronounced at lower frequencies where the magnitudes are higher, and its effect is therefore much greater, as can again be seen in Figure 4.1.

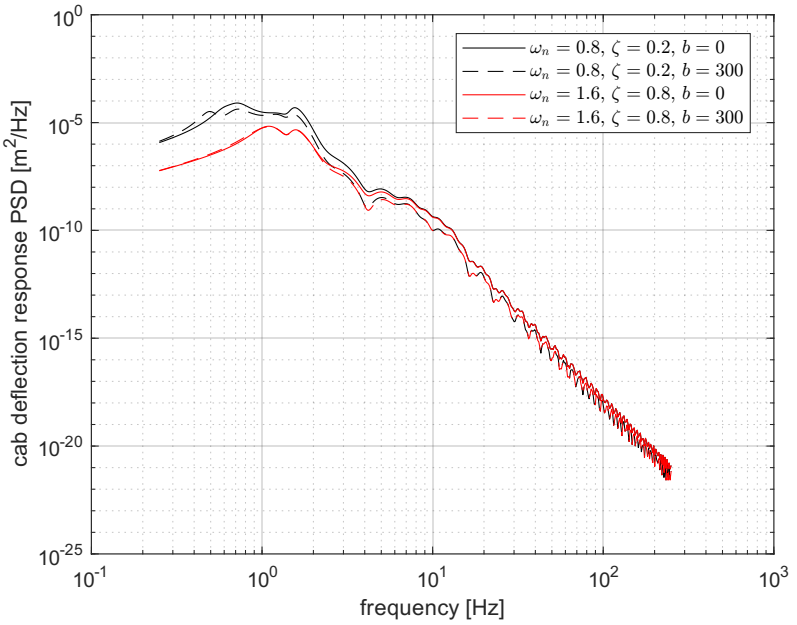

Figure 4.9 Cab deflection PSD plots for the highest and lowest $w_n - \zeta$ pairs, comparing inerter and non-inerter versions, Case 1.

Lastly, the time domain simulation results are presented in Figures 4.10 and 4.11. Both graphs reveal that the response in time is predominantly influenced by the low frequencies up to 1.5 Hz. Smaller magnitude higher frequency content is also noticeable for the high natural frequency-damping ratio pair.

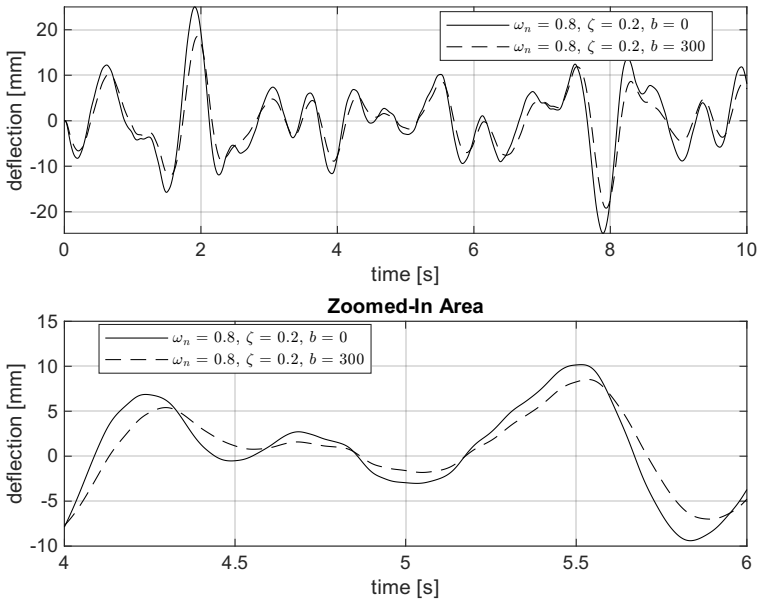

Figure 4.10 Cab deflection plot for the lowest $w_n - \zeta$ pair with and without inerter from Simulink time domain simulation, case-1.

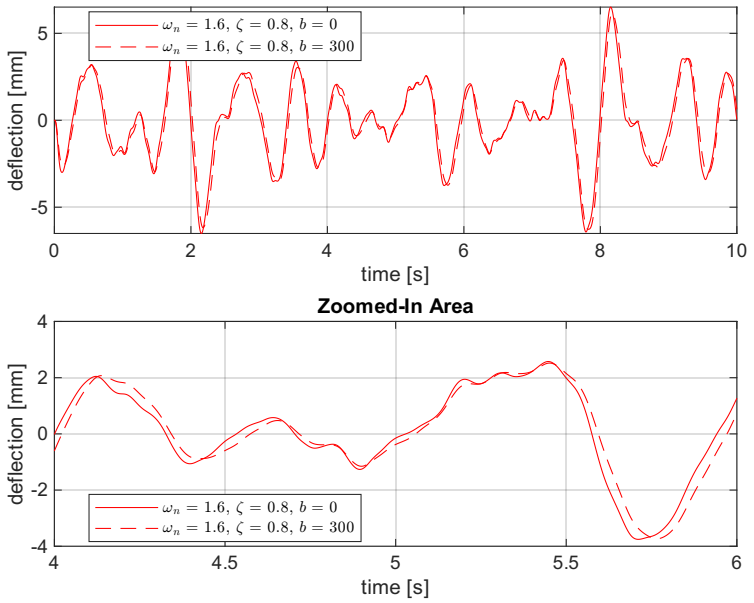

Figure 4.11 Cab deflection plot for the highest $w_n - \zeta$ pair with and without inerter from Simulink time domain simulation, case-1.

4.2. Case 2: Inerter at rear cab suspension, velocity is 90 km/h

The findings for Case 2 exhibit a similar trend to those observed in Case 1. The weighted RMS acceleration and RMS cab deflection results are depicted in Figure 4.12. Generally, it is noted that inertance has a positive effect on isolation performance. For the lowest undamped natural frequency and damping pair, a significant decrease in RMS deflection is evident, accompanied by a considerable reduction in weighted RMS acceleration by 15% and 11% respectively. Following the constant frequency path to the left side, again, the impact diminishes. Conversely, for values corresponding to the highest frequency-damping pair, while the weighted combined RMS acceleration decreases by 5%, the RMS deflection value remains relatively unchanged, with only a 1% reduction.

The results pertaining to each pair with 0 kg of inertance (i.e., no inerter) and with 300 kg of inertance are presented in Table 4.2. The relative changes are also calculated and listed in this table.

Overall, it can be inferred that the impact of an inerter, when applied at the rear cab suspension, is most pronounced with lower damping ratios, as in the case of Case 1.

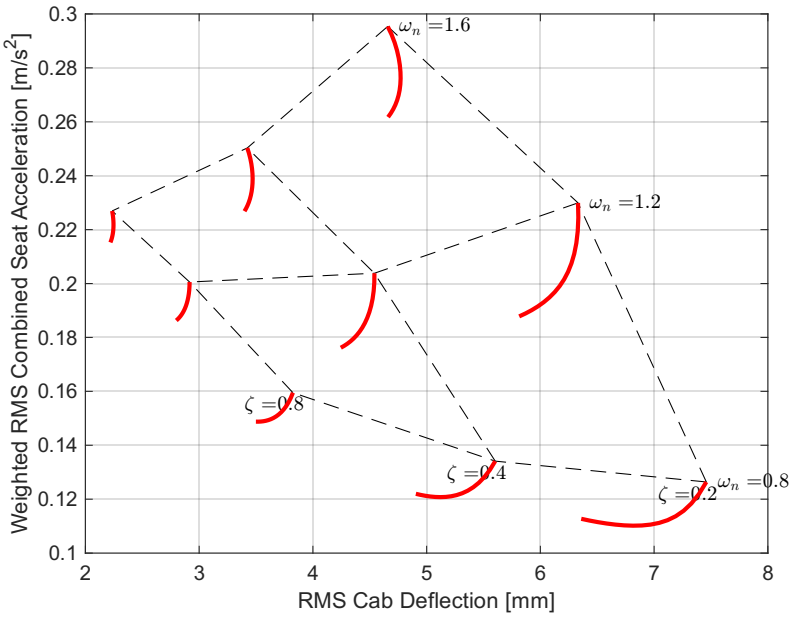

Figure 4.12 Illustration of RMS value changes with increasing inertance for all $w_n - \zeta$ pairs in Case 2.

Table 4.2 Summarized RMS results for case-2.

w_n	ζ	Seat Weighted RMS Acceleration $[m/s^2]$									Cab RMS deflection $[mm]$		
		fore-aft			vertical			combined					
		b=0	b=300	relative change	b=0	b=300	relative change	b=0	b=300	change	b=0	b=300	relative change
0.8	0.2	0.0403	0.0794	97%	0.1198	0.08	-33%	0.1264	0.1127	-11%	7.4591	6.3592	-15%
0.8	0.4	0.0403	0.0666	65%	0.1279	0.1022	-20%	0.1341	0.122	-9%	5.6031	4.9052	-12%
0.8	0.8	0.0426	0.0514	21%	0.1537	0.1396	-9%	0.1595	0.1488	-7%	3.8243	3.4988	-9%
1.2	0.2	0.0418	0.074	77%	0.2261	0.1726	-24%	0.2299	0.1878	-18%	6.331	5.8139	-8%
1.2	0.4	0.0432	0.0535	24%	0.1992	0.1679	-16%	0.2038	0.1762	-14%	4.5408	4.2455	-7%
1.2	0.8	0.0447	0.0403	-10%	0.1955	0.1819	-7%	0.2006	0.1863	-7%	2.9158	2.7989	-4%
1.6	0.2	0.0624	0.0494	-21%	0.2887	0.257	-11%	0.2954	0.2617	-11%	4.6577	4.6609	0%
1.6	0.4	0.0508	0.0339	-33%	0.2451	0.2243	-8%	0.2503	0.2268	-9%	3.423	3.3988	-1%
1.6	0.8	0.0457	0.0346	-24%	0.2223	0.2125	-4%	0.2269	0.2152	-5%	2.2347	2.2196	-1%

The non-dimensional parameter results are depicted in Figure 4.13, echoing the observations made in Case 1. The more pronounced changes with softer suspensions is evident. However,

similar to Case 1, due to high deflections, softer suspensions perform considerably worse than those with higher damping ratios. The best-performing pair, as indicated by the blue dashed line which is the closest point to 0, corresponds to a 1.6 Hz undamped natural frequency and 0.8 damping ratio with a 300 kg inertance. In comparison to the best-performing suspension from Case 1, the suspension with an inerter at the rear cab performs slightly worse, with both providing a 1% reduction in deflection and respectively 8% and 5% reduction in the weighted combined RMS seat acceleration.

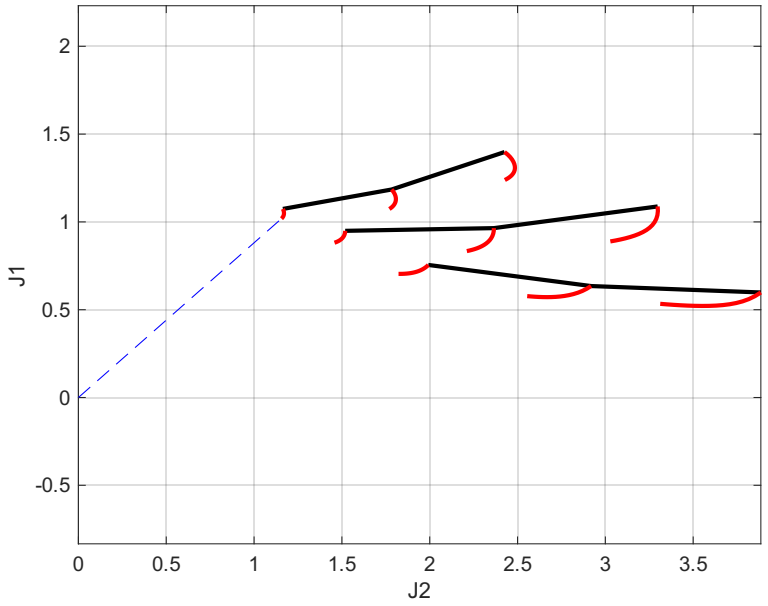

Figure 4.13 Illustration of non-dimensional parameter changes with increasing inertance for all $w_n - \zeta$ pairs in Case 2.

The analytically obtained PSD functions are plotted for the highest and lowest frequency-damping pairs in Figure 4.14. Degraded performance at higher frequencies becomes obvious after roughly 5 Hz for both pairs and the responses around 1.5 Hz are predominant in magnitude. In this region, it is observed that the inerter based suspension has a much higher response for the low natural frequency-damping pair, indicating the performance degradation listed in 4.2 as %97 increase in weigted fore-aft RMS seat acceleration. The improvement is noticeable for the high natural frequency-damping pair around 1.5-2.5 Hz band, where the red dashed line is stays below the red solid line. As the

figure in log scale and the RMS values is the related to the square root of the area under the curve, larger amplitudes on the plot have much more impact on the area than the smaller values. The reduction in weighted RMS acceleration is listed as %24 in table 4.2.

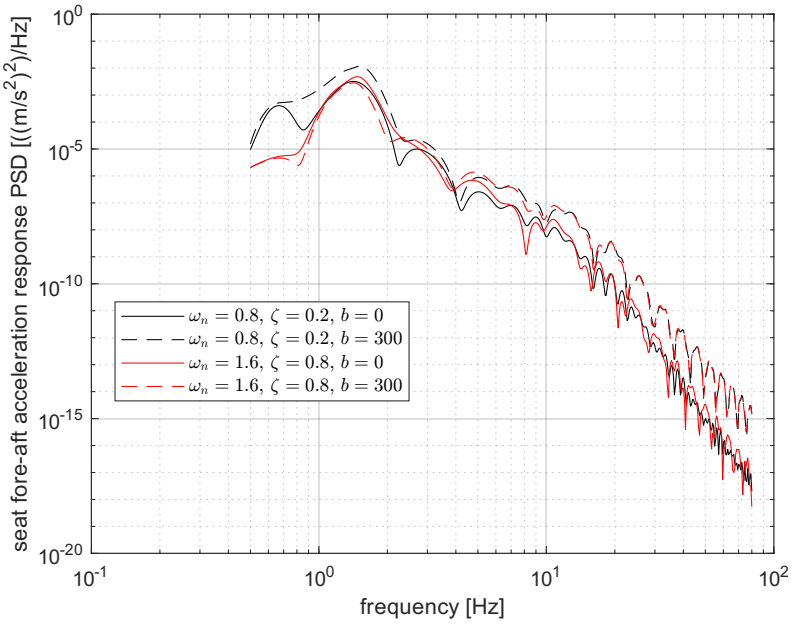

Figure 4.14 Seat fore-aft weighted acceleration PSD plots for the highest and lowest $w_n - \zeta$ pairs, comparing inerter and non-inerter versions, Case 2.

Figures 4.15 and 4.16 depict the seat fore-aft weighted acceleration response in the time domain. These graphs are obtained through time-domain simulations in a Simulink model.

In Figure 4.15, the deteoriated performance of the low frequency-damping pair is observable. The peaks are seen to be larger with the inerter than without. Furthermore, the response is significantly dominated by frequencies around 1.5 Hz which is also the predominant frequeny in the PSD plot.

Conversely, in Figure 4.16, the improvement in the acceleration isolation with inerter is evident. The response becomes much smaller with the inerter at the cab rear suspension for the high natural frequency-damping ratio pair, which reflects the reduction in the PSD plot very well.

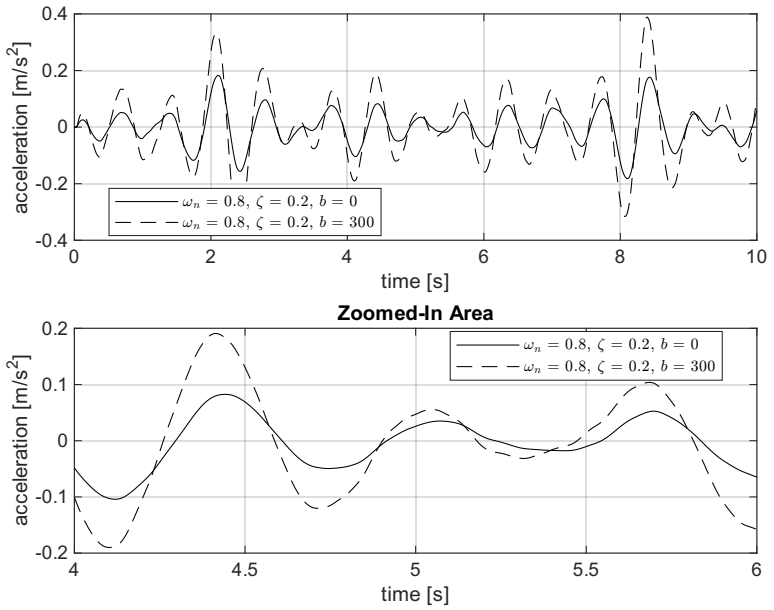

Figure 4.15 Seat fore-aft weighted acceleration plot for the lowest $w_n - \zeta$ pair with and without inerter from Simulink time domain simulation, case-2.

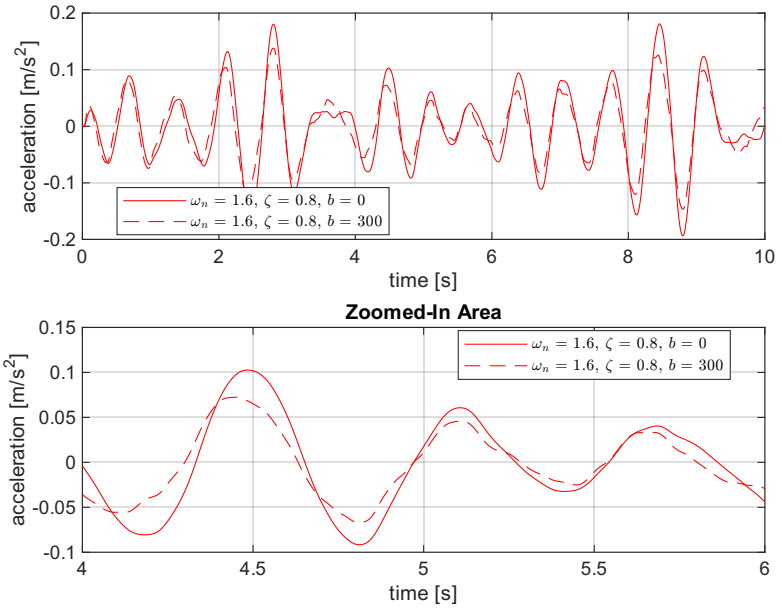

Figure 4.16 Seat fore-aft weighted acceleration plot for the highest $w_n - \zeta$ pair with and without inerter from Simulink time domain simulation, case-2..

The analytically obtained PSD functions for the seat vertical weighted acceleration are plotted in Figure 4.17. Suspension with low natural frequency-damping ratio has much lower acceleration values in 0.6 - 2 Hz band and the detoireted performance is evident after about 3 Hz. In total, from table 4.2, it is seen that the RMS acceleration reduces by %33 for this pair. For the high w_n, ζ pair, inerter provides only a small reduction is 1-7 Hz band and after then isolation deteriorates. However, as the magnitudes are much higher in this band, its impact on the area is also larger and hence, in total %4 percent reduction is seen.

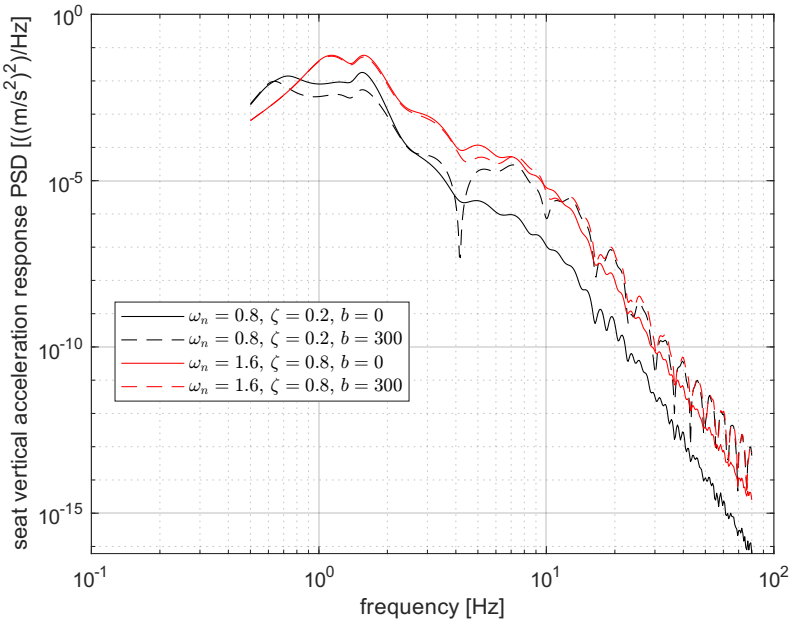

Figure 4.17 Seat vertical weighted acceleration PSD plots for the highest and lowest $w_n - \zeta$ pairs, comparing inerter and non-inerter versions, Case 2.

Time domain simulation results for the weighted vertical seat acceleration responses are given in figures 4.18 and 4.19. In the first figure the reduction in the acceleration peaks with inerter is evident together with the degraded performance at the higher frequencies are still pronounced. In the second plot, there is only a slight reduction is seen as expected and both inerter and non-inerter suspensions has almost the same responses in time.

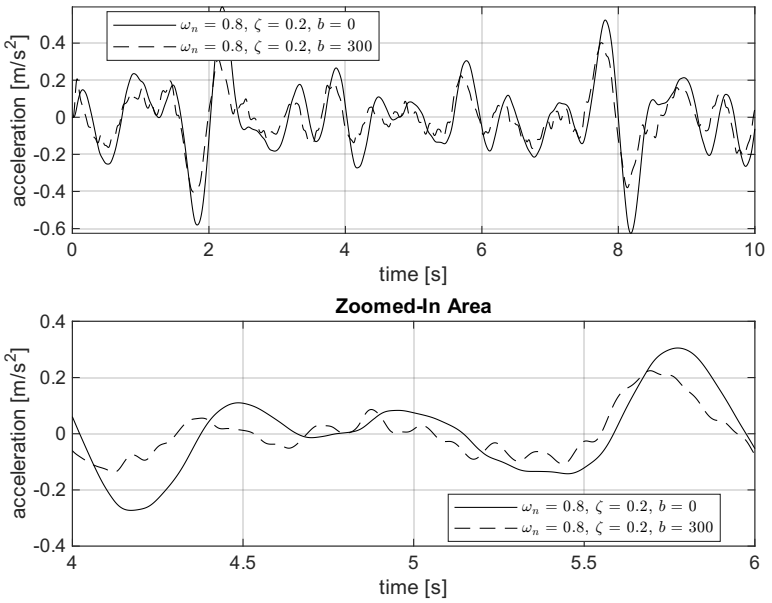

Figure 4.18 Seat vertical weighted acceleration plot for the lowest $w_n - \zeta$ pair with and without inerter from Simulink time domain simulation, case-2.

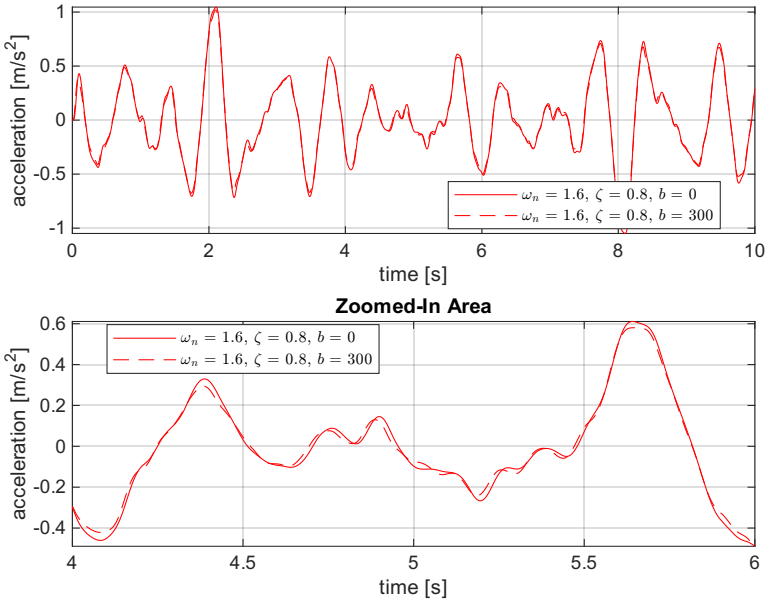

Figure 4.19 Seat vertical weighted acceleration plot for the highset $w_n - \zeta$ pair with and without inerter from Simulink time domain simulation, case-2.

The PSD of the cab deflection is plotted in figure 4.20 from its analytical definition. %15 reduction for the in the deflection for the low frequency-damping pair seen to be provided by the reduction in response after 0.7 Hz. For the high damping and natural frequency pair it was listed only %1 reduction in the deflection and it also seen in the second figure that the deflection responses are almost identical and in RMS value does not change very much.

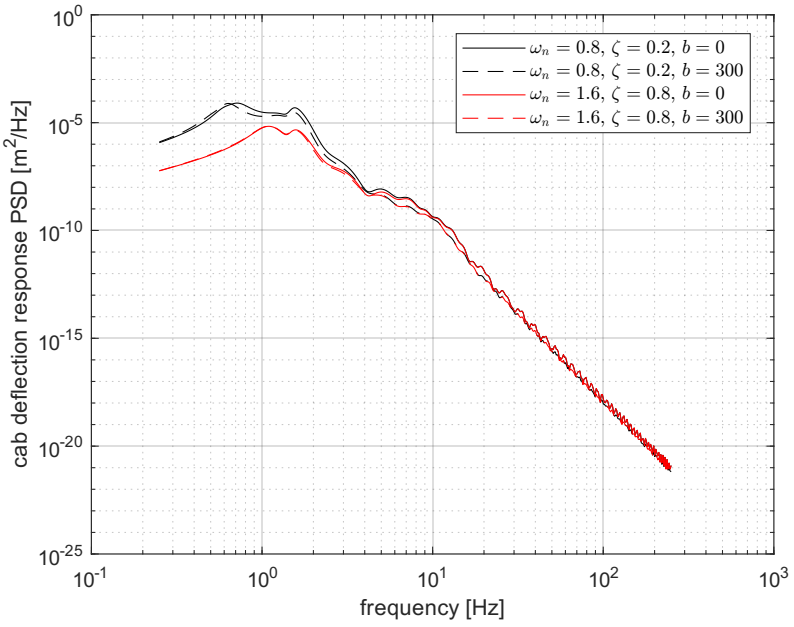

Figure 4.20 Cab deflection PSD plots for the highest and lowest $w_n - \zeta$ pairs, comparing inerter and non-inerter versions, Case 2.

Time domain simulation results for the cab deflection depicted in figures 4.21 and 4.22 also reflect the findings from the PSD plots. Deflections found to be much smaller in magnitude with inerter for the low natural frequency-damping ratio pair which reflects the %15 reduction in the RMS value. Very close response is observable for the high damping pair and this explains the only %1 change in the RMS value.

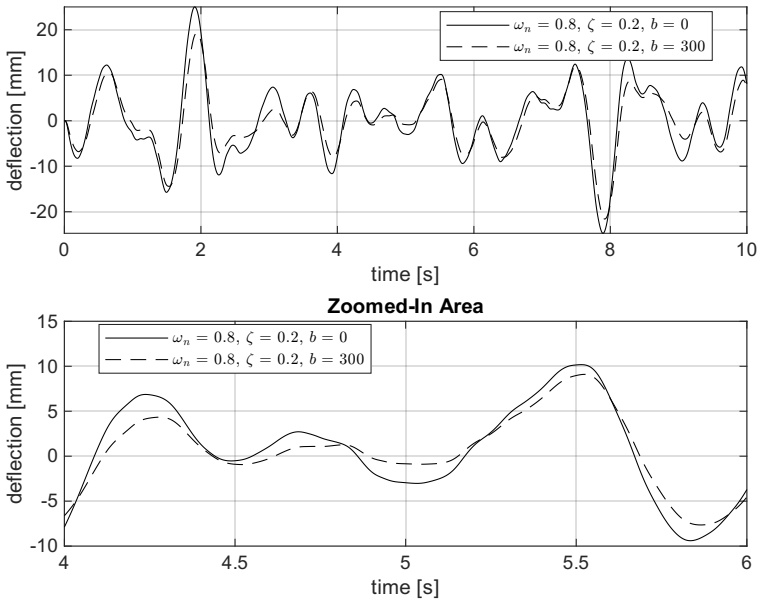

Figure 4.21 Cab deflection plot for the lowest $w_n - \zeta$ pair with and without inerter from Simulink time domain simulation, case-2.

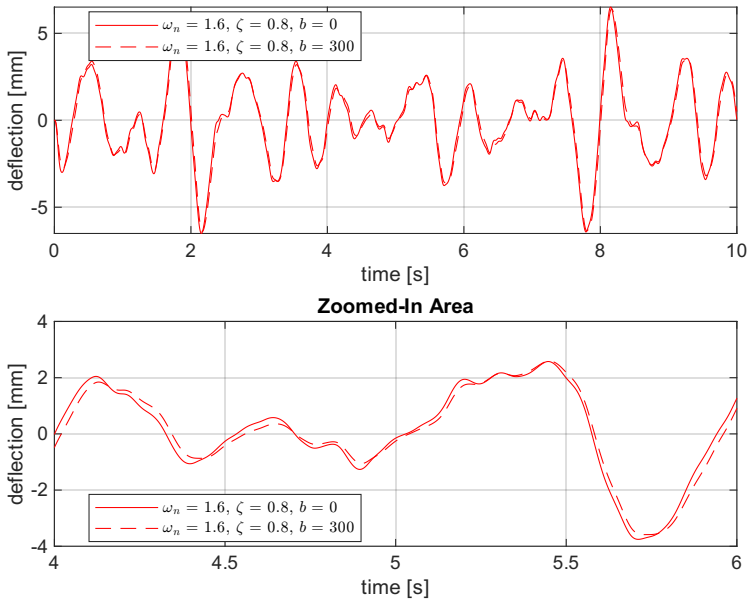

Figure 4.22 Cab deflection plot for the highset $w_n - \zeta$ pair with and without inerter from Simulink time domain simulation, case-2.

4.3. Case 3: Inerter at front and rear cab suspension, velocity is 90 km/h

In case-3, both front and rear suspensions of the cab has an inerter. The RMS results presented in figure 4.23 and the similar pattern is observed as previous cases but with larger effects. This is evident of longer paths of each pairs and cause by the doubled inertance value because both front and rear suspensions have inerters which essentially doubles the total inertance of the cab suspension system. This increase also reveals the limits of reductions in acceleration RMS for all pairs with $w_n = 0.8$, which is evident from the minimas after which the acceleration RMS values are increasing.

The RMS results together with their relative changes are tabulated in table 4.3. Wieghted fore-aft RMS acceleration is increased for all suspension pairs with 0.8 and 1.2 Hz except the pair with $w_n = 1.2, \zeta = 0.8$ which reduces the fore-aft RMS by $\%1$. The vertical and combined weighted RMS values are decreased for all pairs and the deflection RMS values are decreased for all pairs with 0.8 and 1.2 Hz natural frequency. Slight increases in the cab deflection are noted for the pairs with 1.6 Hz of natural frequency.

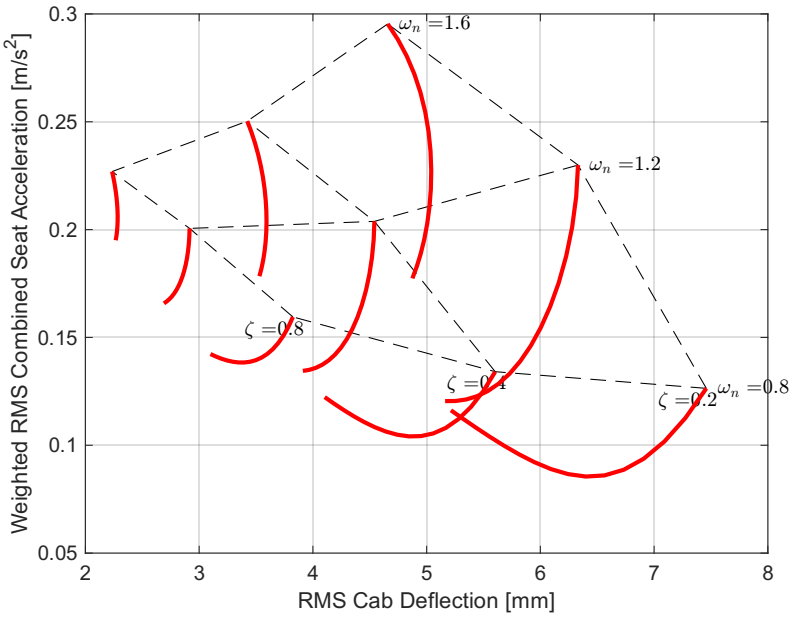

Figure 4.23 Illustration of RMS value changes with increasing inertance for all $w_n - \zeta$ pairs in Case 3.

Table 4.3 Summarized RMS results for case-3

w_n	ζ	Seat Weighted RMS Acceleration $[m/s^2]$									Cab RMS deflection $[mm]$		
		fore-aft			vertical			combined					
		b=0	b=300	relative change	b=0	b=300	relative change	b=0	b=300	change	b=0	b=300	relative change
0.8	0.2	0.0403	0.0479	19%	0.1198	0.1059	-12%	0.1264	0.1162	-8%	7.4591	5.2137	-30%
0.8	0.4	0.0403	0.0465	15%	0.1279	0.1131	-12%	0.1341	0.1223	-9%	5.6031	4.1039	-27%
0.8	0.8	0.0426	0.0449	5%	0.1537	0.135	-12%	0.1595	0.1423	-11%	3.8243	3.0993	-19%
1.2	0.2	0.0418	0.047	12%	0.2261	0.1109	-51%	0.2299	0.1205	-48%	6.331	5.1624	-18%
1.2	0.4	0.0432	0.0452	5%	0.1992	0.1267	-36%	0.2038	0.1345	-34%	4.5408	3.9117	-14%
1.2	0.8	0.0447	0.0442	-1%	0.1955	0.1598	-18%	0.2006	0.1658	-17%	2.9158	2.6901	-8%
1.6	0.2	0.0624	0.0461	-26%	0.2887	0.1713	-41%	0.2954	0.1774	-40%	4.6577	4.8747	5%
1.6	0.4	0.0508	0.0448	-12%	0.2451	0.1727	-30%	0.2503	0.1784	-29%	3.423	3.5298	3%
1.6	0.8	0.0457	0.0442	-3%	0.2223	0.19	-15%	0.2269	0.1951	-14%	2.2347	2.2663	1%

The changes in the non-dimensional parameters are depicted in the figure 4.24. Similar to the previous cases, while softer suspensions having lower J1, due to the high deflections J2

becomes larger and the best performing suspension is the hardest pair with 1.6 Hz natural frequency and 0.8 damping ratio. This pairs J value is indicated with a blue dashed line which is the shortest distance from 0.

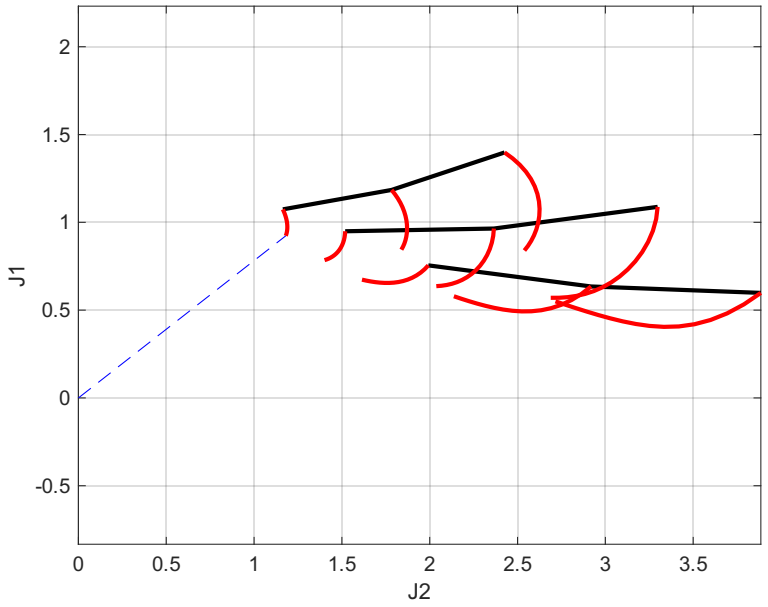

Figure 4.24 Illustration of non-dimensional parameter changes with increasing inertance for all $w_n - \zeta$ pairs in Case 3.

The PSD function of the weighted RMS fore-aft seat acceleration is plotted in the figure 4.25 from which the degraded performances of both pairs after around 10 Hz is evident. %19 increase in the RMS fore-aft acceleration with low damping pair is seen to be because of the higher acceleration magnitudes around 1.5 Hz. The high damping pair seen to be very close to each other with and without inerter and also only %3 reduction is obtained. This reduction is seen to be provided by the lower responses with inerter about 2-6 Hz band.

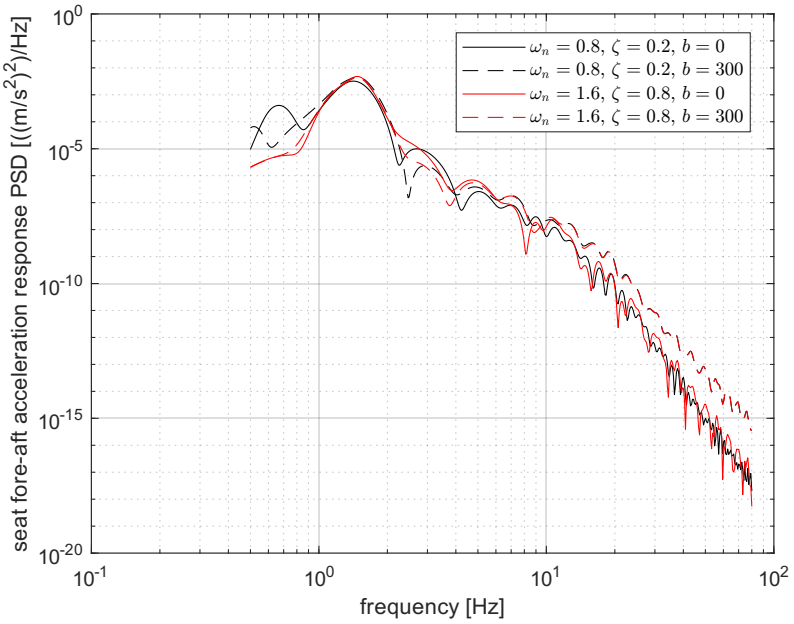

Figure 4.25 Seat fore-aft weighted acceleration PSD plots for the highest and lowest $w_n - \zeta$ pairs, comparing inerter and non-inerter versions, Case 3.

The predominant 1.5 Hz fore-aft acceleration responses are also to be seen in the figures 4.26 and 4.27 which both present the time domain simulation results for both lowest and highest $w_n - \zeta$ pairs, respectively. The increased acceleration is clear on the first plot which reflects the %19 increase in the RMS value and second graph shows that inerter based suspension has slightly lower amplitudes.

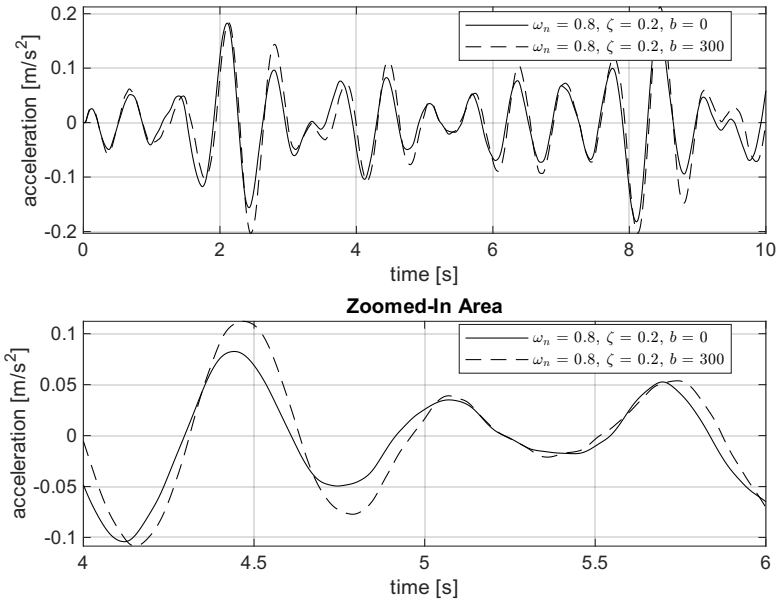

Figure 4.26 Seat fore-aft weighted acceleration plot for the lowest $w_n - \zeta$ pair with and without inerter from Simulink time domain simulation, case-3.

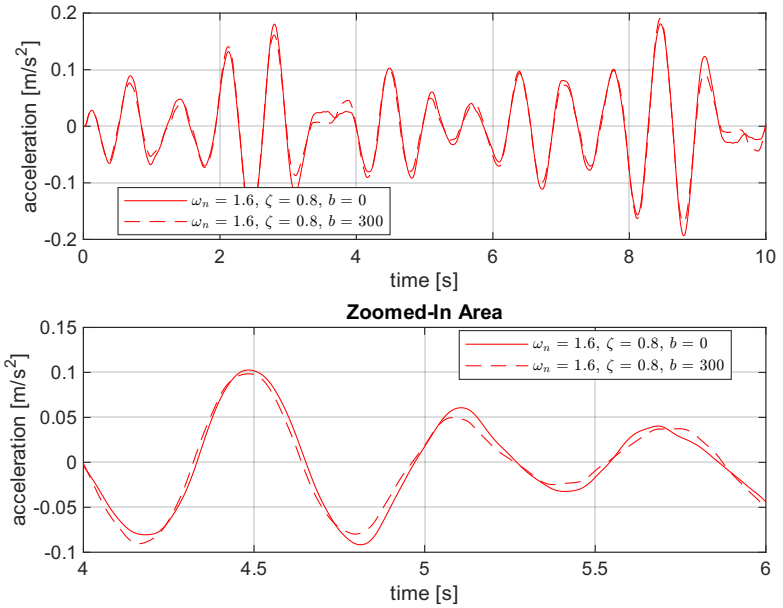

Figure 4.27 Seat fore-aft weighted acceleration plot for the highest $w_n - \zeta$ pair with and without inerter from Simulink time domain simulation, case-3.

Analytically obtained PSD functions of the weighted vertical seat acceleration is plotted in the figure 4.28 for the highest and lowest $w_n - \zeta$ pairs. Degradation in the isolation performance of the lowest $w_n - \zeta$ pair is clearly observable after about 1.5 Hz which is also the predominant for both pairs. %12 reduction in RMS acceleration of the lowest $w_n - \zeta$ pair seen to be caused by the lower amplitudes obtained up to 1.5 Hz, as the magnitudes are much higher at this band, impact on the RMS value is much greater.

High $w_n - \zeta$ pair seen to be having lower magnitudes with inerter from 0.9 Hz up to around 5 Hz which can be related to the listed %15 reduction in the RMS acceleration.

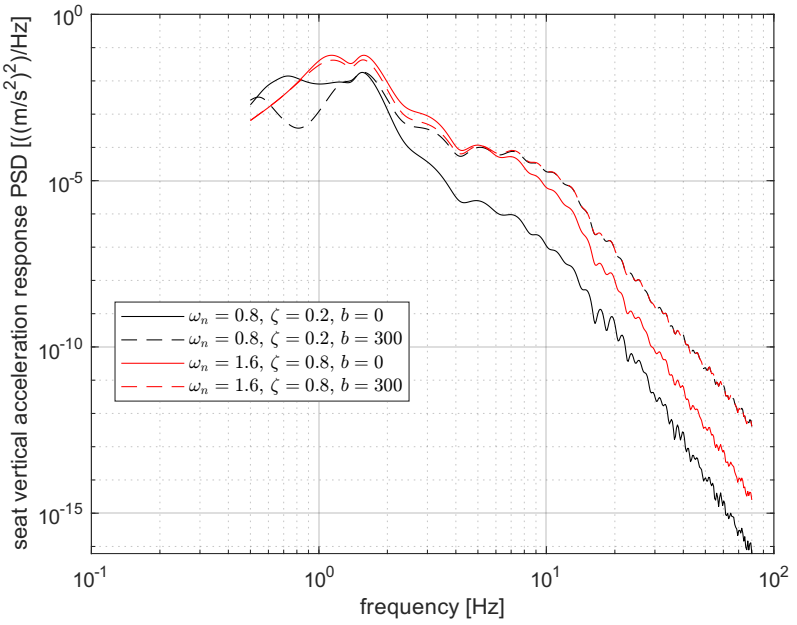

Figure 4.28 Seat vertical weighted acceleration PSD plots for the highest and lowest $w_n - \zeta$ pairs, comparing inerter and non-inerter versions, Case 3.

In PSD plots it was seen that the acceleration responses of both pairs has greater magnitudes at high frequencies. This also be seen in figures 4.29 and 4.30 which present the acceleration responses in time domain obtained through time domain simulations conducted in Simulink model. In both figures, higher frequency contents are pronounced for inerter based suspensions and for the low $w_n - \zeta$ pair with no inerter only lower frequency content is pronounced. The reductions in the RMS values however, are not very clear on time domain plots.

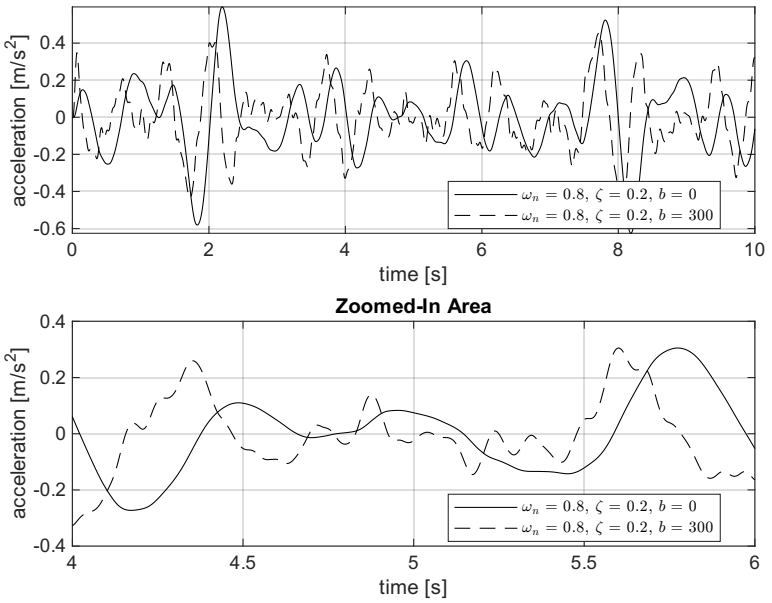

Figure 4.29 Seat vertical weighted acceleration plot for the lowest $w_n - \zeta$ pair with and without inerter from Simulink time domain simulation, case-3.

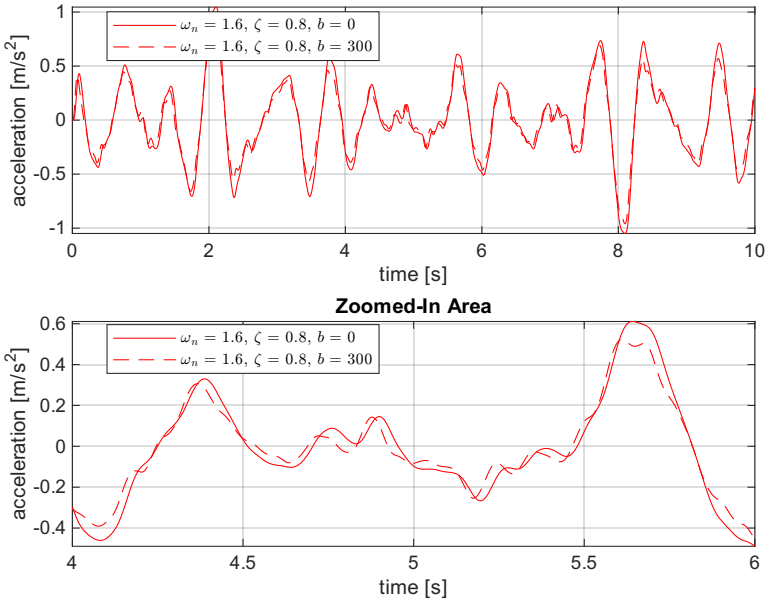

Figure 4.30 Seat vertical weighted acceleration plot for the highest $w_n - \zeta$ pair with and without inerter from Simulink time domain simulation, case-3.

The lower magnitudes after 0.6 Hz for the lowest $w_n - \zeta$ pair with an inerter, compared to its non-inerter response in the PSD graph given in figure 4.31, clearly explain the 30% reduction in the cab deflection listed in Table 4.3, despite the higher magnitudes seen below 0.6 Hz. High $w_n - \zeta$ pair seen to be not influenced by the inerter. Up to 1 Hz, a slight increase in the deflection magnitude is seen and after 2 Hz, the response with inerter becomes smaller in magnitude. However, as the RMS value is related to the area under the PSD curve, and because the graphs are in logarithmic scale, the impact of the high magnitudes on the given plot has much greater then the lower values which ultimately yields to only %1 increase in the RMS value.

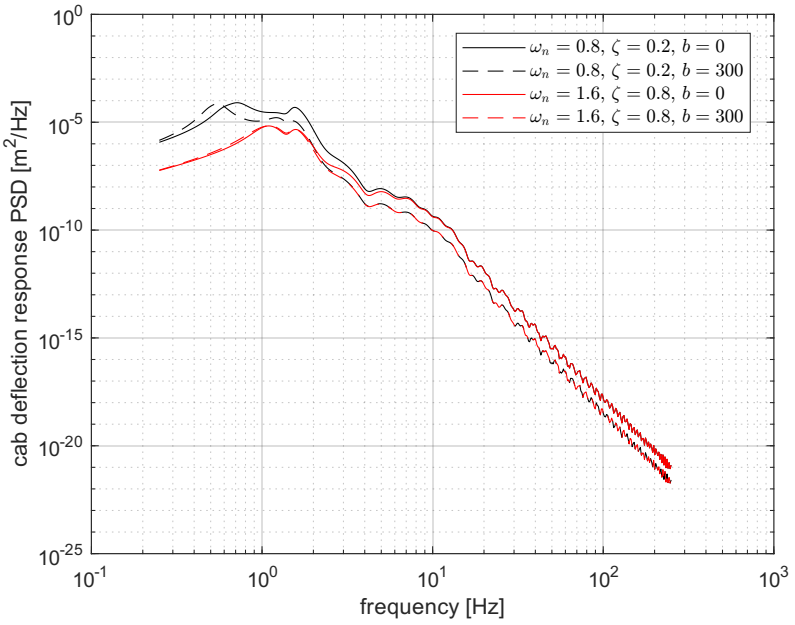

Figure 4.31 Cab deflection PSD plots for the highest and lowest $w_n - \zeta$ pairs, comparing inerter and non-inerter versions, Case 3.

The time domain simulations result are presented in the figures 4.32 and 4.33 which are obtained from Simulink model. Inerter based low $w_n - \zeta$ pair has significantly lower deflection values compared to its non-inerter counterpart and the response is predominated by lower frequency content as expected when the PSD results are considered. High $w_n - \zeta$ pair has very similar deflection values with shift which also evident in the PSD plot by

both inerter and non-inerter counterparts having very close magnitudes in the predominant frequency range.

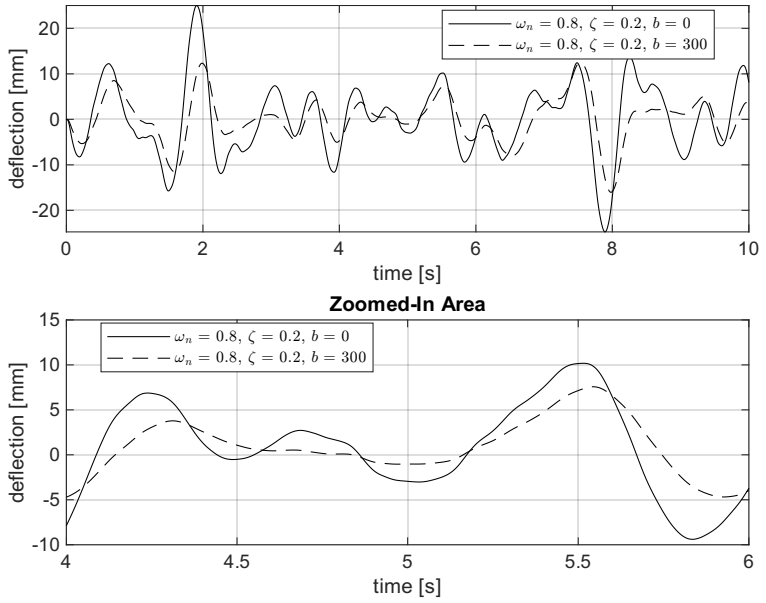

Figure 4.32 Cab deflection plot for the lowest $w_n - \zeta$ pair with and without inerter from Simulink time domain simulation, case-3.

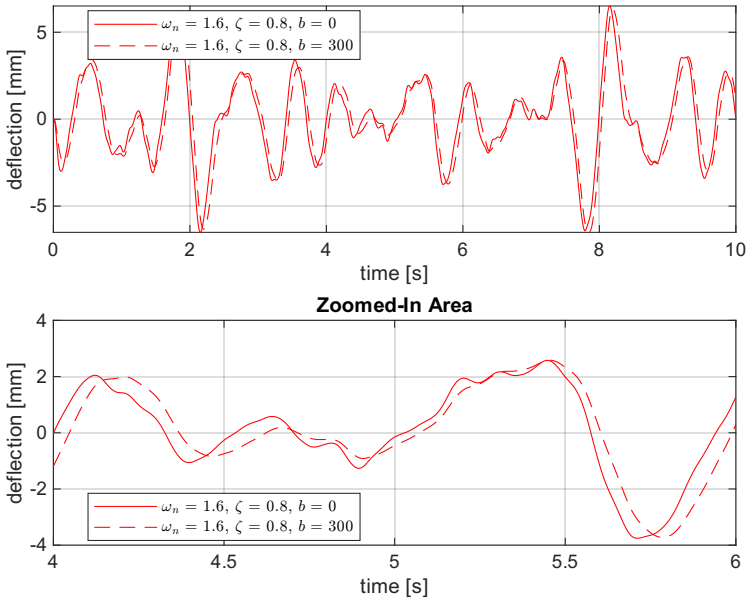

Figure 4.33 Cab deflection plot for the highest $w_n - \zeta$ pair with and without inerter from Simulink time domain simulation, case-3.

4.4. Case 4: Seat suspensions with inerters velocity is 90 km/h

Figure 4.34 presents the RMS fore-aft deflection versus weighted fore-aft RMS acceleration results for each pair and where they are moving with increasing inerter up to 30 kg. All pairs are seen to be moving in decreasing directions as the inertance increasing with larger changes, again as in the cases1 to case3, with softer suspension by the mean of natural frequency and damping ratio.

Figure 4.35 presents the RMS results in the vertical direction for each pair and the changes with increasing inerter up to 30 kg. Unlike the fore-aft direction, all pairs are seen to be moving more vertically which indicates a lower reduction in the deflection than the acceleration.

Table 4.4 summarizes the RMS results for each pairs in the both directions and for when inertances is 0 and its maximum value of 30 kg. The large reductions in acceleration values yields to %23-48 relative change in the fore-aft direction and between %15-30 in the vertical direction. When combined acceleration considered, up to %30 reduction possible with 1.2 Hz undamped natural frequency and 0.2 damping ratio. The changes in the RMS deflection values are higher in the fore-aft aft direction and all pairs have reduced values in this direction.

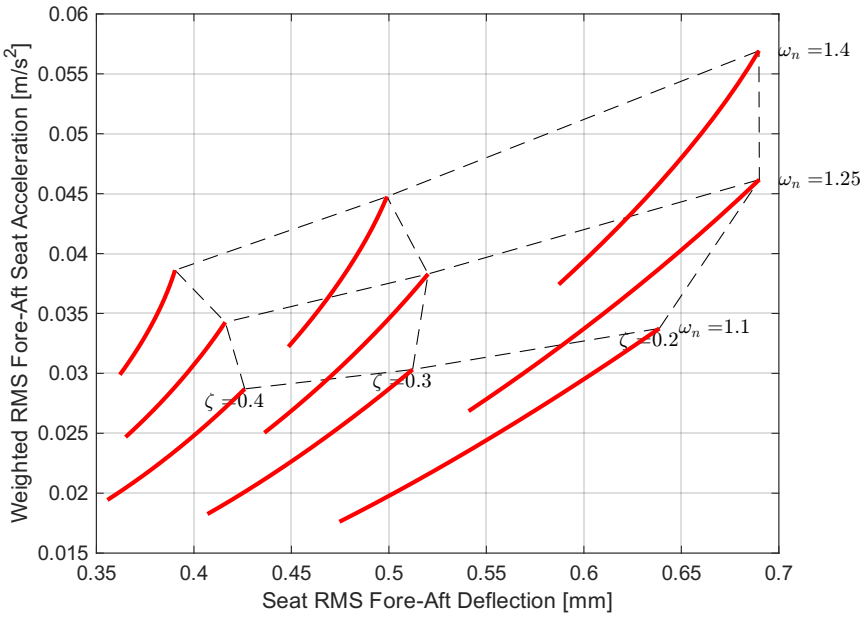

Figure 4.34 Illustration of RMS value changes with increasing seat fore-aft suspension inertance for all $w_n - \zeta$ pairs in Case 4.

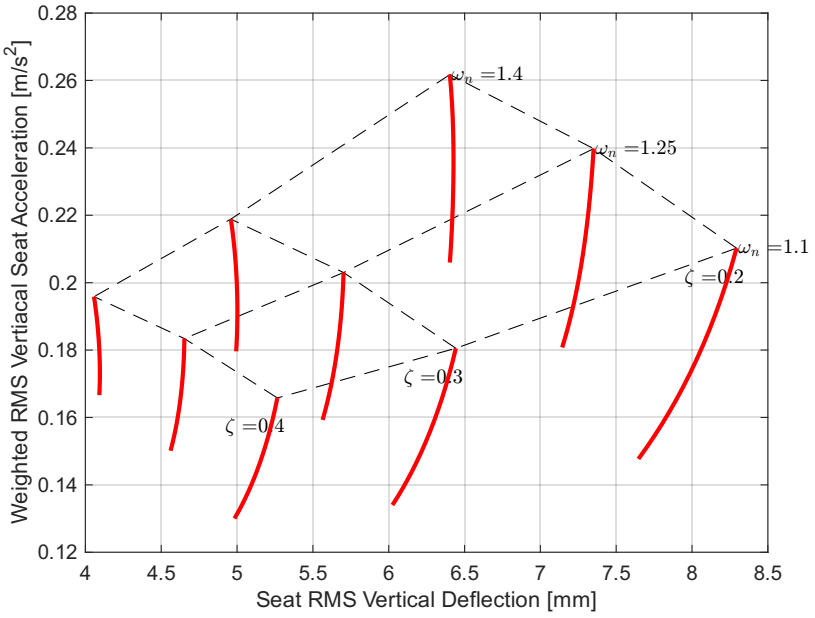

Figure 4.35 Illustration of RMS value changes with increasing seat vertical suspension inertance for all $w_n - \zeta$ pairs in Case 4.

Table 4.4 Summarized RMS values for case-4.

w_n	ζ	Seat Weighted RMS Acceleration $[m/s^2]$									Seat Suspension Deflection $[mm]$					
		fore-aft			vertical			combined			fore-aft			vertical		
		b=0	b=30	relative change	b=0	b=30	relative change	b=0	b=30	change	b=0	b=30	relative change	b=0	b=30	relative change
1.2	0.2	0.0338	0.0176	-48%	0.2102	0.1477	-30%	0.2129	0.1487	-30%	0.6387	0.4746	-26%	8.2937	7.6464	-8%
1.2	0.3	0.0303	0.0183	-40%	0.1805	0.134	-26%	0.1831	0.1353	-26%	0.5122	0.407	-21%	6.4425	6.0245	-6%
1.2	0.4	0.0287	0.0194	-32%	0.1658	0.13	-22%	0.1683	0.1315	-22%	0.4261	0.3556	-17%	5.2657	4.9829	-5%
1.4	0.2	0.0462	0.0269	-42%	0.2398	0.1808	-25%	0.2442	0.1828	-25%	0.69	0.5409	-22%	7.3511	7.144	-3%
1.4	0.3	0.0383	0.025	-35%	0.203	0.1593	-22%	0.2066	0.1612	-22%	0.5201	0.4361	-16%	5.7022	5.5638	-2%
1.4	0.4	0.0343	0.0247	-28%	0.1834	0.1501	-18%	0.1866	0.1522	-18%	0.4161	0.3649	-12%	4.6526	4.5614	-2%
1.6	0.2	0.0569	0.0374	-34%	0.2617	0.206	-21%	0.2679	0.2093	-22%	0.6898	0.5871	-15%	6.4032	6.4031	0%
1.6	0.3	0.0448	0.0322	-28%	0.2189	0.1796	-18%	0.2234	0.1825	-18%	0.499	0.4484	-10%	4.959	4.994	1%
1.6	0.4	0.0386	0.0299	-23%	0.1959	0.1666	-15%	0.1996	0.1693	-15%	0.3903	0.362	-7%	4.0567	4.0917	1%

Normalized non-dimensional parameters $J1$ and $J2$ are presented in the figures 4.36 and 4.37. Higher damping ratio pairs perform better in both directions at each natural frequency which is evident from that each constant frequency path are getting closer to 0 with increasing damping ratio (from right to left). The best performing isolator in the fore aft direction has 1.2 Hz natural frequency and 0.4 damping ratio and 1.6 Hz natural frequency 0.4 damping ratio pair performs the best in the vertical seat suspension.

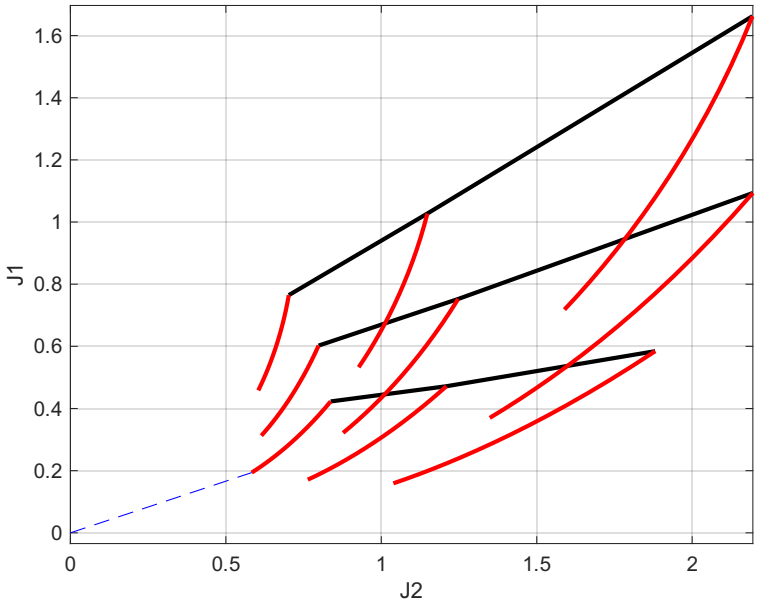

Figure 4.36 Illustration of non-dimensional parameters changes with increasing seat fore-aft suspension inertance for all $w_n - \zeta$ pairs in Case 4.

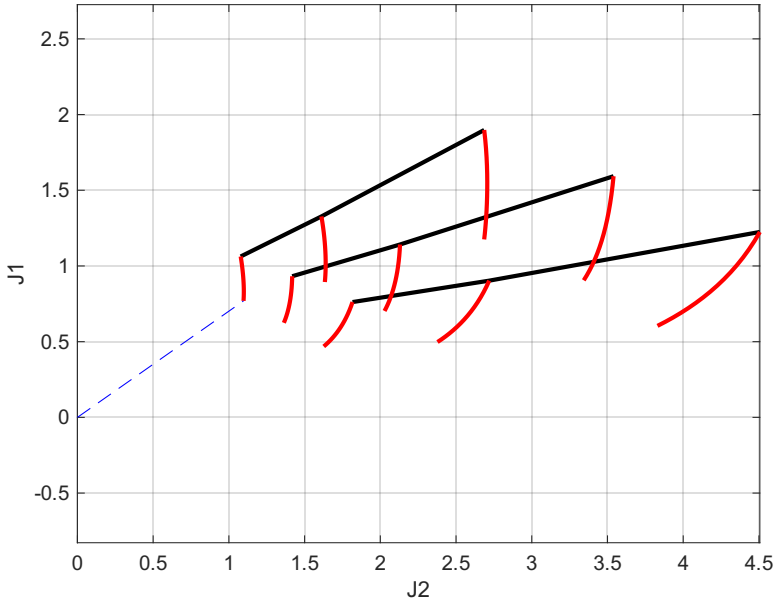

Figure 4.37 Illustration of non-dimensional parameters changes with increasing seat vertical suspension inertance for all $w_n - \zeta$ pairs in Case 4.

PSD of fore-aft weighted seat acceleration from its analytical definition plotted in figure 4.38. As expected and as in the previous cases, the deteriorated isolation performances with inerters at higher frequencies are evident after about 3.5 Hz for the 1.1 Hz pair and after about 5Hz for the pair with 1.4 Hz pair. There are great suppressions around the peak responses which explains the resultant RMS reduction listed in the table 4.4 with %48 and %28 for plotted pairs.

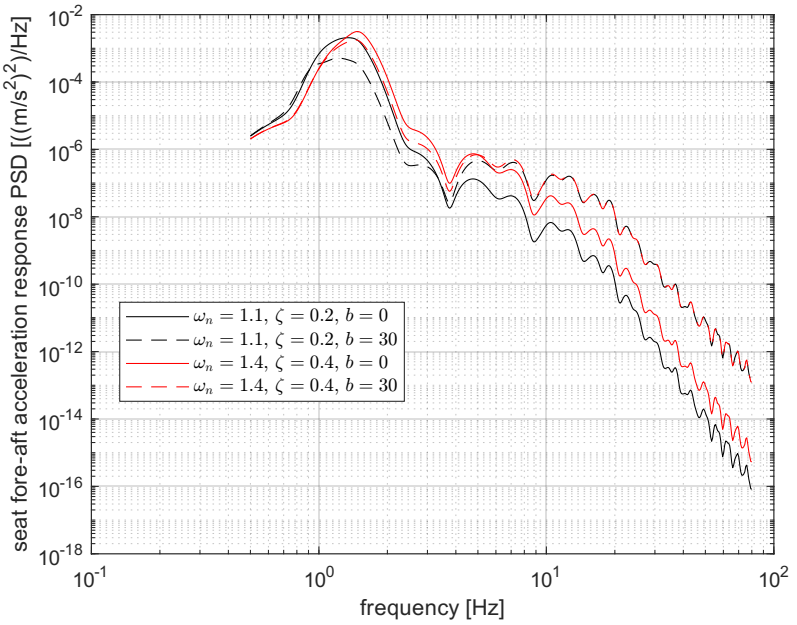

Figure 4.38 Seat fore-aft weighted acceleration PSD plots for the highest and lowest $w_n - \zeta$ pairs, comparing inerter and non-inerter versions, Case 4.

Time domain simulation results for fore-aft direction are presented in 4.39 and 4.40 in which the lower magnitudes with inerters seen. The predominated frequencies seen in the PSD plot observable on the time-domain plots and also due to the higher magnitude responses at higher frequencies with inerters, higher frequency content is also observable on the time history plots with $b = 30$, which is obtained seperately from Simulink simulation.

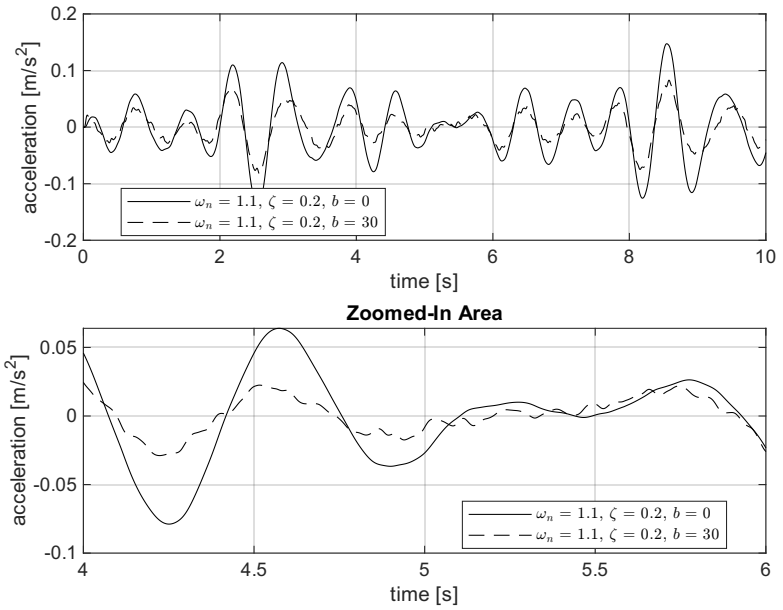

Figure 4.39 Seat fore-aft weighted acceleration plot for the lowest $w_n - \zeta$ pair with and without inerter from Simulink time domain simulation, case-4.

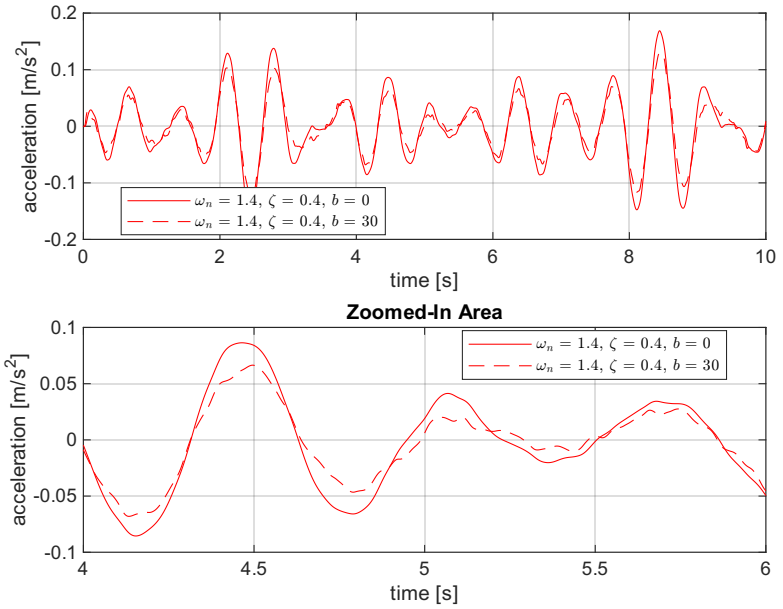

Figure 4.40 Seat fore-aft weighted acceleration plot for the highest $w_n - \zeta$ pair with and without inerter from Simulink time domain simulation, case-4.

The PSD for the vertical weighted seat acceleration is plotted from its analytical definition is plotted in the figure 4.41. Performance degradation is visible at higher frequencies and the suppression in the magnitude around natural frequencies are evident which relates to the reduction in the RMS values of %30 and %15 for the plotted pairs.

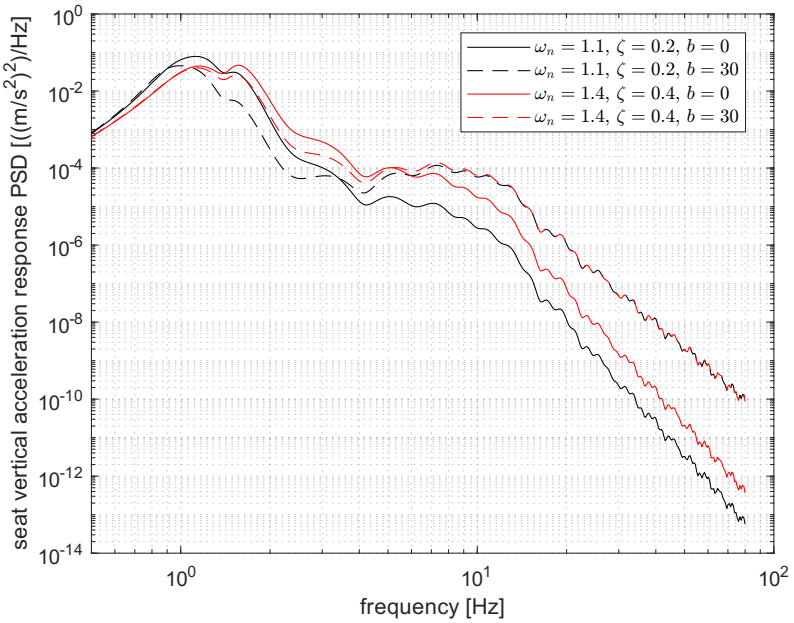

Figure 4.41 Seat vertical weighted acceleration PSD plots for the highest and lowest $w_n - \zeta$ pairs, comparing inerter and non-inerter versions, Case 4.

Time domain simulation results also reflect the reduced responses around the natural frequencies together with the increased increased responses at higher frequencies. In both plots, higher frequency content is more pronounced as depicted in the figures 4.42 and 4.43.

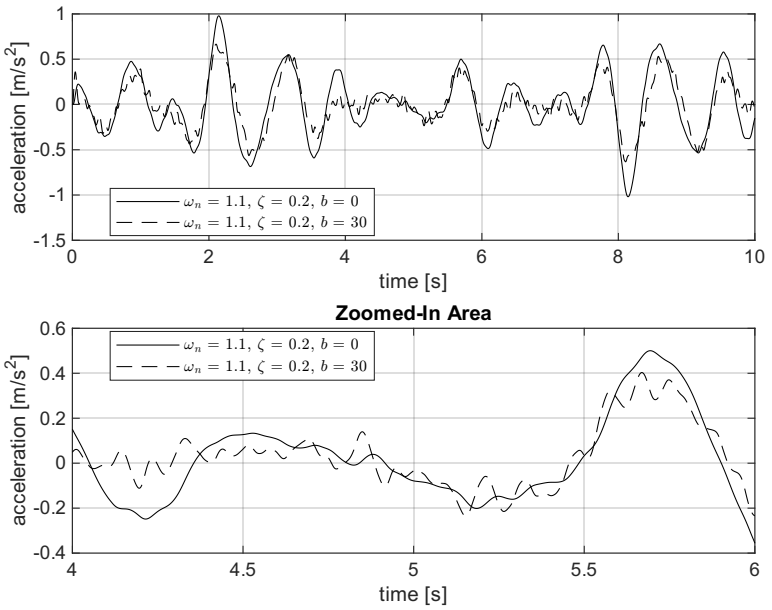

Figure 4.42 Seat vertical weighted acceleration plot for the lowest $w_n - \zeta$ pair with and without inerter from Simulink time domain simulation, case-4.

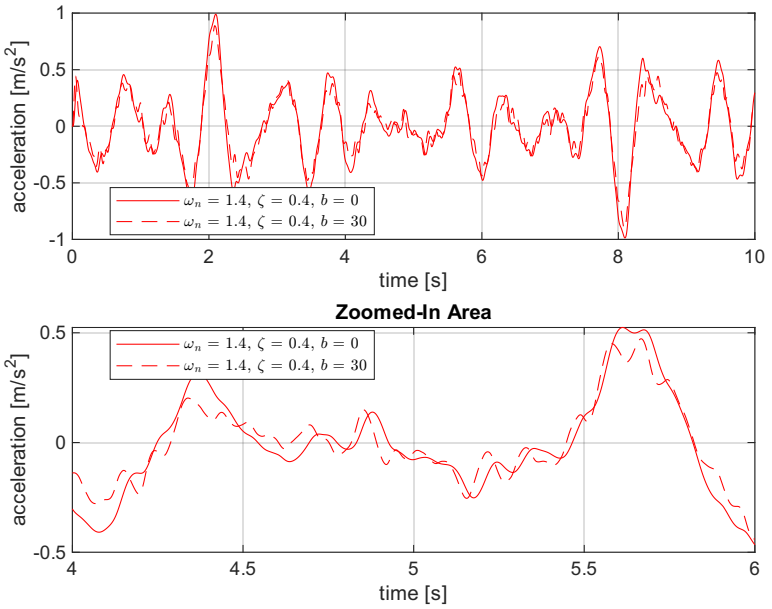

Figure 4.43 Seat vertical weighted acceleration plot for the highest $w_n - \zeta$ pair with and without inerter from Simulink time domain simulation, case-4.

In the PSD plots for the seat fore-aft deflection, it is observed that the pair with $w_n = 1.1, \zeta = 0.2$ more suppressed magnitude around the natural frequency and this reflects the listed change of %26 reduction in the RMS value in the table 4.4. The other plotted pair seen to be less changing in the magnitude with inerter and this explains the tabulated change of %7 reduction. For both pairs, there is slightly less deflection at the high frequencies.

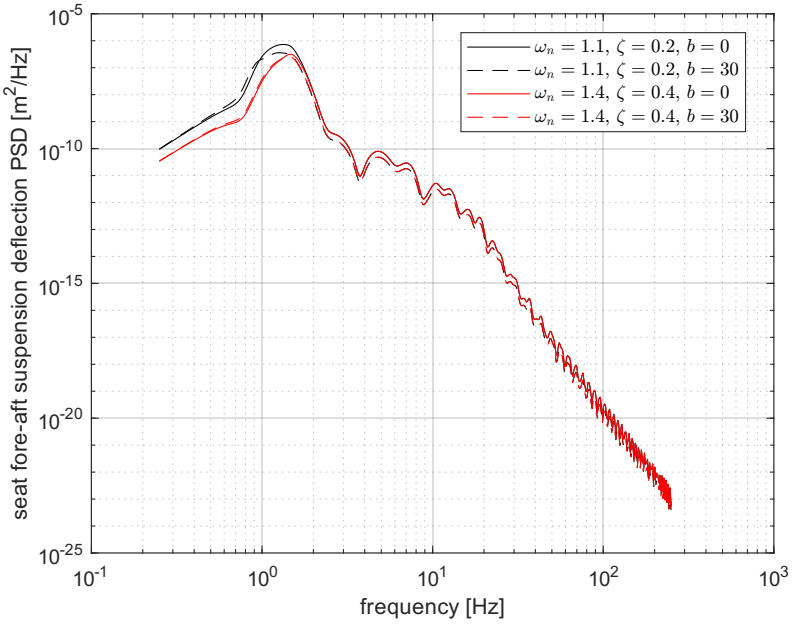

Figure 4.44 Seat fore-aft suspension deflection PSD plots for the highest and lowest $w_n - \zeta$ pairs, comparing inerter and non-inerter versions, Case 4.

Seat fore-aft deflection time history plots are given from the Simulink simulations in below figures 4.45 and 4.46. The reduced magnitude around the natural frequency is clearly represented in the firs plot with lower deflection values. İt is also similar for the second figure but the suppressed amplitudes are less pronounced.

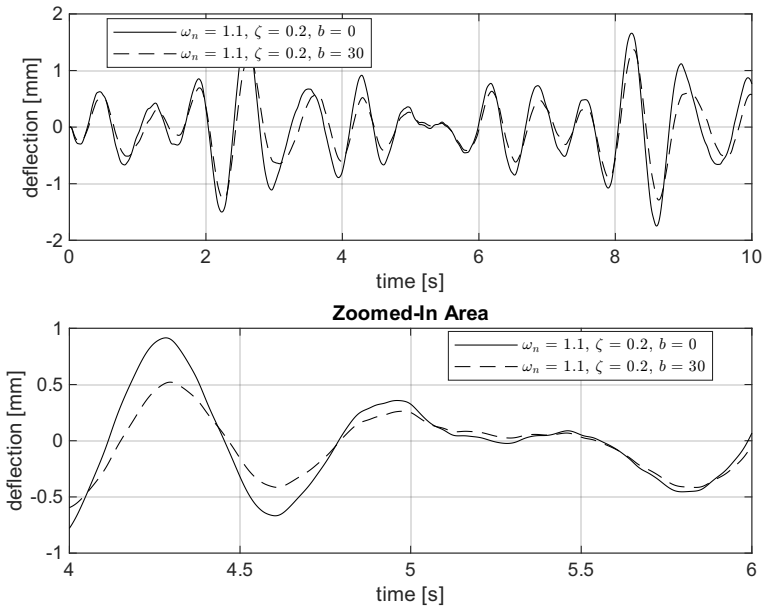

Figure 4.45 Seat suspension fore-aft deflection plot for the lowest $w_n - \zeta$ pair with and without inerter from Simulink time domain simulation, case-4.

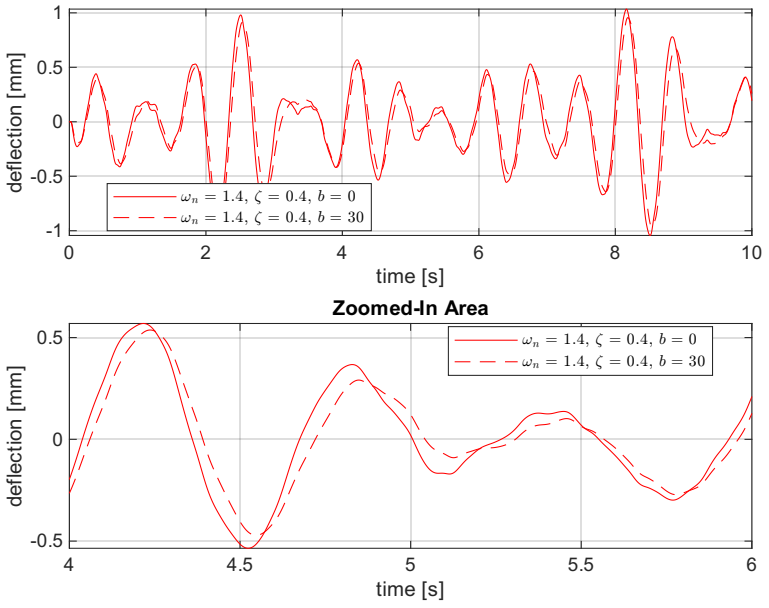

Figure 4.46 Seat suspension fore-aft deflection plot for the highest $w_n - \zeta$ pair with and without inerter from Simulink time domain simulation, case-4.

Seat vertical deflection PSD plot depicted in the figure 4.47 in which the magnitudes of the pair with $w_n = 1.1$ Hz has reduction starting at around 1.1 Hz and before the magnitudes seen to be greater which indicates deteriorated performance before the natural frequency. The same trend is also evident for the 1.4 Hz pair with degraded performance until 1.4 Hz and reduction in the deflection after that point. The changes in magnitudes seen to be more for the $w_n = 1.1Hz$ pair than the other one and this is reflected in the table with the changes in the RMS values of %8 reduction for the 1.1 Hz pair and %1 increase for the 1.4 Hz pair.

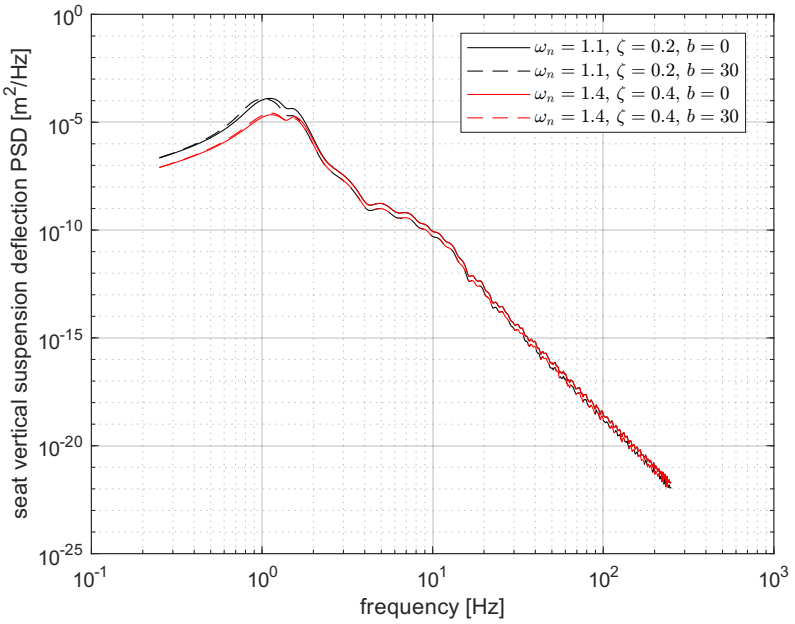

Figure 4.47 Seat vertical suspension deflection PSD plots for the highest and lowest $w_n - \zeta$ pairs, comparing inerter and non-inerter versions, Case 4.

Time domain simulation results are shown in the figures 4.48 and 4.49 both reflecting the findings in the PSD plots. In the first figure, it iseen that the deflection values are generally smaller and the predominant frequency is slightly lower with inerter and in the second figure it is seen that the differences between inerter and non-inerter suspension has closer response in time.

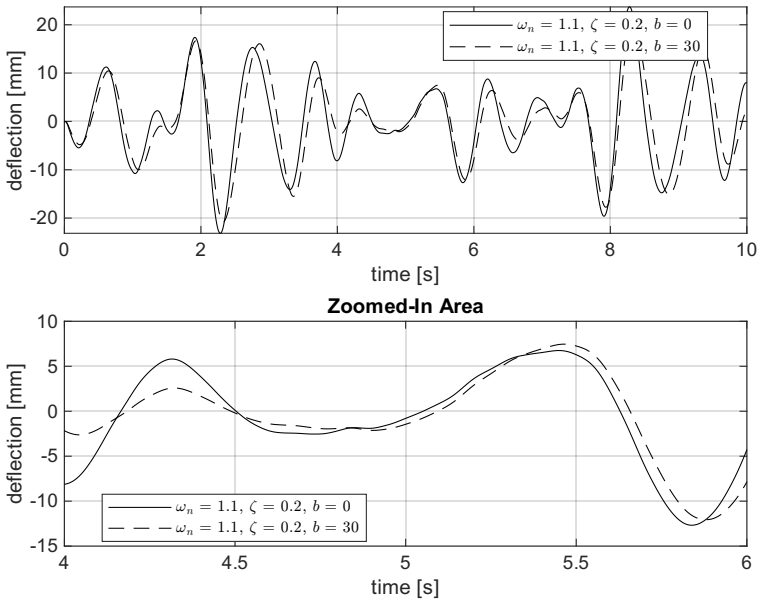

Figure 4.48 Seat suspension vertical deflection plot for the lowest $w_n - \zeta$ pair with and without inerter from Simulink time domain simulation, case-4.

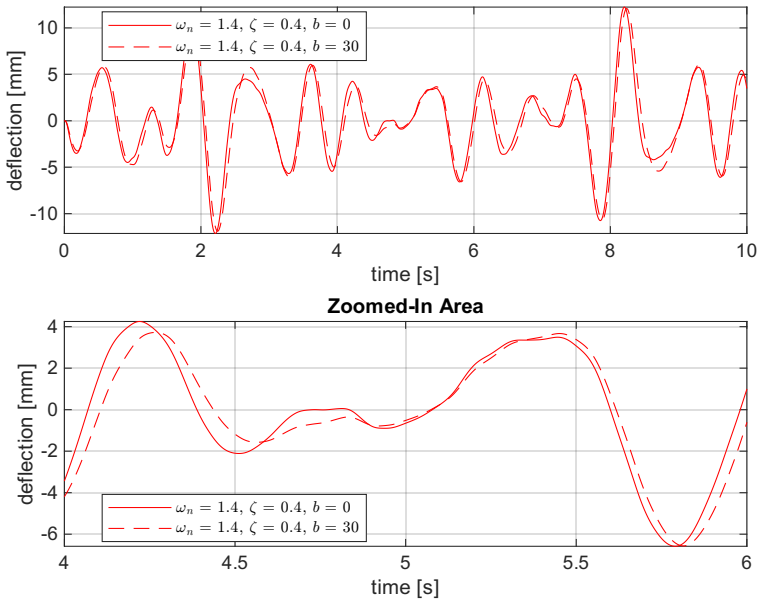

Figure 4.49 Seat suspension vertical deflection plot for the highest $w_n - \zeta$ pair with and without inerter from Simulink time domain simulation, case-4.

5. Conclusion

The ride comfort performance benefit of inerters is investigated for both the cab suspension and seat suspension of a tractor semi-trailer. Since today's vehicle seats typically feature two independent suspensions for vertical and fore-aft directions, an inerter is modeled for each direction. The effects of inerters are then studied across a range of inertance values within a set of natural frequencies and damping ratios of the cab and seat suspensions, in order to broaden the validity of the analysis carried out.

Despite that parallel inerter based suspensions degrade in performance at higher frequencies, the findings indicate that inerters can improve ride comfort when implemented in both the tractor semi-trailer cab and seat suspensions, by decreasing the weighted RMS acceleration values together with RMS suspension deflection which is a crucial factor when designing and assessing suspensions. It is seen that, the most of the contribution into the RMS acceleration content brought by the frequencies near the natural frequencies. There are 2 important factors; the PSD definition of road profile and the acceleration weighting definitions. The excitation magnitude becomes rapidly very small as the frequency increasing. This provide very low excitation amplitudes at the frequencies where the inerter based suspension performance degrades. Furthermore, frequency-dependent acceleration weightings are also becaomes very small at the frequencies where the suspension performance is deteoriated by with inerter. Conversely, both excitation and frequency weighting are found to be much higher at the frequencies where the inerter based suspension have superior performance resulting in, overall better isolation

The different investigation cases showed for the cab suspension the the best performance is achieved with inerters at both the front and rear. It is noted that the fore-aft comfort is affected by the inerter location. While, vertical comfort is always enhanced, fore-aft comfort is negtively affected for some $w_n - \zeta$ pairs when no seat inerter is implemented. However, investigation case-4 shows great improvement in the fore-aft direction with seat inerters.

The seat suspension benefits most from the inclusion of inerters. Comfort improvements of up to 48% are observed in the fore-aft direction, accompanied by a 26% reduction in RMS deflection. In the vertical direction, improvements of up to 30% in weighted RMS acceleration and a 8% reduction in RMS deflection are achievable. The extent to which inerters enhance vibration isolation at the seat suspension depends on the initial configuration, with softer suspensions tending to benefit the most from inerters.

REFERENCES

[1] International Organization for Standardization. Mechanical vibration and shock: Evaluation of human exposure to whole-body vibration. Standard, International Organization for Standardization, Geneva, CH, **1997**.

[2] Alan W Salmoni Adam P Cann and Tammy R Eger. Predictors of whole-body vibration exposure experienced by highway transport truck operators. *Ergonomics*, 47(13):1432–1453, **2004**. doi:10.1080/00140130410001712618. PMID: 15513718.

[3] Malcolm C. Smith and Fu-Cheng Wang. Performance benefits in passive vehicle suspensions employing inerters. *Vehicle System Dynamics*, 42(4):235–257, **2004**. doi:10.1080/00423110412331289871.

[4] D.Sc. J.Y. Wong Ph.D. *Vehicle Ride Characteristics*, chapter 7, pages 469–520. John Wiley & Sons, Ltd, **2022**. ISBN 9781119719984. doi:https://doi.org/10.1002/9781119719984.ch7.

[5] Zhenyu Jiang, Donald Streit, and Moustafa El-Gindy. Heavy vehicle ride comfort: Literature survey. *International Journal of Heavy Vehicle Systems*, 8, **2001**. doi:10.1504/IJHVS.2001.001163.

[6] Oldrich Kropac and Peter Mucka. Indicators of longitudinal unevenness of roads in the usa. *International Journal of Vehicle Design*, 46(4):393–415, **2008**. doi:10.1504/IJVD.2008.020306.

[7] C. Trangsrud, E. H. Law, and I. Janajreh. Ride dynamics and pavement loading of tractor semi-trailers on randomly rough roads. In *SAE Commercial Vehicle Engineering Congress & Exhibition*. SAE International, **2004**. ISSN 0148-7191. doi:https://doi.org/10.4271/2004-01-2622.

[8] Odilon T. Perseguim, A. Costa Neto, Marcos A. Argentino, C. F. Nogueira, P. Federico Neto, M. A. Fogaça, A. Dybal, and M. D. Torre Garcia. Comfort

and vibration study of a tractor and trailer combination using simulation and experimental approaches: the jumping ride behavior. In *International Truck & Bus Meeting & Exposition*. SAE International, **2000**. ISSN 0148-7191. doi:https://doi.org/10.4271/2000-01-3517.

[9] International Organization for Standardization. Mechanical vibration - Road surface profiles - Reporting of measured data. Standard, International Organization for Standardization, Geneva, CH, **2016**.

[10] Giancarlo Genta and Lorenzo Morello. *Comfort Performance*, pages 421–503. Springer International Publishing, Cham, **2020**. ISBN 978-3-030-35709-2. doi:10.1007/978-3-030-35709-2_26.

[11] Malcolm C. Smith. The inerter: A retrospective. *Annual Review of Control, Robotics, and Autonomous Systems*, 3(Volume 3, 2020):361–391, **2020**. ISSN 2573-5144. doi:https://doi.org/10.1146/annurev-control-053018-023917.

[12] Willian M. Kuhnert, Paulo J. Paupitz Gonçalves, Diego F. Ledezma-Ramirez, and Michael J. Brennan. Inerter-like devices used for vibration isolation: A historical perspective. *Journal of the Franklin Institute*, 358(1):1070–1086, **2021**. ISSN 0016-0032. doi:https://doi.org/10.1016/j.jfranklin.2020.11.007.

[13] Donghong Ning, Shuaishuai Sun, Haiping Du, Weihua Li, Nong Zhang, Minyi Zheng, and Liang Luo. An electromagnetic variable inertance device for seat suspension vibration control. *Mechanical Systems and Signal Processing*, 133:106259, **2019**. ISSN 0888-3270. doi:https://doi.org/10.1016/j.ymssp.2019.106259.

[14] Peter F Sweatman and Scott McFarlane. Investigation into the specification of heavy trucks and consequent effects on truck dynamics and drivers: Final report. *FEDERAL OFFICE OF ROAD SAFETY*, **2000**.

[15] Sunder Vaduri and E. Harry Law. Development of a simulation for assessment of ride quality of tractor semi-trailers. In *International Truck & Bus Meeting &*

Exposition. SAE International, **1993**. ISSN 0148-7191. doi:https://doi.org/10.4271/932940.

[16] I.M. Ibrahim, D.A. Crolla, and D.C. Barton. Effect of frame flexibility on the ride vibration of trucks. *Computers & Structures*, 58(4):709–713, **1996**. ISSN 0045-7949. doi:https://doi.org/10.1016/0045-7949(95)00198-P.

[17] M M El Madany. An analytical investigation of isolation systems for cab ride. *Computers and Structures*, 27:679–688, **1987**.

[18] M. A. DOKAINISH and M. M. ELMADANY. Random response of tractor-semitrailer system. *Vehicle System Dynamics*, 9(2):87–112, **1980**. doi:10.1080/00423118008968618.

[19] Tadas Lenkutis, Aurimas Čerškus, Nikolaj Šešok, Andrius Dzedzickis, and Vytautas Bučinskas. Road surface profile synthesis: Assessment of suitability for simulation. *Symmetry*, 13(1), **2021**. ISSN 2073-8994. doi:10.3390/sym13010068.

[20] W.J.E. Evers. *Improving driver comfort in commercial vehicles : modeling and control of a low-power active cabin suspension system*. Phd thesis 1 (research tu/e / graduation tu/e), Mechanical Engineering, **2010**. doi:10.6100/IR673075.

[21] G.J. Stein, R. Zahoranský, T.P. Gunston, L. Burström, and L. Meyer. Modelling and simulation of a fore-and-aft driver's seat suspension system with road excitation. *International Journal of Industrial Ergonomics*, 38(5):396–409, **2008**. ISSN 0169-8141. doi:https://doi.org/10.1016/j.ergon.2007.10.016. Seating Dynamics.

[22] S. Rakheja, P.-É. Boileau, and Z. Wang. Performance analysis of suspension seats under high magnitude vibration excitations: Ii. design parameter study. *Journal of Low Frequency Noise, Vibration and Active Control*, 23(1):7–25, **2004**. doi:10.1260/0263092041456792.

[23] Kang Song, Xiaokai Chen, and Yi Lin. Wheelbase filtering effect on vehicle ride dynamics. In *Proceedings of the FISITA 2012 World Automotive Congress*, pages 1183–1195. Springer Berlin Heidelberg, Berlin, Heidelberg, **2013**.

APPENDIX

APPENDIX 1 - Matlab Function for cab inerter studies

`cabfunc.m` function expects the numeric substitution values `x` for symbolic state-space matrix `A` in the order which can be obtained by `symvar` command, symbolic state-space matrices `A, B, C, D`, numeric wheelbase distance array `wl`, numeric velocity variable `V`, symbolic ISO-2631 filter transfer functions `Wd, Wk` and symbolic road profile PSD function `Gf`.

It returns, seat weighted RMS fore-aft acceleration `wrmsax_s`, seat weighted RMS fore-aft and vertical accelerations `wrmsaz_s`, seat weighted combined acceleration `wrmsac_s`, RMS cab deflection `rmsdz_c`, seat weighted fore-aft, acceleration, vertical acceleration and cab deflection PSD functions `S_wx_s`, `S_wz_s` and `S_dz_c`, respectively.

```
function [wrmsax_s, wrmsaz_s, wrmsac_s,...
    rmsdz_c, S_wx_s, S_wz_s, S_dz_c, H] =...
    cab_func(x,A,B,C,D,wl,V,Wd,Wk,Gf)
syms s f
symvars = symvar(A);
Ad = double(subs(A,symvars,x));
% obtain time delay transfer function
H = sym(zeros(size(A,1),1));
for i=1:size(B,2)   % obtain transfer function
    % from every input to every output
    [b(:,:,i) , a(:,:,i)] = ss2tf(Ad,B,C,D,i);
    for j=1:2   % get seat position pos. response
        % to road and bind transfer functions each
        % input by adding time delay
        H(j,1) = H(j,1) + exp(-wl(i)/V*s) * ...
```

```
            poly2sym(b(j,:,i),s) / poly2sym(a(:,:,i),s);
    end
    for j=5:5   % get cab susp. deflection response to
        % road and bind transfer functions each input by
        % adding time delay
        H(j,1) = H(j,1) + exp(-wl(i)/V*s) *...
            poly2sym(b(j,:,i),s) / poly2sym(a(:,:,i),s);
    end
end
%FRF FUNCTIONS
% seat weighted acceleration FRF
H_wx_s(f) = vpa(abs(subs(s^2*H(1)*Wd,s,1i*2*pi*f)));  % seat
% weighted longitudinal acceleration FRF magnitude
H_wz_s(f) = vpa(abs(subs(s^2*H(2)*Wk,s,1i*2*pi*f)));  % seat
% weighted vertical acceleration FRF magnitude
% cab CoG-chassis vertical distance FRF
H_dz_c(f) = vpa(abs(subs(H(5),s,1i*2*pi*f)));  % cab front
% suspension vert. deflection FRF magnitude
% PSD RESPONSES
% seat weighted acceleration PSD function
S_wx_s(f) = H_wx_s(f)^2 * Gf(f);    % seat weighted
% longitudinal acceleration PSD response function
S_wz_s(f) = H_wz_s(f)^2 * Gf(f);    % seat weighted
% vertical acceleration PSD response function
% cab CoG-chassis distance PSD function
S_dz_c(f) = H_dz_c(f)^2 * Gf(f);   % cab CoG-chassis
% vertical distance PSD function
% RMS VALUES
% seat weighted rms accelerations
```

```
wrmsax_s = sqrt(double(vpaintegral(S_wx_s(f),...
    [0.5 80]))); % seat weighted longitudal rms acceleration
wrmsaz_s = sqrt(double(vpaintegral(S_wz_s(f),...
    [0.5 80]))); % seat weighted vertical rms acceleration
wrmsac_s = sqrt(wrmsax_s^2 + wrmsaz_s^2);   % seat weighted
% combined rms acceleration
% cab CoG-chassis vertical distance rms deflections
rmsdz_c = sqrt(double(vpaintegral(S_dz_c(f),...
    [0.01*V 10*V])));  % cab CoG-chassis vertical
% distance rms deflection
end
```

It returns, seat weighted RMS fore-aft acceleration `wrmsax_s`, seat weighted RMS fore-aft and vertical accelerations `wrmsaz_s`, seat weighted combined acceleration `wrmsac_s`, RMS seat fore-aft suspension deflection `rmsdx_s`, seat RMS vertical suspension deflection `wrmsdz_s` and the PSD function outputs `S_wx_s`, `S_wz_s`, `S_dx_s`, `S_dz_s` are for seat weighted fore-aft acceleraion, seat weighted vertical acceleration, seat fore-aft suspension deflection and seat vertical acceleration deflection, respectively.

```
function [wrmsax_s, wrmsaz_s, wrmsac_s, rmsdx_s,...
    rmsdz_s, S_wx_s, S_wz_s, S_dx_s, S_dz_s] =...
    seat_func(x,A,B,C,D,wl,V,Wd,Wk,Gf)
syms s f
symvars = symvar(A);
Ad = double(subs(A,symvars,x));
% obtain time delay transfer function
H = sym(zeros(size(A,1),1));
for i=1:size(B,2)   % obtain transfer function
    % from every input to every output
    [b(:,:,i) , a(:,:,i)] = ss2tf(Ad,B,C,D,i);
```

```
    for j=1:2   % get seat position pos. response
        % to road and bind transfer functions each
        % input by adding time delay
        H(j,1) = H(j,1) + exp(-wl(i)/V*s) *...
            poly2sym(b(j,:,i),s) / poly2sym(a(:,:,i),s);
    end
    for j=3:4   % get cab susp. deflection response
        % to road and bind transfer functions each input
        % by adding time delay
        H(j,1) = H(j,1) + exp(-wl(i)/V*s) *...
            poly2sym(b(j,:,i),s) / poly2sym(a(:,:,i),s);
    end
end
% FRF FUNCTIONS
% seat suspension deflection FRF
H_dx_s(f) = vpa(abs(subs(H(3),s,1i*2*pi*f)));  % seat
% suspension long. deflection FRF magnitude
H_dz_s(f) = vpa(abs(subs(H(4),s,1i*2*pi*f)));  % seat
% suspension vert. deflection FRF magnitude
% seat weighted acceleration FRF
H_wx_s(f) = vpa(abs(subs(s^2*H(1)*Wd,s,1i*2*pi*f)));  % seat
% weighted longitudinal acceleration FRF magnitude
H_wz_s(f) = vpa(abs(subs(s^2*H(2)*Wk,s,1i*2*pi*f)));  % seat
% weighted vertical acceleration FRF magnitude
% PSD RESPONSES
% seat suspension deflection PSD function
S_dx_s(f) = H_dx_s(f)^2 * Gf(f);  % cab front suspension
% vert. deflection response PSD to road input
S_dz_s(f) = H_dz_s(f)^2 * Gf(f);  % cab rear suspension
```

```
% vert. deflection response PSD to road input
% seat weighted acceleration PSD function
S_wx_s(f) = H_wx_s(f)^2 * Gf(f);
S_wz_s(f) = H_wz_s(f)^2 * Gf(f);
% RMS VALUES
% cab suspension rms deflections
rmsdx_s = sqrt(double(vpaintegral(S_dx_s(f),...
    [0.01*V 10*V],'RelTol', 1e-9,...
    'AbsTol', 1e-12)));  % cab front suspension
% vertical rms deflection
rmsdz_s = sqrt(double(vpaintegral(S_dz_s(f),...
    [0.01*V 10*V],'RelTol', 1e-9,...
    'AbsTol', 1e-12)));  % cab rear suspension
% vertical rms deflection

% seat weighted rms accelerations
wrmsax_s = sqrt(double(vpaintegral(S_wx_s(f),...
    [0.5 80]))); % seat weighted longitudal rms acceleration
wrmsaz_s = sqrt(double(vpaintegral(S_wz_s(f),...
    [0.5 80]))); % seat weighted vertical rms acceleration
wrmsac_s = sqrt(wrmsax_s^2 + wrmsaz_s^2);
end
```

APPENDIX 2 - Main Matlab Code

`main.m` calculates equations of motion and state-space matrices for the system model and must be executed prior to the case study codes.

```
clc, clear
sympref('AbbreviateOutput', false);
```

```
% generalized coordinates in world frame
syms x_s(t) z_s(t)  % seat
syms x_c(t) z_c(t) theta_c(t)   % cab
syms x_tr(t) z_tr(t) theta_tr(t)   % tractor chassis
syms theta_st(t)    % trailer
syms z_1(t) z_2(t)  % tractor axles
syms z_3(t) z_4(t) z_5(t)   % trailer axles
syms u_1(t) u_2(t) u_3(t) u_4(t) u_5(t)  % road inputs
% generalized coordinates x:
x = [x_s;z_s;x_c;z_c;theta_c;x_tr;...
    z_tr;theta_tr;theta_st;z_1;z_2;z_3;z_4;z_5];
x = x(t);
x_dot = diff(x);
x_ddot = diff(x_dot);
% generalized inputs q:
q = [u_1;u_2;u_3;u_4;u_5];
q = q(t);
% mass, inertia, stiffness, damping,
% inertance parameter variables
syms m_s m_c m_tr m_st m_1 m_2 m_3 m_4 m_5
syms I_c I_tr I_st
syms k_sx k_sz k_cfx k_cfz k_crz k_trf k_trr k_st1 k_st2
syms k_st3 k_1 k_2 k_3 k_4 k_5
syms c_sx c_sz c_cfx c_cfz c_crz c_trf c_trr
syms c_st1 c_st2 c_st3
syms b_sx b_sz  % parallel seat inertances
syms b_cfx b_cfz b_crz  % cab parallel inertance
syms l_cf   % Distance from Cab CoG to front
% suspension mount 940mm
```

```
syms h_cf   % Height from cab CoG to front
% suspension mount -970mm
syms l_cr   % Distance from Cab CoG to rear
% suspension mount -1140mm
syms h_cr   % Heigt from cab CoG to rear
% suspension mount -970mm
syms l_cs   % Distance from Cab CoG to Seat CoG 230mm
syms h_cs   % Height from Cab CoG to Seat CoG -245mm
syms l_trfa % Distance from tractor CoG to front axle
% suspension 1460mm+430mm
syms l_trra % Distance from tractor CoG to rear axle
% suspension -2340mm-430mm
syms l_trfc % Distance from tractor CoG to front cab
% suspension mount 2570mm
syms l_trrc % Distance from tractor CoG to rear cab
% suspension mount 490mm
syms l_tr5 % Distance from tractor CoG to 5th wheel
% coupling -1820mm
syms h_tr5 % Height from tractor CoG to 5th wheel
% coupling 250mm
syms l_5st % Distance from 5th wheel coupling to
% trailer CoG -5610mm
syms h_5st % Height from 5th wheel coupling to
% trailer CoG 100mm
syms l_st1 % Distance from 5th wheel coupling to
% trailer 1st axle -6310mm
syms l_st2 % Distance from 5th wheel coupling to
% trailer 2nd axle -7620mm
syms l_st3 % Distance from 5th wheel coupling to
```

```
% trialer 3rd axle -8930mm
% Energy functions
% KINETIC ENERGIES
% Seat mass
KE_s = 1/2*m_s*diff(x_s)^2 +...
    1/2*m_s*diff(z_s)^2;
% Seat Parallel Inerters
KE_ip = 1/2*b_sx*diff(x_s - (x_c + theta_c*h_cs))^2 + ...
    1/2*b_sz*diff(z_s - (z_c - theta_c*l_cs))^2;
% Cab mass
KE_c = 1/2*m_c*diff(x_c)^2 +...
    1/2*m_c*diff(z_c)^2 +...
    1/2*I_c*diff(theta_c)^2;
% Cab parallel Inerters
KE_ic = 1/2*b_cfx*diff((x_c + theta_c*h_cf)...
    - (x_tr))^2 + 1/2*b_cfz*diff((z_c - theta_c*l_cf)...
    - (z_tr - theta_tr*l_trfc))^2 + 1/2*b_crz*...
    diff((z_c - theta_c*l_cr) - (z_tr - theta_tr*l_trrc))^2;
% Tractor mass
KE_tr = 1/2*m_tr*diff(x_tr)^2 +...
    1/2*m_tr*diff(z_tr)^2 +...
    1/2*I_tr*diff(theta_tr)^2;
% Trailer mass
KE_st = 1/2*m_st*...
    diff(x_tr+theta_tr*h_tr5+theta_st*h_5st)^2+1/2*m_st*...
    diff(z_tr-theta_tr*l_tr5-theta_st*l_5st)^2+...
    1/2*I_st*diff(theta_st)^2;
% Axles mass
KE_axles = 1/2*m_1*diff(z_1)^2 +...
```

```
    1/2*m_2*diff(z_2)^2 +...
    1/2*m_3*diff(z_3)^2 +...
    1/2*m_4*diff(z_4)^2 +...
    1/2*m_5*diff(z_5)^2;
%TOTAL KINETIC ENERGY
KE = KE_s + KE_ip + KE_c + KE_ic + KE_tr + KE_st + KE_axles;
% POTENTIAL ENERGIES
% Seat Springs
PE_s = 1/2*k_sx*(x_s - (x_c + theta_c*h_cs))^2 + ...
    1/2*k_sz*(z_s - (z_c - theta_c*l_cs))^2;
% Cab springs
PE_c = 1/2*k_cfx*((x_c+theta_c*h_cf)-(x_tr))^2+...
    1/2*k_cfz*((z_c-theta_c*l_cf)-...
    (z_tr-theta_tr*l_trfc))^2 + ...
    1/2*k_crz*((z_c-theta_c*l_cr)-...
    (z_tr-theta_tr*l_trrc))^2;
% Tractor springs
PE_tr = 1/2*k_trf*((z_tr-theta_tr*l_trfa)-(z_1))^2+...
    1/2*k_trr*((z_tr-theta_tr*l_trra)-(z_2))^2;
% Semi-Trailer springs
PE_st = 1/2*k_st1*...
    (z_tr-theta_tr*l_tr5-theta_st*l_st1-z_3)^2+1/2*...
    k_st2*(z_tr-theta_tr*l_tr5-theta_st*l_st2-z_4)^2+...
    1/2*k_st3*(z_tr-theta_tr*l_tr5-theta_st*l_st3-z_5)^2;
% Tyre springs
PE_tyres = 1/2*k_1*(z_1-u_1)^2 + ...
    1/2*k_2*(z_2-u_2)^2 + ...
    1/2*k_3*(z_3-u_3)^2 + ...
    1/2*k_4*(z_4-u_4)^2 + ...
```

```
    1/2*k_5*(z_5-u_5)^2;
% TOTAL POTENTIAL ENERGY
PE = PE_s + PE_c + PE_tr + PE_st + PE_tyres;
% DISSIPATIVE ENERGIES
% Seat dampers
DE_s = 1/2*c_sx*diff(x_s-(x_c+theta_c*h_cs))^2 + ...
    1/2*c_sz*diff(z_s-(z_c-theta_c*l_cs))^2;
% Cab dampers
DE_c = 1/2*c_cfx*diff((x_c+theta_c*h_cf)-(x_tr))^2+...
    1/2*c_cfz*diff((z_c-theta_c*l_cf)...
    -(z_tr - theta_tr*l_trfc))^2+...
    1/2*c_crz*diff((z_c-theta_c*l_cr)-...
    (z_tr - theta_tr*l_trrc))^2;
% Tractor dampers
DE_tr = 1/2*c_trf*diff((z_tr-theta_tr*l_trfa)-(z_1))^2+...
    1/2*c_trr*diff((z_tr-theta_tr*l_trra)-(z_2))^2;
% Semi-Trailer dampers
DE_st = 1/2*c_st1*...
    diff(z_tr-theta_tr*l_tr5-theta_st*l_st1-z_3)^2+...
    1/2*c_st2*...
    diff(z_tr-theta_tr*l_tr5-theta_st*l_st2-z_4)^2+...
    1/2*c_st3*...
    diff(z_tr-theta_tr*l_tr5-theta_st*l_st3-z_5)^2;
% TOTAL DISSIPATIVE ENERGY
DE = DE_s + DE_c + DE_tr + DE_st;
L = KE - PE;
% derive equations of motion
eqms = sym(zeros(size(x)));
for i=1:height(x)
```

```
    eqms(i,1) = diff(diff(L,diff(x(i),t)),t)...
        -diff(L,x(i))+diff(DE,diff(x(i),t))==0;
end
% MASS,STIFFNESS,DAMPING MATRICES
for i=1:height(eqms)
    for j=1:height(x_ddot)
        MM(i,j) = diff(lhs(eqms(i)),x_ddot(j));
    end
end
% STIFFNESS MATRIX
for i=1:height(eqms)
    for j=1:height(x)
        KK(i,j) = diff(lhs(eqms(i)),x(j));
    end
end
% DAMPING MATRIX
for i=1:height(eqms)
    for j=1:height(x_dot)
        CC(i,j) = diff(lhs(eqms(i)),x_dot(j));
    end
end
% INPUT
for i=1:height(eqms)
    for j=1:height(q)
        U(i,j) = diff(lhs(eqms(i)),q(j));
    end
end
%Parameters
m_s = 105.4;    % fore-aft model heavy subject reduced
```

```
% model mass inc. seat&human [kg]
m_c = 1300/2;   % PARAMETERS: 9DOF pitch heave model,
% half of the cab mass [kg]
I_c = 1100/2;   % half of the cab pitch inertia [kgm^2]
m_tr = 2503/2+1785/2;   % half of tractor chassis and
% engine mass [kg]
I_tr = 46590/2; % TRANSGRUD: half of the tractor chassis
% and engine inertia [kgm^2]
m_st = 15170;   % PARAMETERS: half of the trailer
% mass inc load [kg]
I_st = 200000/2;    % Generic laden trailer inertia [kgm^2]
m_1 = 700/2;    % PARAMETERS: half of front axle mass [kg]
m_2 = 1240/2;   % half of tractor rear axle mass [kg]
m_3 = 450;  % Generic half of trailer axle mass [kg]
m_4 = 450;  % half of trailer axle mass [kg]
m_5 = 450;  % half of trailer axle mass [kg]
k_sx0 = 8510;    % FORE-AFT: low friction model seat
% fore-aft stiffness [N/m]
k_sz0 = 7961.6;  % RAKHEJA PART-1: Seat B seat vert.
% stiffness [N/m] (for 105.4)
k_cfx = 6000000;    % PARAMETERS: cab front long.
% spring stiff [N/m]
k_cfz0 = 20000;  % cab front vert. spring stiff. [N/m]
k_crz0 = 20000;  % cab rear vert. spring stiff [N/m]
k_trf = 300000; % tractor front susp. stiff. [N/m]
k_trr = 300000; % tractor rear susp. stiff. [N/m]
k_st1 = 400000; % trailer suspension stiff. [N/m]
k_st2 = 400000; % trailer suspension stiff. [N/m]
k_st3 = 400000; % trailer suspension stiff. [N/m]
```

```
k_1 = 1200000;  % tractor front tyre stiff. [N/m]
k_2 = 2200000;  % tractor rear tyre
% stiff. 4 TYRE PER AXLE!!  [N/m]
k_3 = 1200000;  % trailer tyre stiff [N/m]
% (trangsrud+parameters)
k_4 = 1200000;  % trailer tyre stiff [N/m]
k_5 = 1200000;  % trailer tyre stiff [N/m]
c_sx0 = 606; % FORE-AFT low friction: seat
% long. damping [Ns/m]
c_sz0 = 788; % RAKHEJA SEAT B: calculated
% for damped nat. freq. 1.25 Hz. [Ns/m]
c_cfx = 25000;  % PARAMETERS: cab front
% susp. long. damping [Ns/m]
c_cfz0 = 7400;   % cab front susp. vert. damping [Ns/m]
c_crz0 = 5900;   % cab rear susp. vert. damping [Ns/m]
c_trf = 11000;  % tractor front axle susp. damping [Ns/m]
c_trr = 22000;  % tractor rear axle susp. damping [Ns/m]
c_st1 = 10000;  % trailer axle susp. damping [Ns/m]
c_st2 = 10000;  % trailer axle susp. damping [Ns/m]
c_st3 = 10000;  % trailer axle susp. damping [Ns/m]
l_cf = 0.94;
h_cf = -0.97;
l_cr = -1.14;
l_cs = 0.23;
h_cs = -0.65;
l_trfa = 1.46-0.43;
l_trra = -2.34-0.43;
l_trfc = 2.57;
l_trrc = 0.49;
```

```
l_tr5 = -1.82;
h_tr5 = 0.25;
l_5st = -5.61;
h_5st = 0.5;
l_st1 = -6.31;
l_st2 = -7.62;
l_st3 = -8.93;
symeqms = eqms;
eqms = subs(eqms);
MM = subs(MM);
KK = subs(KK);
CC = subs(CC);
Minv = MM^-1;
eqms2 = x_ddot == -Minv*KK*x - Minv*CC*x_dot - Minv*U*q;
% STATE SPACE
xss = [x ; x_dot];
xss_dot = diff(xss);
Ass = [zeros(14,14) , eye(14,14) ; -Minv*KK , -Minv*CC];
Bss = [zeros(14,5) ; -Minv*U];
Css = eye(height(xss));
Css(1,1) = 1;   % seat longitudinal position
Css(2,2) = 1;   % seat vertical position
Css(3,1:5) = [1 0 -1 0 -h_cs];    % seat suspension
% long. deflection
Css(4,1:5) = [0 1 0 -1 l_cs];     % seat suspension
% vert. deflection
Css(5,1:8) = [0 0 0 1 0 0 -1 l_trrc-l_cr];   % cab
% CoG-Chassis distance
Dss = zeros(size(Bss));
```

```
wl = [0 ; 3.8 ; 9.59 ; 10.9 ; 12.21];   % axle
% distances from first axle [m]
% ROAD PSD FUNCTION
syms n f V
Gd0 = 16*10^-6; % road degree of roughness mean value
% for road class A ISO8608:2016
w = 2;  % fit exponent defined by ISO8608:2016
n0 = 0.1;   % degree of roughness reference
% spatial frequency [cycles/m]
G(n) = vpa(Gd0*(n/n0)^-w);
fplot(G,[0.004 10])
set(gca,'Xscale','log','Yscale','log')
grid on
xlabel('Spatial Frequency [cycle/m]')
ylabel('Displacement PSD [m^3]')
title('Displacement PSD Graph for ISO8608 Class:A')
xlim([0.004 10])
ylim([10^-8 1])
% Road PSD definition in frequency
Gf(f) = subs(G/V,n,f/V); % PSD definition
% in time frequency dependent on V [Hz]
Vels = [90/3.6 ; 70/3.6 ; 50/3.6];
for j=1:length(Vels)
    S_temp = subs(Gf,V,Vels(j));
    fplot(S_temp,[0.01 10]*Vels(j),'LineWidth',2)
    hold on
end
set(gca , 'Xscale', 'log', 'Yscale', 'log')
% xlim([0.1 100])
```

```
% ylim([1e-9 1e-3])
grid on
xlabel('Frequency [Hz]')
ylabel(sprintf("Displacement PSD [m^2/Hz]"))
title('PSD Graphs for different velocities')
legend('V = 90 km/h','V = 70 km/h','V = 50 km/h')
hold off
% ISO FILTERS
[Wd, Wk] = ISO_filter;
syms s f
tempfunWd(f) = 20*log10(abs(subs(Wd,s,2i*pi*f)));
tempfunWk(f) = 20*log10(abs(subs(Wk,s,2i*pi*f)));
% Calculate Third Octave Bands
% (base 10) in Matlab // wikipedia
fcentre = 10.^(0.1.*[-18:26]);
semilogx(fcentre(9:end),tempfunWk(fcentre(9:end)))
hold on
semilogx(fcentre(9:end),tempfunWd(fcentre(9:end)))
xlim([fcentre(1) fcentre(end)])
ylim([-90 10])
xticks(fcentre(1:3:end))
xline(fcentre)
yline(-90:10:10)
title(['ISO2631:1997 Frequency...' ...
    ' Weighting Curves for Principal Weightings'])
xlabel('Frequency [Hz]')
ylabel('Frequency weightings [dB]')
legend('W_k','W_d')
ax = gca;
```

```
ax.XAxis.TickLabelFormat = '%.2f';
hold off
```

APPENDIX 3 - Matlab Code for Case-1

This code runs the calculations for the case-1 and plots the results. The simulink model must be constructed and placed within the same directory with this code.

To obtain code for case-2 and case-3, below changes should be made, in their respective places in the code for case-1.

Necessary chages for case-2;

```
caseindex =2;
resultname='case2';
b_cabf_v(i,j,k)=0;
b_cabr_v(i,j,k)=b_c(k);
A1 = subs(A1,symvars(2),0);
A1 = subs(A1,symvars(3),b_c(1));
A2 = subs(A2,symvars(2),0;
A2 = subs(A2,symvars(3),b_c(end));
A3 = subs(A1,symvars(2),0;
A3 = subs(A1,symvars(3),b_c(1));
A4 = subs(A2,symvars(2),0;
A4 = subs(A2,symvars(3),b_c(end));
```

Necessary chages for case-3;

```
caseindex =3;
resultname='case3';
b_cabf_v(i,j,k)=b_c(k);
b_cabr_v(i,j,k)=b_c(k);
```

```
A1 = subs(A1,symvars(2),b_c(1));
A1 = subs(A1,symvars(3),b_c(1));
A2 = subs(A2,symvars(2),b_c(end));
A2 = subs(A2,symvars(3),b_c(end));
A3 = subs(A1,symvars(2),b_c(1));
A3 = subs(A1,symvars(3),b_c(1));
A4 = subs(A2,symvars(2),b_c(end));
A4 = subs(A2,symvars(3),b_c(end));
```

```
caseindex = 1;
resultname = 'case1';
Vels = 90/3.6;  % vehicle velocity
w_n_c = [0.8 1.2 1.6];  % cab vertical natural
% frequency range
zeta_c = [0.2 0.4 0.8];  % cab damping ratio range
b_c = 0:20:300; % cab vertical inerters range
Atemp = subs(Ass);  % substitute fix parameters
Bd = double(subs(Bss));
Cd = double(Css);
Dd = double(Dss);
% construct spring, damper and inerter
% values for simulation separately in
% order to be able to use parfor
k_cabf_v = zeros(length(w_n_c),length(zeta_c),length(b_c));
k_cabr_v = zeros(length(w_n_c),length(zeta_c),length(b_c));
c_cabf_v = zeros(length(w_n_c),length(zeta_c),length(b_c));
c_cabr_v = zeros(length(w_n_c),length(zeta_c),length(b_c));
b_cabf_v = zeros(length(w_n_c),length(zeta_c),length(b_c));
b_cabr_v = zeros(length(w_n_c),length(zeta_c),length(b_c));
```

```
for i = 1:length(w_n_c)
    for j = 1:length(zeta_c)
        parfor k = 1:length(b_c)
            % calculate cab spring for the
            % current natural frequency
            k_cabf_v(i,j,k) = double(solve(1/2/pi*...
                sqrt((k_cfz+k_cfz)/m_c)==w_n_c(i)));
            k_cabr_v(i,j,k) = k_cabf_v(i,j,k);
            % calculate cab damper for the
            % current damping ratio
            c_cabf_v(i,j,k)=double(solve((c_cfz+c_cfz)/...
                (2*sqrt((k_cabf_v(i,j,k)+...
                k_cabr_v(i,j,k))*m_c))...
                ==zeta_c(j)));
            c_cabr_v(i,j,k)=c_cabf_v(i,j,k);
            % inerter values
            b_cabf_v(i,j,k)=b_c(k);
            b_cabr_v(i,j,k)=0;
        end
    end
end
% simulate base model
[wrmsax_s0, wrmsaz_s0, wrmsac_s0, rmsdz_c0,...
    S_wx_s0, S_wz_s0, S_dz_c0] =...
    cab_func([0 0 0 0 0 c_cfz0 c_crz0 c_sx0 c_sz0 k_cfz0...
    k_crz0 k_sx0 k_sz0],Atemp,Bd,Cd,Dd,wl,Vels,Wd,Wk,...
    subs(Gf,V,Vels));
% Call simulation function to get
% results and store in the struct
```

```
for i=1:length(w_n_c)   % loop for cab
    % vertical natural frequency
    for j=1:length(zeta_c)    % loop for
        % cab vertical damping
        parfor k=1:length(b_c)    % loop for
            % cab vertical inerter
            [wrmsax_s(i,j,k), wrmsaz_s(i,j,k),...
                wrmsac_s(i,j,k), rmsdz_c(i,j,k),...
                S_wx_s(i,j,k), S_wz_s(i,j,k),...
                S_dz_c(i,j,k)] =...
                cab_func([0 b_cabf_v(i,j,k)...
                b_cabr_v(i,j,k) 0 0 c_cabf_v(i,j,k)...
                c_cabr_v(i,j,k) c_sx0 c_sz0...
                k_cabf_v(i,j,k) k_cabr_v(i,j,k)...
                k_sx0 k_sz0],Atemp,Bd,Cd,Dd,wl,Vels,...
                Wd,Wk,subs(Gf,V,Vels));
        end
    end
end
% store results in struct variable
result = struct('V', {}, 'w_n_c', {}, 'zeta_c', {},...
    'b_c', {}, 'k_cabf_v', {}, 'k_cabr_v', {},...
    'c_cabf_v', {}, 'c_cabr_v', {}, 'b_cabf_v', {},...
    'b_cabr_v',{},'wrmsax_s', {} , 'wrmsaz_s', {} ,...
    'wrmsac_s', {} , 'rmsdz_c', {} , 'J1', {} , 'J2',...
    {} , 'J', {}, 'S_wx_s', {}, 'S_wz_s', {}, 'S_dz_c', {});
for i = 1:length(w_n_c)
    for j = 1:length(zeta_c)
        for k = 1:length(b_c)
```

```
            index = (i - 1) * length(zeta_c) *...
                length(b_c) + (j - 1) * length(b_c) + k;
            result(index).V = Vels;
            result(index).w_n_c = w_n_c(i);
            result(index).zeta_c = zeta_c(j);
            result(index).b_c = b_c(k);
            result(index).k_cabf_v = k_cabf_v(i,j,k);
            result(index).k_cabr_v = k_cabr_v(i,j,k);
            result(index).c_cabf_v = c_cabf_v(i,j,k);
            result(index).c_cabr_v = c_cabr_v(i,j,k);
            result(index).b_cabf_v = b_cabf_v(i,j,k);
            result(index).b_cabr_v = b_cabr_v(i,j,k);
            result(index).wrmsax_s = wrmsax_s(i,j,k);
            result(index).wrmsaz_s = wrmsaz_s(i,j,k);
            result(index).wrmsac_s = wrmsac_s(i,j,k);
            result(index).rmsdz_c = rmsdz_c(i,j,k);
            result(index).J1 = wrmsac_s(i,j,k)/wrmsac_s0;
            result(index).J2 = (rmsdz_c(i,j,k))/(rmsdz_c0);
            result(index).J = sqrt((result(index).J1^2) +...
                (result(index).J2^2));
            result(index).S_wx_s = S_wx_s(i,j,k);
            result(index).S_wz_s = S_wz_s(i,j,k);
            result(index).S_dz_c = S_dz_c(i,j,k);
        end
    end
end
% hold results in another struct
results.(resultname) = result;
figure
```

```
for i = 1:length(w_n_c)
    for j = 1:length(zeta_c)
        indeces = find(and([results.(resultname).w_n_c]==...
            w_n_c(i),and([results.(resultname).zeta_c]==...
            zeta_c(j),[results.(resultname).b_c]==0)));
        scatter([results.(resultname)(indeces).rmsdz_c]*...
            1000,...
            [results.(resultname)(indeces).wrmsac_s],...
            'k', 'filled')
        text([results.(resultname)(indeces).rmsdz_c]*...
            1000+0.1,...
            [results.(resultname)(indeces).wrmsac_s],...
            ['$\omega_n=$', sprintf('%s\n' ,...
            num2str(w_n_c(i))),'$\zeta=$',sprintf('%s\n',...
            num2str(zeta_c(j))),'$b=0$'],...
            'HorizontalAlignment', 'left',...
            'VerticalAlignment', 'middle',...
            'Interpreter', 'latex');
        hold on
    end
end
grid on
xlabel('RMS Cab Deflection [mm]')
ylabel('Weighted RMS Combined Seat Acceleration [m/s^2]')
hold off
figure
for i = 1:length(w_n_c)
    for j = 1:length(zeta_c)
        indeces = find(and([results.(resultname).w_n_c]==...
```

```
            w_n_c(i),and([results.(resultname).zeta_c]==...
            zeta_c(j),[results.(resultname).b_c] == 0)));
        scatter( [results.(resultname)(indeces).rmsdz_c]*...
            1000,...
            [results.(resultname)(indeces).wrmsac_s],...
            'k', 'filled')
        text([results.(resultname)(indeces).rmsdz_c]*...
            1000+0.1,...
            [results.(resultname)(indeces).wrmsac_s],...
            ['$\omega_n=$', sprintf('%s\n',...
            num2str(w_n_c(i))),'$\zeta=$',sprintf('%s\n',...
            num2str(zeta_c(j))),'$b=0$' ],...
            'HorizontalAlignment', 'left',...
            'VerticalAlignment', 'middle',...
            'Interpreter', 'latex');
        hold on
        indeces = find(and([results.(resultname).w_n_c]==...
            w_n_c(i),...
            [results.(resultname).zeta_c]==zeta_c(j)));
        plot([results.(resultname)(indeces).rmsdz_c]*...
            1000,...
            [results.(resultname)(indeces).wrmsac_s],...
            'r','LineWidth',2)
    end
end
grid on
xlabel('RMS Cab Deflection [mm]')
ylabel('Weighted RMS Combined Seat Acceleration [m/s^2]')
hold off
```

```
figure
for i = 1:length(w_n_c)
    for j = 1:length(zeta_c)
        indeces = find(and([results.(resultname).w_n_c]==...
            w_n_c(i),[results.(resultname).zeta_c]==...
            zeta_c(j)));
        plot([results.(resultname)(indeces).rmsdz_c]*...
            1000,...
            [results.(resultname)(indeces).wrmsac_s],...
            'r','LineWidth',2)
        hold on

        indeces = find(and([results.(resultname).w_n_c]==...
            w_n_c(i),and([results.(resultname).zeta_c]==...
            zeta_c(j),[results.(resultname).b_c]==...
            b_c(end))));
        scatter([results.(resultname)(indeces).rmsdz_c]*...
            1000,...
            [results.(resultname)(indeces).wrmsac_s],...
            'k', 'filled')
        text([results.(resultname)(indeces).rmsdz_c]*...
            1000+0.1 ,...
            [results.(resultname)(indeces).wrmsac_s],...
            ['$\omega_n=$',sprintf('%s\n',...
            num2str(w_n_c(i))),'$\zeta=$',sprintf('%s\n',...
            num2str(zeta_c(j))),'$b=$',...
            sprintf('%s',num2str(b_c(end)))],...
            'HorizontalAlignment', 'left',...
            'VerticalAlignment', 'middle',...
```

```
            'Interpreter', 'latex');
    end
end
grid on
xlabel('RMS Cab Deflection [mm]')
ylabel('Weighted RMS Combined Seat Acceleration [m/s^2]')
hold off
figure
for i = 1:length(w_n_c)
    indeces = find(and([results.(resultname).w_n_c]==...
        w_n_c(i),[results.(resultname).b_c] == 0) );
    plot([results.(resultname)(indeces).rmsdz_c]*1000,...
        [results.(resultname)(indeces).wrmsac_s],'--k')
    text([results.(resultname)(indeces(1)).rmsdz_c]*...
        1000+0.1,...
        [results.(resultname)(indeces(1)).wrmsac_s],...
        ['$\omega_n=$',sprintf('%s',num2str(w_n_c(i)))],...
        'HorizontalAlignment', 'left',...
        'VerticalAlignment','middle','Interpreter','latex');
    hold on
end
for i = 1:length(zeta_c)
    indeces = find(and([results.(resultname).zeta_c]==...
        zeta_c(i) , [results.(resultname).b_c] == 0) );
    plot([results.(resultname)(indeces).rmsdz_c]*1000,...
        [results.(resultname)(indeces).wrmsac_s],'--k')
    text([results.(resultname)(indeces(1)).rmsdz_c]*...
        1000+0.1,...
        [results.(resultname)(indeces(1)).wrmsac_s],...
```

```
        ['$\zeta=$', sprintf('%s' , num2str(zeta_c(i)))],...
        'HorizontalAlignment', 'right',...
        'VerticalAlignment', 'top', 'Interpreter', 'latex');
    hold on
end
for i = 1:length(w_n_c)
    for j = 1:length(zeta_c)
        indeces = find(and([results.(resultname).w_n_c]==...
            w_n_c(i),[results.(resultname).zeta_c]==...
            zeta_c(j)));
        plot([results.(resultname)(indeces).rmsdz_c]*...
            1000,...
            [results.(resultname)(indeces).wrmsac_s],...
            'r','LineWidth',2)
        hold on
    end
end
grid on
xlabel('RMS Cab Deflection [mm]')
ylabel('Weighted RMS Combined Seat Acceleration [m/s^2]')
hold off
figure
for i = 1:length(w_n_c)
    indeces = find( and( [results.(resultname).w_n_c]==...
        w_n_c(i) ,  [results.(resultname).b_c] == 0));
    plot( [results.(resultname)(indeces).J2],...
        [results.(resultname)(indeces).J1],...
        '-k','LineWidth',2)
    hold on
```

```
    for j = 1:length(zeta_c)
        indeces = find(and([results.(resultname).w_n_c]==...
            w_n_c(i),[results.(resultname).zeta_c]==...
            zeta_c(j)));
        plot([results.(resultname)(indeces).J2],...
            [results.(resultname)(indeces).J1],...
            'r','LineWidth',2)
        hold on
    end
end
grid on
xlabel('J2')
ylabel('J1')
optindex1 = find([results.(resultname).J]==...
    min([results.(resultname).J]));
plot([0 [results.(resultname)(optindex1).J2]],...
    [0 [results.(resultname)(optindex1).J1] ],'--b')
indeces = find([results.(resultname).b_c]==0);
axis equal
hold off
% INITILIZATION FOR PLOTTING AND SIMULATION
load('road.mat');   % load road data
t_end = (road(1,end)-wl(end))/Vels; % simulation end time
[num, den] = numden(Wk);
numWk = double(coeffs(num,'All'));
denWk = double(coeffs(den,'All'));
[num, den] = numden(Wd);
numWd = double(coeffs(num,'All'));
denWd = double(coeffs(den,'All'));
```

```
% result numbers for plottings
index1 = find(and([results.(resultname).w_n_c]==w_n_c(1),...
    and([results.(resultname).zeta_c]==zeta_c(1),...
    [results.(resultname).b_c]==b_c(1))));
index2 = find(and([results.(resultname).w_n_c]==w_n_c(1),...
    and([results.(resultname).zeta_c]==zeta_c(1),...
    [results.(resultname).b_c]==b_c(end))));
index3 = find(and([results.(resultname).w_n_c]==...
    w_n_c(end),and([results.(resultname).zeta_c]==...
    zeta_c(end),[results.(resultname).b_c]==b_c(1))));
index4 = find(and([results.(resultname).w_n_c]==...
    w_n_c(end),and([results.(resultname).zeta_c]==...
    zeta_c(end),[results.(resultname).b_c] == b_c(end))));
% state space matrices for plottings
symvars = symvar(Ass);
A1 = subs(Ass,symvars(1),0);
A1 = subs(A1,symvars(2),b_c(1));
A1 = subs(A1,symvars(3),0);
A1 = subs(A1,symvars(4),0);
A1 = subs(A1,symvars(5),0);
A1 = subs(A1,symvars(6),results.(resultname)...
    (index1).c_cabf_v);
A1 = subs(A1,symvars(7),results.(resultname)...
    (index1).c_cabr_v);
A1 = subs(A1,symvars(8),c_sx0);
A1 = subs(A1,symvars(9),c_sz0);
A1 = subs(A1,symvars(10),results.(resultname)...
    (index1).k_cabf_v);
```

```
A1 = subs(A1,symvars(11),results.(resultname)...
    (index1).k_cabr_v);
A1 = subs(A1,symvars(12),k_sx0);
A1 = subs(A1,symvars(13),k_sz0);
A1 = double(A1);
B1 = double(subs(Bss));
C1 = double(Css);
D1 = double(Dss);
A2 = subs(Ass,symvars(1),0);
A2 = subs(A2,symvars(2),b_c(end));
A2 = subs(A2,symvars(3),0);
A2 = subs(A2,symvars(4),0);
A2 = subs(A2,symvars(5),0);
A2 = subs(A2,symvars(6),results.(resultname)...
    (index2).c_cabf_v);
A2 = subs(A2,symvars(7),results.(resultname)...
    (index2).c_cabr_v);
A2 = subs(A2,symvars(8),c_sx0);
A2 = subs(A2,symvars(9),c_sz0);
A2 = subs(A2,symvars(10),results.(resultname)...
    (index2).k_cabf_v);
A2 = subs(A2,symvars(11),results.(resultname)...
    (index2).k_cabr_v);
A2 = subs(A2,symvars(12),k_sx0);
A2 = subs(A2,symvars(13),k_sz0);
A2 = double(A2);
B2 = double(subs(Bss));
C2 = double(Css);
D2 = double(Dss);
```

```
A3 = subs(Ass,symvars(1),0);
A3 = subs(A3,symvars(2),b_c(1));
A3 = subs(A3,symvars(3),0);
A3 = subs(A3,symvars(4),0);
A3 = subs(A3,symvars(5),0);
A3 = subs(A3,symvars(6),results.(resultname)...
    (index3).c_cabf_v);
A3 = subs(A3,symvars(7),results.(resultname)...
    (index3).c_cabr_v);
A3 = subs(A3,symvars(8),c_sx0);
A3 = subs(A3,symvars(9),c_sz0);
A3 = subs(A3,symvars(10),results.(resultname)...
    (index3).k_cabf_v);
A3 = subs(A3,symvars(11),results.(resultname)...
    (index3).k_cabr_v);
A3 = subs(A3,symvars(12),k_sx0);
A3 = subs(A3,symvars(13),k_sz0);
A3 = double(A3);
B3 = double(subs(Bss));
C3 = double(Css);
D3 = double(Dss);
A4 = subs(Ass,symvars(1),0);
A4 = subs(A4,symvars(2),b_c(end));
A4 = subs(A4,symvars(3),0);
A4 = subs(A4,symvars(4),0);
A4 = subs(A4,symvars(5),0);
A4 = subs(A4,symvars(6),results.(resultname)...
    (index4).c_cabf_v);
A4 = subs(A4,symvars(7),results.(resultname)...
```

```
    (index4).c_cabr_v);
A4 = subs(A4,symvars(8),c_sx0);
A4 = subs(A4,symvars(9),c_sz0);
A4 = subs(A4,symvars(10),results.(resultname)...
    (index4).k_cabf_v);
A4 = subs(A4,symvars(11),results.(resultname)...
    (index4).k_cabr_v);
A4 = subs(A4,symvars(12),k_sx0);
A4 = subs(A4,symvars(13),k_sz0);
A4 = double(A4);
B4 = double(subs(Bss));
C4 = double(Css);
D4 = double(Dss);
% SEAT FORE-AFT RESULTS
u=logspace(log10(.5),log10(80),500);
tempfunb0(f) = results.(resultname)(index1).S_wx_s;
tempfunbmax(f) = results.(resultname)(index2).S_wx_s;
figure
loglog(u,tempfunb0(u),'-k')
hold on
loglog(u,tempfunbmax(u),'--k')
tempfunb0(f) = results.(resultname)(index3).S_wx_s;
tempfunbmax(f) = results.(resultname)(index4).S_wx_s;
loglog(u,tempfunb0(u),'-r')
loglog(u,tempfunbmax(u),'--r')
xlim([0.1 100])
grid on
xlabel('frequency [Hz]')
ylabel(['seat fore-aft acceleration response PSD ' ...
```

```
    '[(m/s^2)^2)/Hz]'])
legend(sprintf('$\\omega_n=%s$, $\\zeta=%s$, $b=%s$',...
    num2str(w_n_c(1)), num2str(zeta_c(1)),...
    num2str(b_c(1))),...
    sprintf('$\\omega_n=%s$, $\\zeta=%s$, $b=%s$',...
    num2str(w_n_c(1)), num2str(zeta_c(1)),...
    num2str(b_c(end))),...
    sprintf('$\\omega_n=%s$, $\\zeta=%s$, $b=%s$',...
    num2str(w_n_c(end)), num2str(zeta_c(end)),...
    num2str(b_c(1))),...
    sprintf('$\\omega_n=%s$, $\\zeta=%s$, $b=%s$',...
    num2str(w_n_c(end)), num2str(zeta_c(end)),...
    num2str(b_c(end))),...
    'Location', 'best', 'Interpreter', 'latex');
hold off
A=A1; B=B1; C=C1; D=D1; % set state-space
% matrices for simulink
% Run the simulation for the first set
% of matrices (A1, B1, C1, D1)
out1 = sim('time_domain_simulation');
time1 = out1.logsout{4}.Values.Time;  % Extract time data
data1 = out1.logsout{4}.Values.Data;  % Extract
% acceleration data
A=A2; B=B2; C=C2; D=D2; % set state-space
% matrices for simulink
% Run the simulation for the second set
% of matrices (A2, B2, C2, D2)
out2 = sim('time_domain_simulation');
time2 = out2.logsout{4}.Values.Time;  % Extract time data
```

```
data2 = out2.logsout{4}.Values.Data;  % Extract
% acceleration data
% Plot the main figure
figure;
% Plot the full data
subplot(2,1,1);
plot(time1, data1, '-k');
hold on;
plot(time2, data2, '--k');
xlabel('time [s]');
ylabel('acceleration [m/s^2]');
grid on;
legend(sprintf('$\\omega_n=%s$, $\\zeta=%s$, $b=%s$',...
    num2str(w_n_c(1)), num2str(zeta_c(1)),...
    num2str(b_c(1))),...
    sprintf('$\\omega_n=%s$, $\\zeta=%s$, $b=%s$',...
    num2str(w_n_c(1)), num2str(zeta_c(1)),...
    num2str(b_c(end))),...
    'Location', 'best', 'Interpreter', 'latex');
% Define the zoomed-in region
zoom_region_start = 4;  % Define the start
% of the zoomed region
zoom_region_end = 6;    % Define the end
% of the zoomed region
% Plot the zoomed-in area
subplot(2,1,2);
plot(time1, data1, '-k');
hold on;
plot(time2, data2, '--k');
```

```
xlim([zoom_region_start, zoom_region_end]);
xlabel('time [s]');
ylabel('acceleration [m/s^2]');
grid on;
legend(sprintf('$\\omega_n=%s$, $\\zeta=%s$, $b=%s$',...
    num2str(w_n_c(1)), num2str(zeta_c(1)),...
    num2str(b_c(1))),...
    sprintf('$\\omega_n=%s$, $\\zeta=%s$, $b=%s$',...
    num2str(w_n_c(1)), num2str(zeta_c(1)),...
    num2str(b_c(end))),...
    'Location', 'best', 'Interpreter', 'latex');
title('Zoomed-In Area');
hold off
A=A3; B=B3; C=C3; D=D3; % set state-space
% matrices for simulink
% Run the simulation for the first set
% of matrices (A1, B1, C1, D1)
out1 = sim('time_domain_simulation');
time1 = out1.logsout{4}.Values.Time;  % Extract time data
data1 = out1.logsout{4}.Values.Data;  % Extract
% acceleration data
A=A4; B=B4; C=C4; D=D4; % set state-space
% matrices for simulink
% Run the simulation for the second set
% of matrices (A2, B2, C2, D2)
out2 = sim('time_domain_simulation');
time2 = out2.logsout{4}.Values.Time;  % Extract time data
data2 = out2.logsout{4}.Values.Data;  % Extract
% acceleration data
```

```
% Plot the main figure
figure;
% Plot the full data
subplot(2,1,1);
plot(time1, data1, '-r');
hold on;
plot(time2, data2, '--r');
xlabel('time [s]');
ylabel('acceleration [m/s^2]');
grid on;
legend(sprintf('$\\omega_n=%s$, $\\zeta=%s$, $b=%s$',...
    num2str(w_n_c(end)), num2str(zeta_c(end)),...
    num2str(b_c(1))),...
    sprintf('$\\omega_n=%s$, $\\zeta=%s$, $b=%s$',...
    num2str(w_n_c(end)), num2str(zeta_c(end)),...
    num2str(b_c(end))),...
    'Location', 'best', 'Interpreter', 'latex');
% Define the zoomed-in region
zoom_region_start = 4;  % Define the start
% of the zoomed region
zoom_region_end = 6;    % Define the end
% of the zoomed region

% Plot the zoomed-in area
subplot(2,1,2);
plot(time1, data1, '-r');
hold on;
plot(time2, data2, '--r');
xlim([zoom_region_start, zoom_region_end]);
```

```
xlabel('time [s]');
ylabel('acceleration [m/s^2]');
grid on;
legend(sprintf('$\\omega_n=%s$, $\\zeta=%s$, $b=%s$',...
    num2str(w_n_c(end)), num2str(zeta_c(end)),...
    num2str(b_c(1))),...
    sprintf('$\\omega_n=%s$, $\\zeta=%s$, $b=%s$',...
    num2str(w_n_c(end)), num2str(zeta_c(end)),...
    num2str(b_c(end))),...
    'Location', 'best', 'Interpreter', 'latex');
title('Zoomed-In Area');
hold off
% SEAT VERTICAL RESULTS
u=logspace(log10(.5),log10(80),500);
tempfunb0(f) = results.(resultname)(index1).S_wz_s;
tempfunbmax(f) = results.(resultname)(index2).S_wz_s;
figure;
loglog(u,tempfunb0(u),'-k')
hold on
loglog(u,tempfunbmax(u),'--k')
tempfunb0(f) = results.(resultname)(index3).S_wz_s;
tempfunbmax(f) = results.(resultname)(index4).S_wz_s;
loglog(u,tempfunb0(u),'-r')
loglog(u,tempfunbmax(u),'--r')
xlim([0.1 100])
grid on
xlabel('frequency [Hz]')
ylabel(['seat vertical acceleration response PSD ' ...
    '[((m/s^2)^2)/Hz]'])
```

```
legend(sprintf('$\\omega_n=%s$, $\\zeta=%s$, $b=%s$',...
    num2str(w_n_c(1)), num2str(zeta_c(1)),...
    num2str(b_c(1))),...
    sprintf('$\\omega_n=%s$, $\\zeta=%s$, $b=%s$',...
    num2str(w_n_c(1)), num2str(zeta_c(1)),...
    num2str(b_c(end))),...
    sprintf('$\\omega_n=%s$, $\\zeta=%s$, $b=%s$',...
    num2str(w_n_c(end)), num2str(zeta_c(end)),...
    num2str(b_c(1))),...
    sprintf('$\\omega_n=%s$, $\\zeta=%s$, $b=%s$',...
    num2str(w_n_c(end)), num2str(zeta_c(end)),...
    num2str(b_c(end))),...
    'Location', 'best', 'Interpreter', 'latex');
hold off
A=A1; B=B1; C=C1; D=D1; % set state-space
% matrices for simulink
% Run the simulation for the first set of
% matrices (A1, B1, C1, D1)
out1 = sim('time_domain_simulation');
time1 = out1.logsout{5}.Values.Time;  % Extract time data
data1 = out1.logsout{5}.Values.Data;  % Extract
% acceleration data
A=A2; B=B2; C=C2; D=D2; % set state-space
% matrices for simulink
% Run the simulation for the second set of
% matrices (A2, B2, C2, D2)
out2 = sim('time_domain_simulation');
time2 = out2.logsout{5}.Values.Time;  % Extract time data
data2 = out2.logsout{5}.Values.Data;  % Extract
```

```
% acceleration data
% Plot the main figure
figure;
% Plot the full data
subplot(2,1,1);
plot(time1, data1, '-k');
hold on;
plot(time2, data2, '--k');
xlabel('time [s]');
ylabel('acceleration [m/s^2]');
grid on;
legend(sprintf('$\\omega_n=%s$, $\\zeta=%s$, $b=%s$',...
    num2str(w_n_c(1)), num2str(zeta_c(1)),...
    num2str(b_c(1))),...
    sprintf('$\\omega_n=%s$, $\\zeta=%s$, $b=%s$',...
    num2str(w_n_c(1)), num2str(zeta_c(1)),...
    num2str(b_c(end))),...
    'Location', 'best', 'Interpreter', 'latex');
% Define the zoomed-in region
zoom_region_start = 4;  % Define the start of
% the zoomed region
zoom_region_end = 6;    % Define the end of
% the zoomed region
% Plot the zoomed-in area
subplot(2,1,2);
plot(time1, data1, '-k');
hold on;
plot(time2, data2, '--k');
xlim([zoom_region_start, zoom_region_end]);
```

```
xlabel('time [s]');
ylabel('acceleration [m/s^2]');
grid on;
legend(sprintf('$\\omega_n=%s$, $\\zeta=%s$, $b=%s$',...
    num2str(w_n_c(1)), num2str(zeta_c(1)),...
    num2str(b_c(1))),...
    sprintf('$\\omega_n=%s$, $\\zeta=%s$, $b=%s$',...
    num2str(w_n_c(1)), num2str(zeta_c(1)),...
    num2str(b_c(end))),...
    'Location', 'best', 'Interpreter', 'latex');
title('Zoomed-In Area');
hold off
A=A3; B=B3; C=C3; D=D3; % set state-space
% matrices for simulink
% Run the simulation for the first set of
% matrices (A1, B1, C1, D1)
out1 = sim('time_domain_simulation');
time1 = out1.logsout{5}.Values.Time;  % Extract time data
data1 = out1.logsout{5}.Values.Data;  % Extract
% acceleration data
A=A4; B=B4; C=C4; D=D4; % set state-space
% matrices for simulink
% Run the simulation for the second set of
% matrices (A2, B2, C2, D2)
out2 = sim('time_domain_simulation');
time2 = out2.logsout{5}.Values.Time;  % Extract time data
data2 = out2.logsout{5}.Values.Data;  % Extract
% acceleration data
% Plot the main figure
```

```
figure;
% Plot the full data
subplot(2,1,1);
plot(time1, data1, '-r');
hold on;
plot(time2, data2, '--r');
xlabel('time [s]');
ylabel('acceleration [m/s^2]');
grid on;
legend(sprintf('$\\omega_n=%s$, $\\zeta=%s$, $b=%s$',...
    num2str(w_n_c(end)), num2str(zeta_c(end)),...
    num2str(b_c(1))),...
    sprintf('$\\omega_n=%s$, $\\zeta=%s$, $b=%s$',...
    num2str(w_n_c(end)), num2str(zeta_c(end)),...
    num2str(b_c(end))),...
    'Location', 'best', 'Interpreter', 'latex');
% Define the zoomed-in region
zoom_region_start = 4;  % Define the start of
% the zoomed region
zoom_region_end = 6;    % Define the end of
% the zoomed region
% Plot the zoomed-in area
subplot(2,1,2);
plot(time1, data1, '-r');
hold on;
plot(time2, data2, '--r');
xlim([zoom_region_start, zoom_region_end]);
xlabel('time [s]');
ylabel('acceleration [m/s^2]');
```

```
grid on;
legend(sprintf('$\\omega_n=%s$, $\\zeta=%s$, $b=%s$',...
    num2str(w_n_c(end)), num2str(zeta_c(end)),...
    num2str(b_c(1))),...
    sprintf('$\\omega_n=%s$, $\\zeta=%s$, $b=%s$',...
    num2str(w_n_c(end)), num2str(zeta_c(end)),...
    num2str(b_c(end))),...
    'Location', 'best', 'Interpreter', 'latex');
title('Zoomed-In Area');
hold off
% CAB DEFLECTION
u=logspace(log10(0.01*Vels),log10(10*Vels),500);
% first points
indeces = find(and([results.(resultname).w_n_c]==...
    w_n_c(1), and([results.(resultname).zeta_c] ==...
    zeta_c(1),  [results.(resultname).b_c] == b_c(1))) );
tempfunb0(f) = results.(resultname)(indeces).S_dz_c;
indeces = find(and([results.(resultname).w_n_c]==...
    w_n_c(1),and([results.(resultname).zeta_c]==...
    zeta_c(1),[results.(resultname).b_c]==b_c(end))));
tempfunbmax(f) = results.(resultname)(indeces).S_dz_c;
figure
loglog(u,tempfunb0(u),'-k')
hold on
loglog(u,tempfunbmax(u),'--k')
% last points
indeces = find(and([results.(resultname).w_n_c]==...
    w_n_c(end),and([results.(resultname).zeta_c]==...
    zeta_c(end),[results.(resultname).b_c]==b_c(1))));
```

```
tempfunb0(f) = results.(resultname)(indeces).S_dz_c;
indeces = find(and([results.(resultname).w_n_c]==...
    w_n_c(end),...
    and([results.(resultname).zeta_c] == zeta_c(end),...
    [results.(resultname).b_c] == b_c(end))) );
tempfunbmax(f) = results.(resultname)(indeces).S_dz_c;
loglog(u,tempfunb0(u),'-r')
loglog(u,tempfunbmax(u),'--r')
grid on
xlabel('frequency [Hz]')
ylabel('cab deflection response PSD [m^2/Hz]')
legend(sprintf('$\\omega_n=%s$, $\\zeta=%s$, $b=%s$',...
    num2str(w_n_c(1)), num2str(zeta_c(1)),...
    num2str(b_c(1))),...
    sprintf('$\\omega_n=%s$, $\\zeta=%s$, $b=%s$',...
    num2str(w_n_c(1)), num2str(zeta_c(1)),...
    num2str(b_c(end))),...
    sprintf('$\\omega_n=%s$, $\\zeta=%s$, $b=%s$',...
    num2str(w_n_c(end)), num2str(zeta_c(end)),...
    num2str(b_c(1))),...
    sprintf('$\\omega_n=%s$, $\\zeta=%s$, $b=%s$',...
    num2str(w_n_c(end)), num2str(zeta_c(end)),...
    num2str(b_c(end))),...
    'Location', 'best', 'Interpreter', 'latex');
hold off
A=A1; B=B1; C=C1; D=D1; % set state-space
% matrices for simulink
% Run the simulation for the first set of
% matrices (A1, B1, C1, D1)
```

```
out1 = sim('time_domain_simulation');
time1 = out1.logsout{1}.Values.Time;  % Extract time data
data1 = out1.logsout{1}.Values.Data;  % Extract
% acceleration data
A=A2; B=B2; C=C2; D=D2; % set state-space
% matrices for simulink
% Run the simulation for the second set of
% matrices (A2, B2, C2, D2)
out2 = sim('time_domain_simulation');
time2 = out2.logsout{1}.Values.Time;  % Extract time data
data2 = out2.logsout{1}.Values.Data;  % Extract
% deflection data
% Plot the main figure
figure;
% Plot the full data
subplot(2,1,1);
plot(time1, data1*1000, '-k');
hold on;
plot(time2, data2*1000, '--k');
xlabel('time [s]');
ylabel('deflection [mm]');
grid on;
legend(sprintf('$\\omega_n=%s$, $\\zeta=%s$, $b=%s$',...
    num2str(w_n_c(1)), num2str(zeta_c(1)),...
    num2str(b_c(1))),...
    sprintf('$\\omega_n=%s$, $\\zeta=%s$, $b=%s$',...
    num2str(w_n_c(1)), num2str(zeta_c(1)),...
    num2str(b_c(end))),...
    'Location', 'best', 'Interpreter', 'latex');
```

```
% Define the zoomed-in region
zoom_region_start = 4;  % Define the start
% of the zoomed region
zoom_region_end = 6;    % Define the end
% of the zoomed region
% Plot the zoomed-in area
subplot(2,1,2);
plot(time1, data1*1000, '-k');
hold on;
plot(time2, data2*1000, '--k');
xlim([zoom_region_start, zoom_region_end]);
xlabel('time [s]');
ylabel('deflection [mm]');
grid on;
legend(sprintf('$\\omega_n=%s$, $\\zeta=%s$, $b=%s$',...
    num2str(w_n_c(1)), num2str(zeta_c(1)),...
    num2str(b_c(1))),...
    sprintf('$\\omega_n=%s$, $\\zeta=%s$, $b=%s$',...
    num2str(w_n_c(1)), num2str(zeta_c(1)),...
    num2str(b_c(end))),...
    'Location', 'best', 'Interpreter', 'latex');
title('Zoomed-In Area');
hold off
A=A3; B=B3; C=C3; D=D3; % set state-space
% matrices for simulink
% Run the simulation for the first set of
% matrices (A1, B1, C1, D1)
out1 = sim('time_domain_simulation');
time1 = out1.logsout{1}.Values.Time;  % Extract time data
```

```
data1 = out1.logsout{1}.Values.Data;  % Extract
% acceleration data
A=A4; B=B4; C=C4; D=D4; % set state-space
% matrices for simulink
% Run the simulation for the second set of
% matrices (A2, B2, C2, D2)
out2 = sim('time_domain_simulation');
time2 = out2.logsout{1}.Values.Time;  % Extract
% time data
data2 = out2.logsout{1}.Values.Data;  % Extract
% deflection data
% Plot the main figure
figure;
% Plot the full data
subplot(2,1,1);
plot(time1, data1*1000, '-r');
hold on;
plot(time2, data2*1000, '--r');
xlabel('time [s]');
ylabel('deflection [mm]');
grid on;
legend(sprintf('$\\omega_n=%s$, $\\zeta=%s$, $b=%s$',...
    num2str(w_n_c(end)), num2str(zeta_c(end)),...
    num2str(b_c(1))),...
    sprintf('$\\omega_n=%s$, $\\zeta=%s$, $b=%s$',...
    num2str(w_n_c(end)), num2str(zeta_c(end)),...
    num2str(b_c(end))),...
    'Location', 'best', 'Interpreter', 'latex');
% Define the zoomed-in region
```

```
zoom_region_start = 4;  % Define the start
% of the zoomed region
zoom_region_end = 6;    % Define the end
% of the zoomed region
% Plot the zoomed-in area
subplot(2,1,2);
plot(time1, data1*1000, '-r');
hold on;
plot(time2, data2*1000, '--r');
xlim([zoom_region_start, zoom_region_end]);
xlabel('time [s]');
ylabel('deflection [mm]');
grid on;
legend(sprintf('$\\omega_n=%s$, $\\zeta=%s$, $b=%s$',...
    num2str(w_n_c(end)), num2str(zeta_c(end)),...
    num2str(b_c(1))),...
    sprintf('$\\omega_n=%s$, $\\zeta=%s$, $b=%s$',...
    num2str(w_n_c(end)), num2str(zeta_c(end)),...
    num2str(b_c(end))),...
    'Location', 'best', 'Interpreter', 'latex');
title('Zoomed-In Area');
hold off
```

APPENDIX 4 - Simscape Model

Design description of the simscape model generated through System Design Report tool of the Simulink is given below.

Table of Contents

Chapter 1. Root System

Figure 1.1. v11_verification

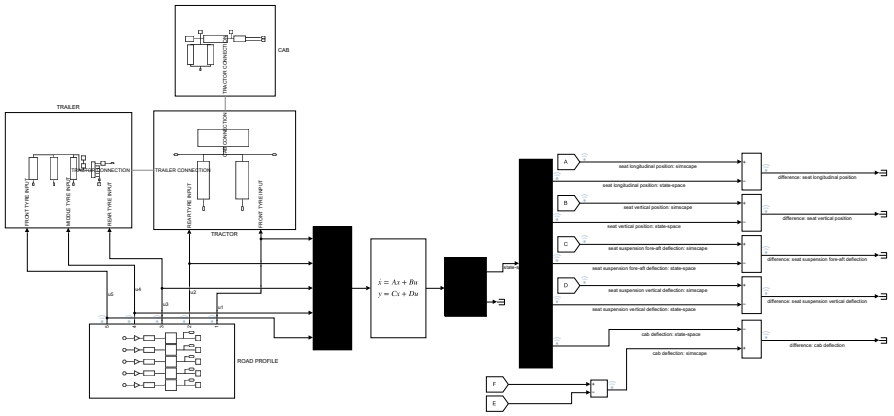

Chapter 2. Subsystems

CAB

Figure 2.1. v11_verification/CAB

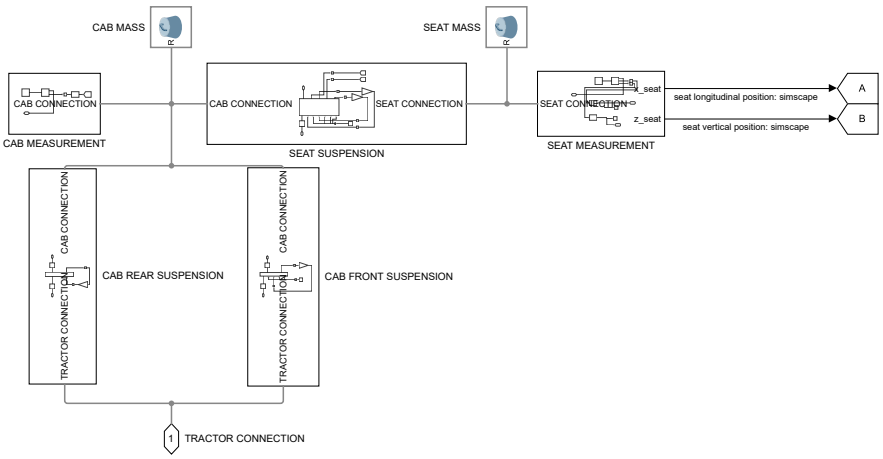

CAB FRONT SUSPENSION

Figure 2.2. v11_verification/CAB/CAB FRONT SUSPENSION

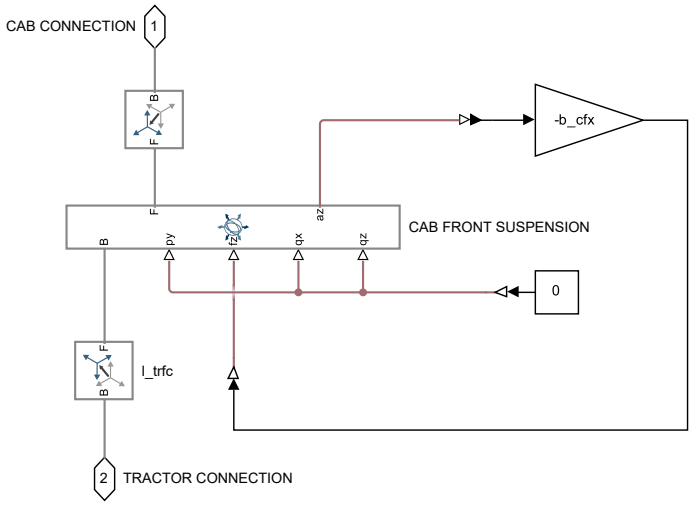

CAB MEASUREMENT

Figure 2.3. v11_verification/CAB/CAB MEASUREMENT

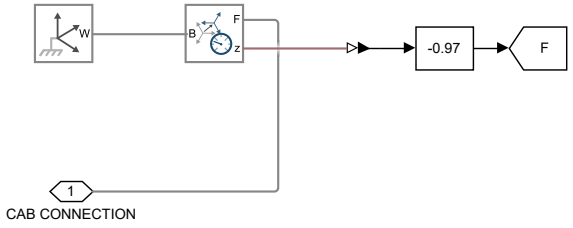

CAB REAR SUSPENSION

Figure 2.4. v11_verification/CAB/CAB REAR SUSPENSION

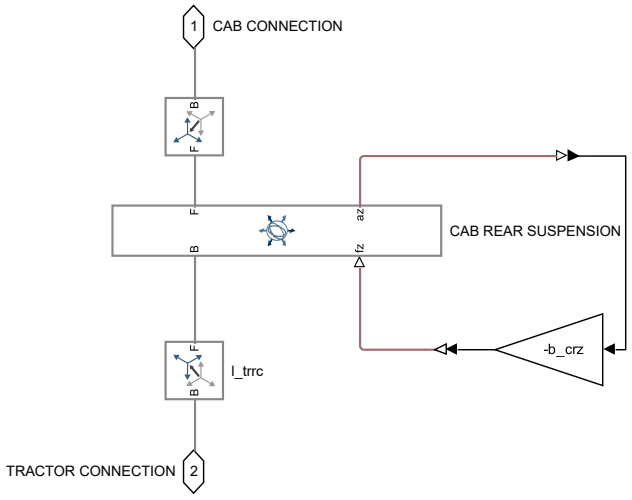

ROAD PROFILE

Figure 2.5. v11_verification/ROAD PROFILE

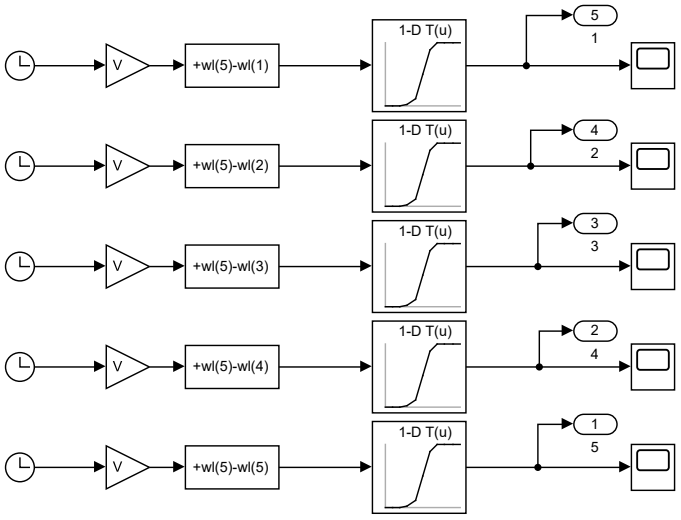

SEAT MEASUREMENT

Figure 2.6. v11_verification/CAB/SEAT MEASUREMENT

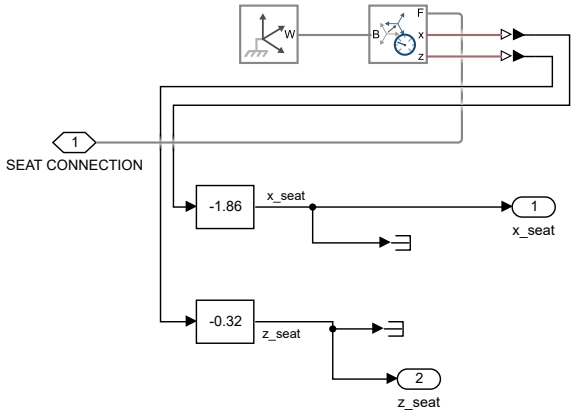

SEAT SUSPENSION

Figure 2.7. v11_verification/CAB/SEAT SUSPENSION

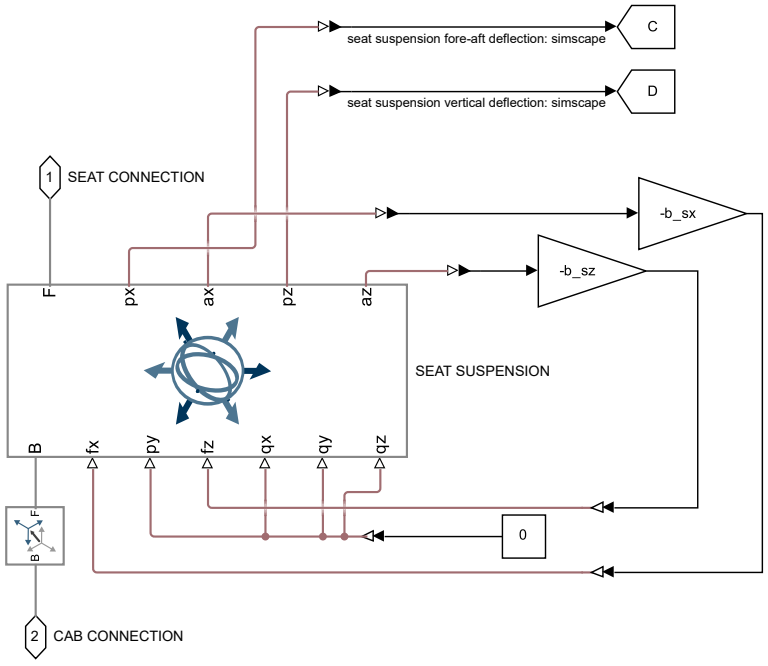

TRACTOR

Figure 2.8. v11_verification/TRACTOR

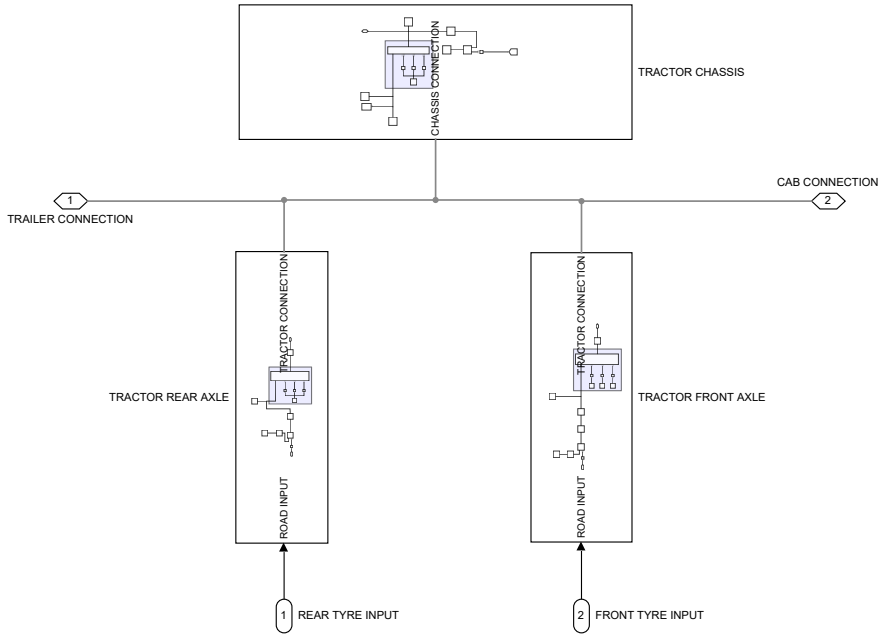

TRACTOR CHASSIS

Figure 2.9. v11_verification/TRACTOR/TRACTOR CHASSIS

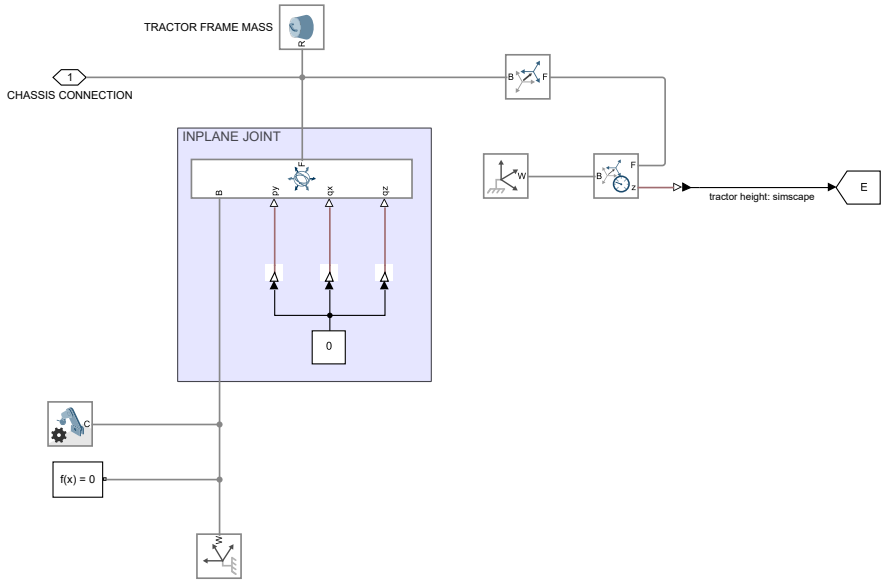

TRACTOR FRONT AXLE

Figure 2.10. v11_verification/TRACTOR/TRACTOR FRONT AXLE

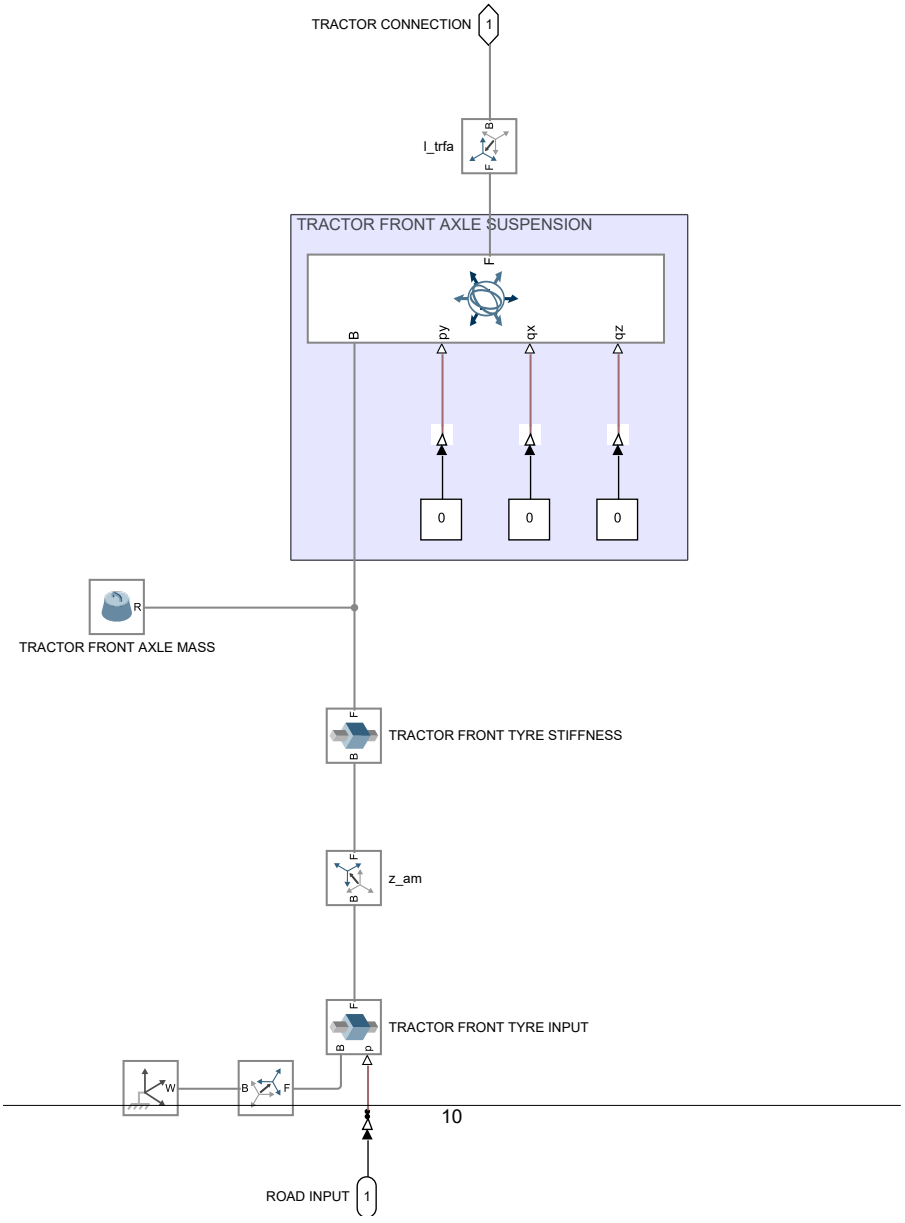

TRACTOR REAR AXLE

Figure 2.11. v11_verification/TRACTOR/TRACTOR REAR AXLE

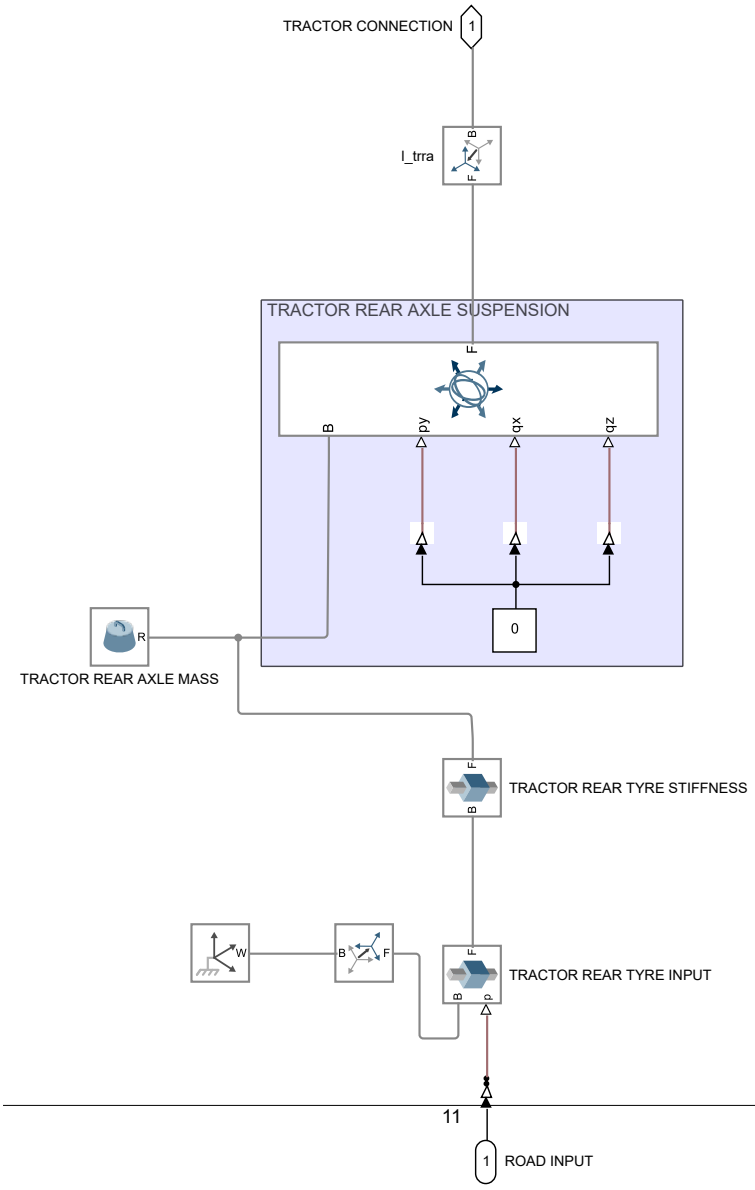

TRAILER

Figure 2.12. v11_verification/TRAILER

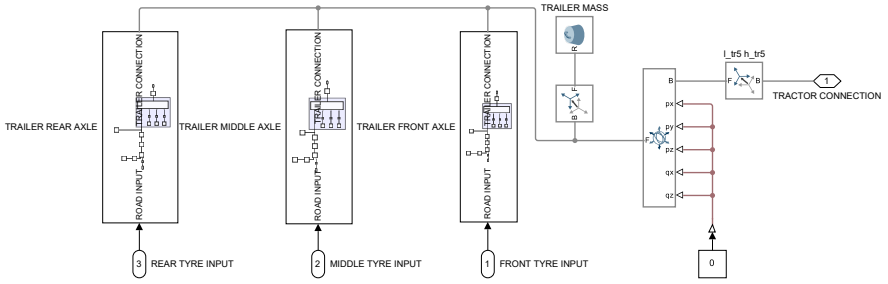

TRAILER FRONT AXLE

Figure 2.13. v11_verification/TRAILER/TRAILER FRONT AXLE

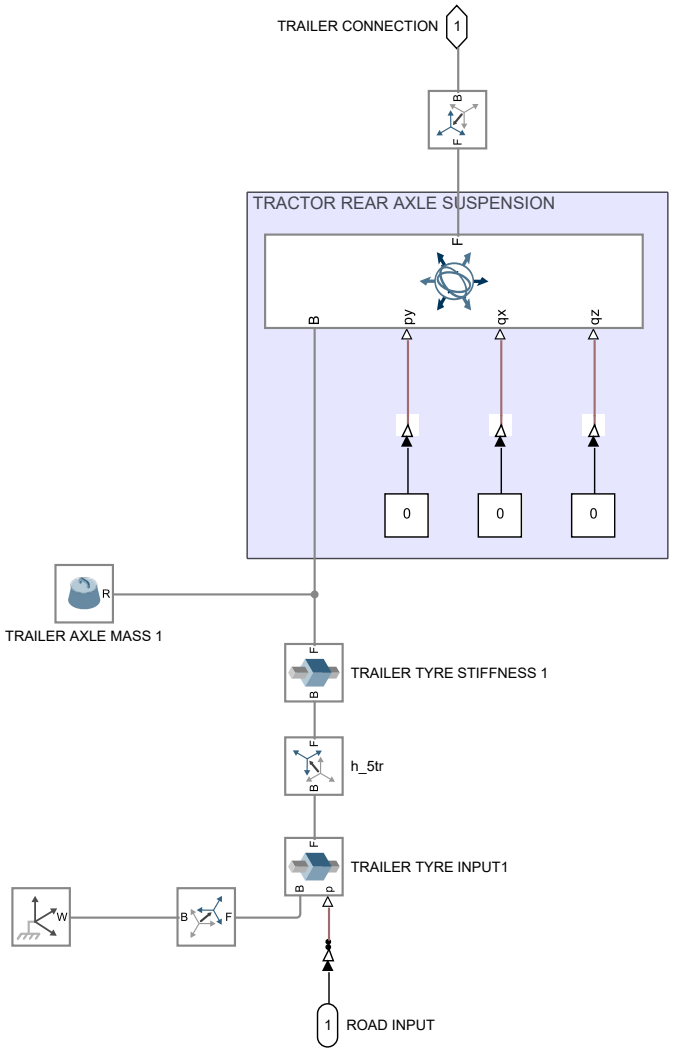

TRAILER MIDDLE AXLE

Figure 2.14. v11_verification/TRAILER/TRAILER MIDDLE AXLE

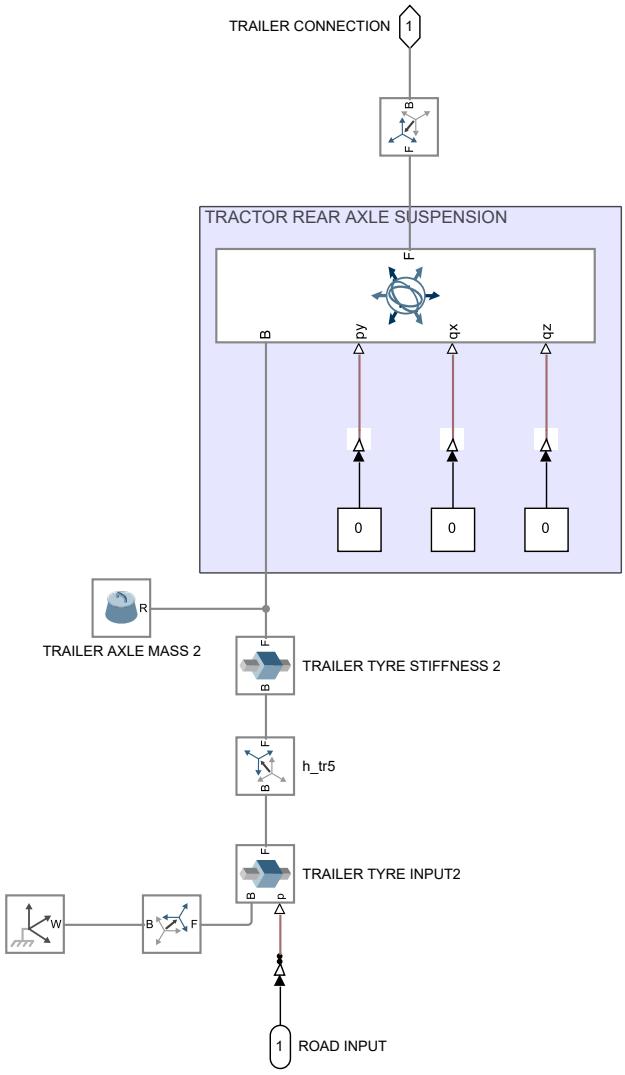

TRAILER REAR AXLE

Figure 2.15. v11_verification/TRAILER/TRAILER REAR AXLE

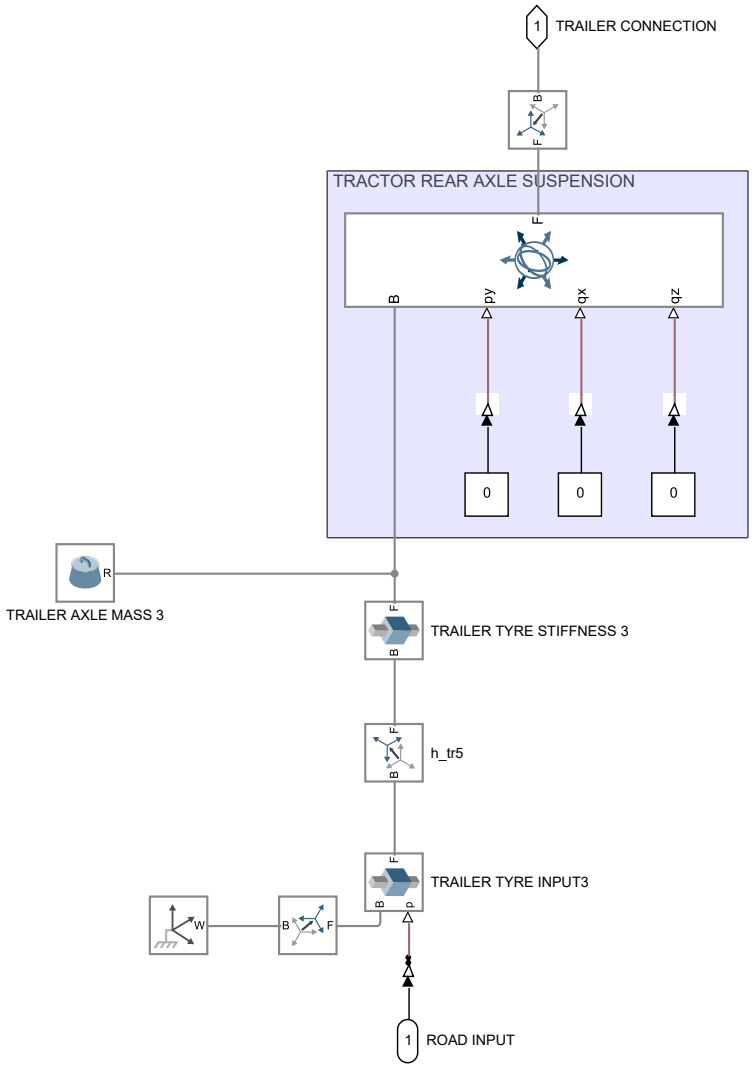

Chapter 3. System Design Variables

Table 3.1. Design Variables

Variable Name	Parent Blocks	Size	Class
A	State-Space	28x28	double
B	State-Space	28x5	double
C	State-Space	28x28	double
D	State-Space	28x5	double
I_c	CAB MASS CAB MASS	1x1	double
I_st	TRAILER MASS TRAILER MASS	1x1	double
I_tr	TRACTOR FRAME MASS TRACTOR FRAME MASS	1x1	double
V	Gain2 Gain3 Gain4 Gain5 Gain6	1x1	double
b_cfx	Gain Gain	1x1	double
b_crz	Gain2 Gain2	1x1	double
b_sx	Gain3 Gain3	1x1	double
b_sz	Gain4 Gain4	1x1	double
c_cfx	CAB FRONT SUSPENSION	1x1	double
c_cfz	CAB FRONT SUSPENSION	1x1	double
c_crz	CAB REAR SUSPENSION	1x1	double
c_st1	Bushing Joint	1x1	double
c_st2	Bushing Joint	1x1	double
c_st3	Bushing Joint	1x1	double
c_sx	SEAT SUSPENSION	1x1	double
c_sz	SEAT SUSPENSION	1x1	double
c_trf	Bushing Joint	1x1	double
c_trr	Bushing Joint	1x1	double

Variable Name	Parent Blocks	Size	Class
h_5st	Rigid Transform5	1x1	double
h_cf	Rigid Transform2 Rigid Transform3	1x1	double
h_cs	Rigid Transform4	1x1	double
h_tr5	h_5tr h_tr5 h_tr5 l_tr5 h_tr5	1x1	double
k_1	TRACTOR FRONT TYRE STIFFNESS	1x1	double
k_2	TRACTOR REAR TYRE STIFFNESS	1x1	double
k_3	TRAILER TYRE STIFFNESS 1	1x1	double
k_4	TRAILER TYRE STIFFNESS 2	1x1	double
k_5	TRAILER TYRE STIFFNESS 3	1x1	double
k_cfx	CAB FRONT SUSPENSION	1x1	double
k_cfz	CAB FRONT SUSPENSION	1x1	double
k_crz	CAB REAR SUSPENSION	1x1	double
k_st1	Bushing Joint	1x1	double
k_st2	Bushing Joint	1x1	double
k_st3	Bushing Joint	1x1	double
k_sx	SEAT SUSPENSION	1x1	double
k_sz	SEAT SUSPENSION	1x1	double
k_trf	Bushing Joint	1x1	double
k_trr	Bushing Joint	1x1	double
l_5st	Rigid Transform5	1x1	double
l_cf	Rigid Transform2	1x1	double
l_cr	Rigid Transform3 Rigid Transform	1x1	double
l_cs	Rigid Transform4	1x1	double
l_st1	Rigid Transform8 Rigid Transform9	1x1	double
l_st2	Rigid Transform10 Rigid Transform11	1x1	double
l_st3	Rigid Transform6 Rigid Transform7	1x1	double
l_tr5	Rigid Transform9 Rigid Transform11 Rigid Transform7 l_tr5 h_tr5	1x1	double

Variable Name	Parent Blocks	Size	Class
l_trfa	Rigid Transform l_trfa	1x1	double
l_trfc	l_trfc	1x1	double
l_trra	Rigid Transform1 l_trra	1x1	double
l_trrc	l_trrc Rigid Transform	1x1	double
m_1	TRACTOR FRONT AXLE MASS	1x1	double
m_2	TRACTOR REAR AXLE MASS	1x1	double
m_3	TRAILER AXLE MASS 1	1x1	double
m_4	TRAILER AXLE MASS 2	1x1	double
m_5	TRAILER AXLE MASS 3	1x1	double
m_c	CAB MASS	1x1	double
m_s	SEAT MASS	1x1	double
m_st	TRAILER MASS	1x1	double
m_tr	TRACTOR FRAME MASS	1x1	double
road	1-D Lookup Table 1-D Lookup Table1 1-D Lookup Table2 1-D Lookup Table3 1-D Lookup Table4 1-D Lookup Table 1-D Lookup Table1 1-D Lookup Table2 1-D Lookup Table3 1-D Lookup Table4 1-D Lookup Table 1-D Lookup Table1 1-D Lookup Table2 1-D Lookup Table3 1-D Lookup Table4	2x20001	double
wl	Bias Bias1 Bias2 Bias3 Bias4 Bias Bias1 Bias2 Bias3 Bias4	5x1	double